

# 第28届武汉国际珠宝学术年会

THE 28TH WUHAN INTERNATIONAL JEWELRY CONFERENCE

暨第一届湖北省珠宝工程技术研究中心学术会议论文集 (2020)



2020.10

《宝石和宝石学杂志（中英文）》编辑部 编

内部资料，请勿外传

第二十八届武汉国际珠宝学术年会  
暨湖北省珠宝工程技术研究中心学术会议

日  
程  
表

中国地质大学（武汉）珠宝学院

2020. 10. 17-10. 18



时间		会议内容	报告人	主持人
17 日 上 午	8:40-8:50	开幕式 Opening Ceremony	中国地质大学 (武汉) 党常委、副校长 王华教授	中国地质大学 (武汉) 珠宝学院 薛保山 书记
	8:50-10:00	彩色钻石优化处理与鉴定 Color Diamond Treatment and its Identification (特邀报告)	王五一博士 美国宝石学院 (GIA)	中国地质大学 (武汉) 珠宝学院 沈锡田教授
17 AM	10:00-10:10	休息 (Break)		
	10:10-11:20	矿物颜色与价态变化 Mineral Color and the Role of Changing Oxidation States (特邀报告)	Prof. George Rossman 加州理工学院 (Caltech.)	中国地质大学 (武汉) 珠宝学院 沈锡田教授
午休 (Lunch break)				
17 日 下 午  17 PM	13:00-14:10	视频报告 Video poster presentation	各位作者 Poster authors	中国地质大学 (武汉) 珠宝学院 沈锡田教授
	14:10-15:20	定年法在宝石学上的应用/ 红宝石或是粉色蓝宝石, 这才是问题 Age dating applied as a testing procedure to gemstones and biogenic materials/Red ruby or pink sapphire, that's the question	Dr. Michael Krzemnicki  瑞士宝石学院 (SSEF)	中国地质大学 (武汉) 珠宝学院 沈锡田教授
	15:20-15:30	休息 (Break)		
	15:30-16:40	重建一顶盎格鲁撒克逊国王的头盔 The reconstruction of a Anglo Saxon Golden Kings Helmet	Frank Cooper 英国伯明翰城市 大学珠宝学院 (Birmingham City University)	中国地质大学 (武汉) 珠宝学院副院长 郝亮教授
休会 (Break)				

18 日 上午	9:00-10:30	EDXRF 原理及实践 Theory and Practice of EDXRF (研习分会 1)	沈锡田教授 中国地质大学 (武汉)	中国地质大学 (武汉) 珠宝学院 沈锡田教授
	10:30-10:40	休息 (Break)		
	10:40-11:40	昌化鸡血石及其相似品的鉴别 Identification of Chicken Blood stone from Changhua and the Similar Species (研习分会 1)	陈涛教授 中国地质大学 (武汉)	中国地质大学 (武汉) 珠宝学院 沈锡田教授
18 AM	午休 (Lunch break)			
18 日 下午	14:00-14:45	合成钻石 Synthetic Diamonds (研习分会 2)	单崇新教授 郑州大学	中国地质大学 (武汉) 珠宝学院副院长 郝亮教授
	14:45-15:30	珠宝首饰工程技术与先进制造 Engineering Technology and Advanced Manufacturing in Gems and Jewellery (研习分会 2)	郝亮教授 中国地质大学 (武汉)	中国地质大学 (武汉) 珠宝学院 李妍副教授
	15:30-15:40	休息 (Break)		
	15:40-16:50	Boltenstern Fine Jewelry – 手工编码, 技术制造 Boltenstern Fine Jewelry, coded by hand - crafted by technology (研习分会 2)	Marie Boltenstern  Boltenstern 公司	中国地质大学 (武汉) 珠宝学院副院长 郝亮教授
	16:50-17:00	闭幕 Closing		中国地质大学 (武汉) 珠宝学院院长 杨明星教授
18 PM				



微信号: gicchina



# 目 次

埃塞俄比亚祖母绿的宝石学特征 .....	胡晓君,裴景成(1)
含重晶石包裹体的石英硬玉岩的宝石岩相学特征及成因初探.....	陈梓贤,沈雁翱,林哲琼(5)
铝硼锆钙石(Painite)的宝石学特征测试分析 .....	郭 杰,廖任庆,郑秋菊(11)
墨西哥红蓝料琥珀的宝石学特征.....	赵 彤,苏小鹏,王雅玫,李 妍(20)
萤石的宝石学特征及荧光特性研究.....	穆宏赫,林静韬,李 妍,卢 勒(23)
寿山金狮峰田石石皮的谱学特征.....	郑金宇,陈 涛,姚春茂,周征宇,李梦阳,徐 行(27)
浙江省遂昌县好川墓地绿松石料珠的宝石学特征及工艺评价.....	姜 炎,杨明星(33)
The Glory of Turquoise from Neolithic to Bronze Age in Persia .....	..... Bahareh Shirdam , Yang Mingxing, Andy H. Shen(38)
中国某公司合成粉色—红色系钻石的宝石学特征研究 .....	张传政,李建军,程佑法,范春丽,王礼胜(42)
水热法合成蓝绿色绿柱石的宝石学及光谱学特征.....	张嘉麟,张 倩,裴景成,黄伟志(46)
合成水晶晶簇的鉴定特征 .....	代会茹,周丹怡,宋中华,苏 隽,李海波,陆太进,马永旺(51)
3D 打印技术在首饰设计创客教育中的应用探索 .....	姜婷煜,杨金凤,李 妍,何 萌(55)
面向智能首饰的大规模个性化的生产模式研究 .....	李星枰,李 妍,潘瑞琪(59)
辽代契丹文化中的融合与包容——以金属工艺纹样为例 .....	文尚佳,卢 勒,刘艺苗(62)
初探首饰日用之中的价值旨归——以乌木首饰为例 .....	曾义平(69)
从应用型技术本科的角度构想珠宝专业本科人才培养模式改革 .....	..... 刘衍宇,赵靖娜,吴 璠,杨天畅,徐娅芬(72)

# 埃塞俄比亚祖母绿的宝石学特征

胡晓君<sup>1</sup>, 裴景成<sup>2</sup>

(1. 中南大学, 湖南 长沙 410012; 2. 中国地质大学珠宝学院, 湖北 武汉 430074)

**摘要:**运用常规宝石学测试方法,结合 LA-ICP-MS 测试、紫外-可见吸收光谱对埃塞俄比亚祖母绿的宝石学特征、化学成分及紫外-可见光谱进行了系统的研究。常规宝石学测试结果表明:埃塞俄比亚祖母绿自形程度较高,整体透明度较好,呈深浅不一的绿色,伴有蓝色或黄色色调,折射率为 1.581~1.589,双折率为 0.007~0.008,相对密度为 2.68~2.73。结果显示,埃塞俄比亚祖母绿内部的包裹体十分丰富:存在大量的流体包裹体,主要为气液两相包裹体,成群存在时可形成“雨状”“浪花状”等特殊形态。黑云母在样品祖母绿也较为常见,部分样品中可见色带和生长纹。LA-ICP-MS 测试结果表明:埃塞俄比亚祖母绿中的碱金属含量在 1.44%~1.68%之间,以 Na 元素为主。影响埃塞俄比亚祖母绿颜色的元素中,Cr 元素和 Fe 元素含量较高,V 元素含量较低。紫外-可见吸收光谱表明,埃塞俄比亚祖母绿的颜色成因是  $\text{Cr}^{3+}$ 、 $\text{V}^{3+}$ 、 $\text{Fe}^{2+}$  和  $\text{Fe}^{3+}$  的共同作用所致,相比于其他地区的祖母绿的紫外-可见光谱,埃塞俄比亚祖母绿在 850 nm 附近的  $\text{Fe}^{2+}$  的特征吸收峰较强。

**关键词:**祖母绿;紫外-可见吸收光谱;激光剥蚀电感耦合等离子体质谱;埃塞俄比亚

## Gemmological Characteristic of Emerald from Ethiopia

HU Xiaojun<sup>1</sup>, PEI Jingcheng<sup>2</sup>

(1. Center South University, Changsha 410012, China; 2. Gemmological Institute, China University of Geosciences, Wuhan 430074, China)

**Abstract:** In this paper, emerald from Ethiopia was selected as the research object. We used conventional instruments to study its basic gemmological features, combining with LA-ICP-MS, UV-Vis-Infrared Spectrum to study the locality features of emerald from Ethiopia.

The results of conventional instruments tests show that emerald from Ethiopia has good euhedral and transparency. The colour of emeralds from Ethiopia are mostly light green to deep green, with blue or yellow tone. The range of refractive index is 1.581—1.589, and DR is between 0.007—0.008. The relative density is from 2.68—2.73. It is

收稿日期:2020-09-30

作者简介:胡晓君(1998—),女,学士,主要从事宝石材料及工艺学研究。

通讯作者:裴景成(1974—),男,副教授,主要从事彩色宝石及产地教学及研究工作。E-mail:peijc@cug.edu.cn



observed that the inclusions in emerald from Ethiopia are rich; there are a large number of fluid inclusions, mainly gas-liquid two-phase inclusions, which can form rain-like, spray-like and other special shapes when they exist in groups. Biotite is also frequently seen in samples, and some of the samples have colour bands and growth pattern. The results of LA-ICP-MS show that emerald from Ethiopia presents a medium to high sum of alkali metals from 1.44% to 1.68%, in which the content of Na is the highest. Of all the chemical elements responsible for the colour of the emeralds, the content of Cr and Fe is relatively high and the content of V is relatively low.

The UV-Vis-Infrared spectrum proves that the colour of emerald from Ethiopia is mainly caused by  $\text{Cr}^{3+}$ ,  $\text{V}^{3+}$ ,  $\text{Fe}^{2+}$  and  $\text{Fe}^{3+}$  in crystal. Compared with the UV-Vis spectrum of emerald from other origins, emerald from Ethiopia has a strong absorption around 850 nm, which belongs to  $\text{Fe}^{2+}$ .

**Key words:** emerald; UV-Vis spectrum; LA-ICP-MS; Ethiopia



图1 埃塞俄比亚祖母绿样品

Fig.1 Emerald samples from Ethiopia

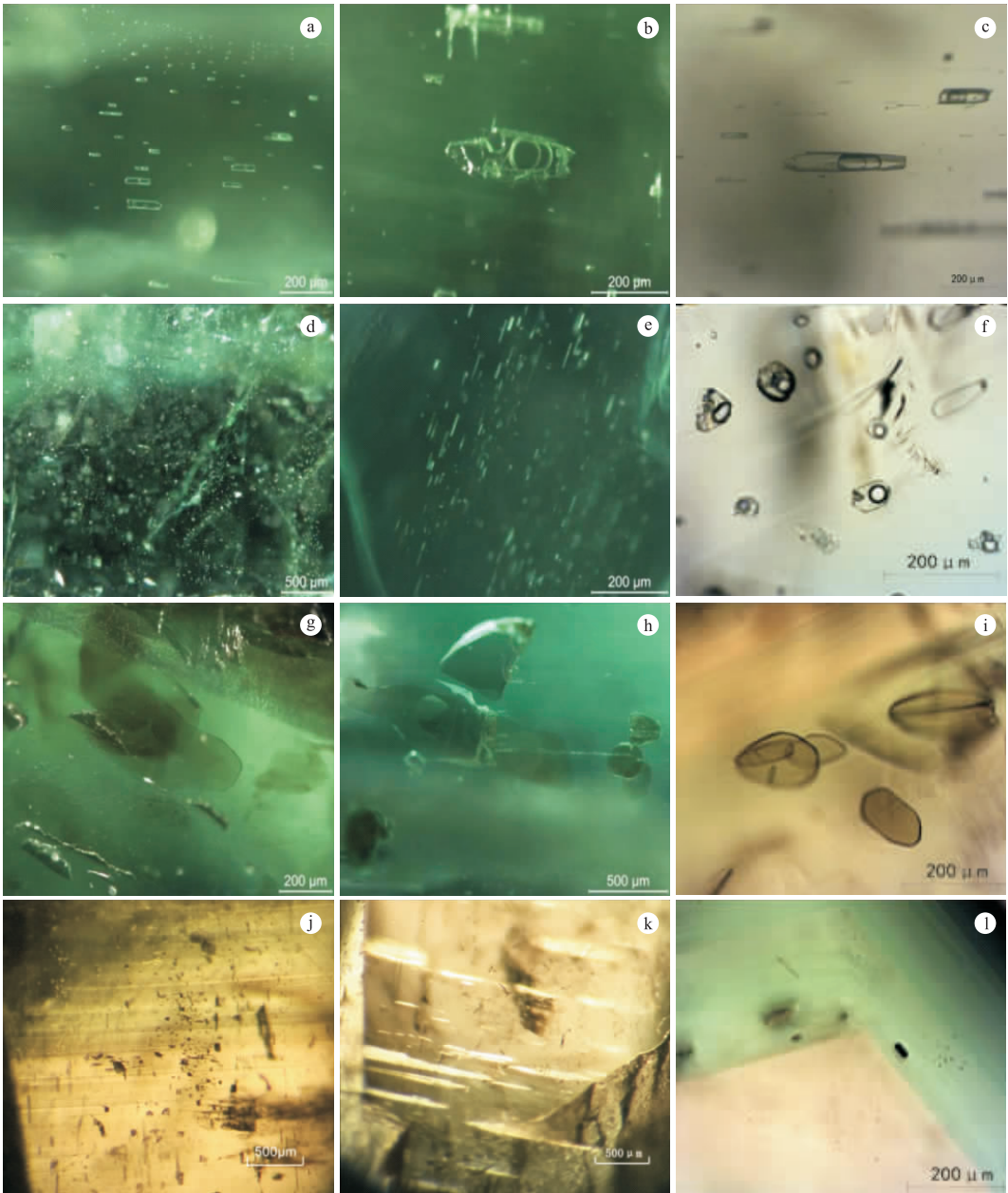


图 2 埃塞俄比亚祖母绿的内部包裹体

Fig. 2 Internal inclusions of emeralds from Ethiopia

a—f. 流体包裹体;g—i. 黑云母包裹体;j. 生长纹;k. 不完全解理纹;l. 角状色带(//C 切面)

表 1 埃塞俄比亚祖母绿的主要化学成分

Table 1 The chemical compositions of emeralds from Ethiopia						$w_B/\%$
成分	EE-1	EE-2	EE-3	EE-4	EE-6	EE-7
SiO <sub>2</sub>	65.30	65.90	65.20	65.40	65.10	65.60
Al <sub>2</sub> O <sub>3</sub>	16.20	15.30	16.30	16.50	16.10	15.90
BeO	13.30	13.00	13.30	13.20	13.70	13.30
Na <sub>2</sub> O	1.94	2.11	1.92	1.82	1.92	1.89
MgO	2.30	2.46	2.29	2.16	2.34	2.25
Na <sub>2</sub> O/ MgO	0.84	0.86	0.84	0.84	0.82	0.84
Alkalis*	1.55	1.68	1.50	1.44	1.51	1.51

Alkalis\* : <sup>7</sup>Li+<sup>23</sup>Na+<sup>39</sup>K+<sup>85</sup>Rb+<sup>133</sup>Cs

表 2 埃塞俄比亚祖母绿的微量元素  
Table 2 Trace elements of emeralds from Ethiopia /ppm

成分	EE-1	EE-2	EE-3	EE-4	EE-5	EE-6	EE-7
Li	238	248	215	270	214	230	274
K	382	349	249	274	332	282	349
Sc	67.9	103	89.8	157	99.8	71.9	57.6
V	100	108	100.2	102	111	110	101
Cr	965	2 095	845	1 050	1 239	717	1 419
Mn	45.7	13.2	10.8	7.0	27.1	10.1	44.9
Fe	4 589	5 056	3 889	4 122	4 978	4 433	4 978
Co	1.39	1.41	1.01	1.49	1.51	1.46	1.36
Ni	11.9	10.37	11.40	9.9	6.56	6.98	10.14
Zn	45.0	35.2	22.0	31.9	41.2	24.8	46.9
Ga	21.5	22.1	18.1	15.5	22.0	17.5	20.9
Rb	67.6	62.6	35.2	32.8	66.5	39.2	70.7
Cs	391	446	261	271	406	341	411

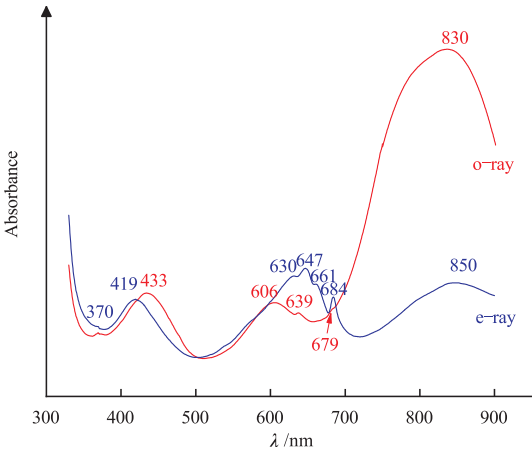


图 3 埃塞俄比亚祖母绿的紫外-可见光谱  
Fig. 3 UV-Vis spectra of emeralds from Ethiopia

# 含重晶石包裹体的石英硬玉岩的宝石 岩相学特征及成因初探

陈梓贤<sup>1</sup>, 沈雁翱<sup>2</sup>, 林哲琼<sup>1</sup>

(1. 国家珠宝检测中心有限责任公司, 广东 广州 511400; 2. 广东谷值资产评估有限公司, 广东 广州 511400)

**摘要:**以宝石学和岩石学的研究方法,对一种紫色硬玉岩进行研究。偏光显微镜显示,岩石的系统鉴定为含钠长石石英微晶硬玉岩,同时发现石英中含有柱状、板状、粒状重晶石包裹体。宝石学仪器和红外光谱测试确定了样品紫色部分为硬玉,白色部分为石英。拉曼光谱确认了石英中的包裹体是重晶石,辅证了偏光显微镜的包裹体鉴定结果。紫外-可见光谱和能量色散型 X 射线荧光光谱分析结果说明,由锰引起的大致以 580 nm 黄绿光为中心的 500~600 nm 最强吸收带是该紫色硬玉岩的呈色原因。基于岩相学特征认为,该岩石是硬玉岩成岩后,压力缓慢降低导致少部分硬玉与石英反应成微细粒钠长石混杂在硬玉集合体中,而吸附有  $\text{Ba}^{2+}$  的富含  $\text{SiO}_2$  胶体热液沿硬玉岩裂隙侵入,在  $\text{SiO}_2$  胶体聚沉阶段,释放出的  $\text{Ba}^{2+}$  与  $\text{SO}_4^{2-}$  反应析出细小且自形的重晶石,被后续晶化的石英包裹,最终形成了石英包裹重晶石呈流动构造状分布于硬玉岩中的罕见现象。

**关键词:**重晶石;石英;钠长石;硬玉岩;包裹体

## Gemmological, Petrographic Characteristics and Petrogenesis of Jadeitite Accompanied Barite Included Quartz

CHEN Zixian<sup>1</sup>, SHEN Yan'ao<sup>2</sup>, LIN Zheqiong<sup>1</sup>

(1. National Gemstone Testing Center Co., Ltd, Guangzhou 511400, China;

2. Guzhi Assets Appraisal Co., Ltd, Guangzhou 511400, China)

**Abstract:** A kind of purple jadeitite is studied by gemmological and petrological methods. System identification of the rock by polarizing microscope find it is albite quartz microcrystalline jadeitite, and the quartz contains columnar, slaty and granular barite inclusions. The purple parts of the sample are jadeite and the white parts are quartzs. Raman spectrum confirms that the inclusions in quartz are barite, which supports the inclusion identification results of polarizing microscope. UV-Vis and the qualitative analysis results of energy dispersive X-ray fluorescence spectrum show that the strongest absorption band between 500—600 nm, with about 580 nm as the center, caused by manganese, is the cause of the colour of the purple jadeitite. Based on the petrographic characteristics, it is considered that a few jadeite reacted with quartz to form micro-grained albite mixed in the jadeite aggregates with the slowly decrease of pressure after



the jadeitite metamorphic crystallization, while the  $\text{SiO}_2$  rich colloidal hydrothermal adsorbed with  $\text{Ba}^{2+}$  intruded along the fractures of jadeitite. The  $\text{Ba}^{2+}$  released in the  $\text{SiO}_2$  colloidal flocculation stage and reacted with  $\text{SO}_4^{2-}$  to form tiny, idiomorphic barite, which were then included by crystallized quartzs, then a rare phenomenon that included in quartzs barite and distributed in jadeite as the form of flow structure in jadeitite.

**Key words:** barite; quartz; albite; jadeitite; inclusion

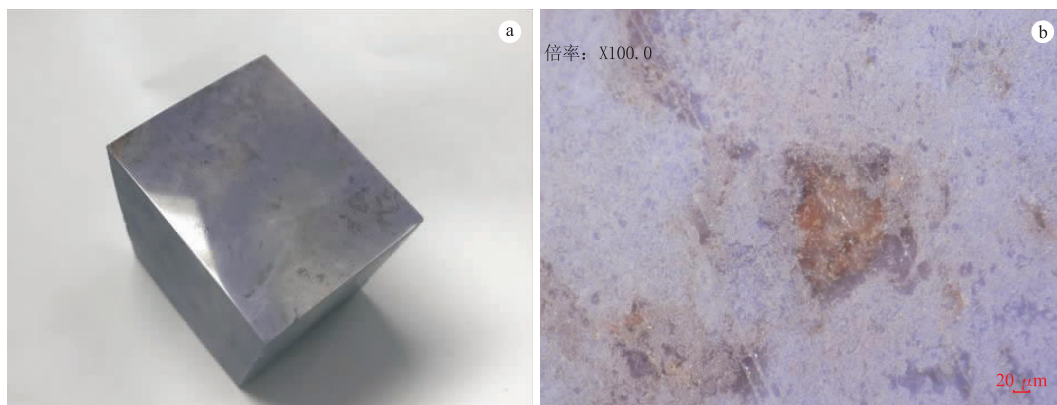


图1 样品中白色斑块和呈流动状白色条带(a)和样品的超景深显微图(b)

Fig. 1 The white clots and fluxion banding in the sample(a) and image of the sample under super depth of field microscope(b)

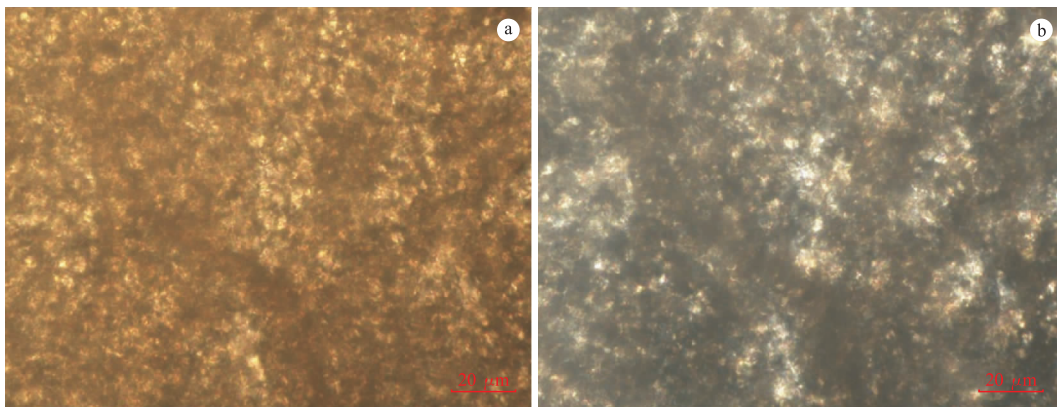


图2 样品中的硬玉以及掺夹的少量钠长石

Fig. 2 Jadeite and a few albite in the sample

a. —; b. +

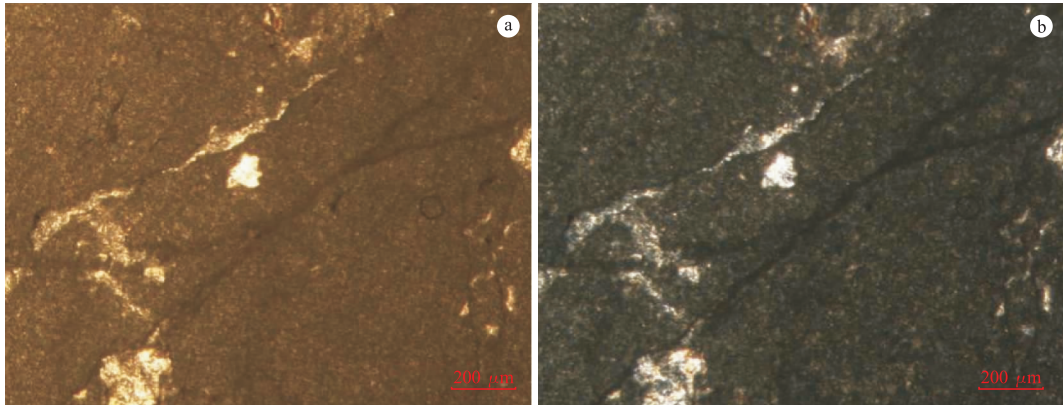


图 3 流动状的含重晶石石英脉

Fig. 3 Barite included fluxion quartz veins in the sample

a. —; b. +

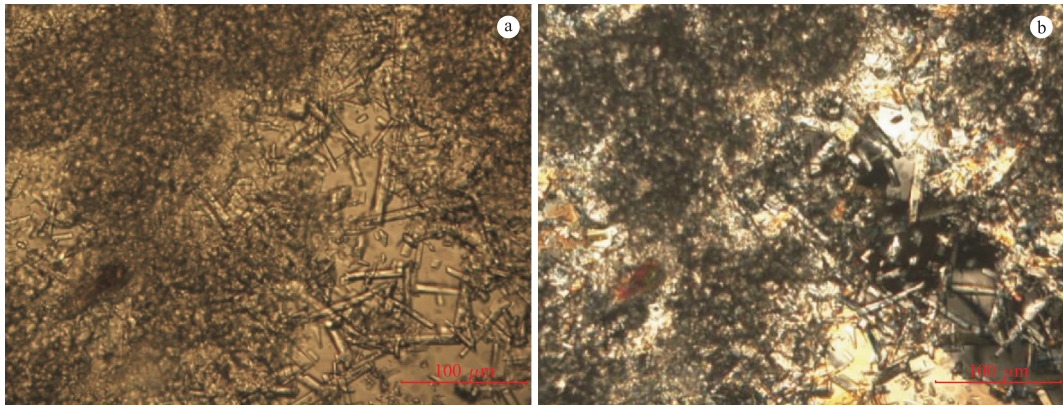


图 4 石英及其中柱状、板状、粒状重晶石包裹体

Fig. 4 Quartzs and the columnar, slaty, granular barite inclusions

a. —; b. +

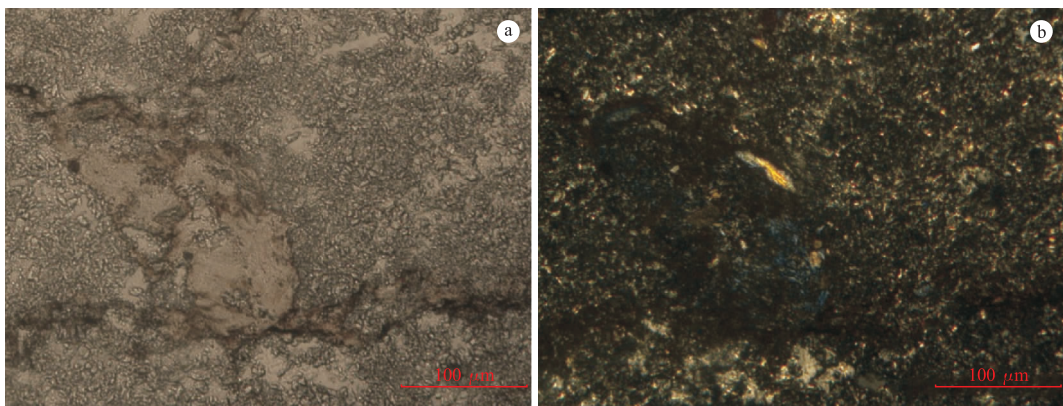


图 5 少量片状黑云母

Fig. 5 A few of schistic biotite

a. —; b. +

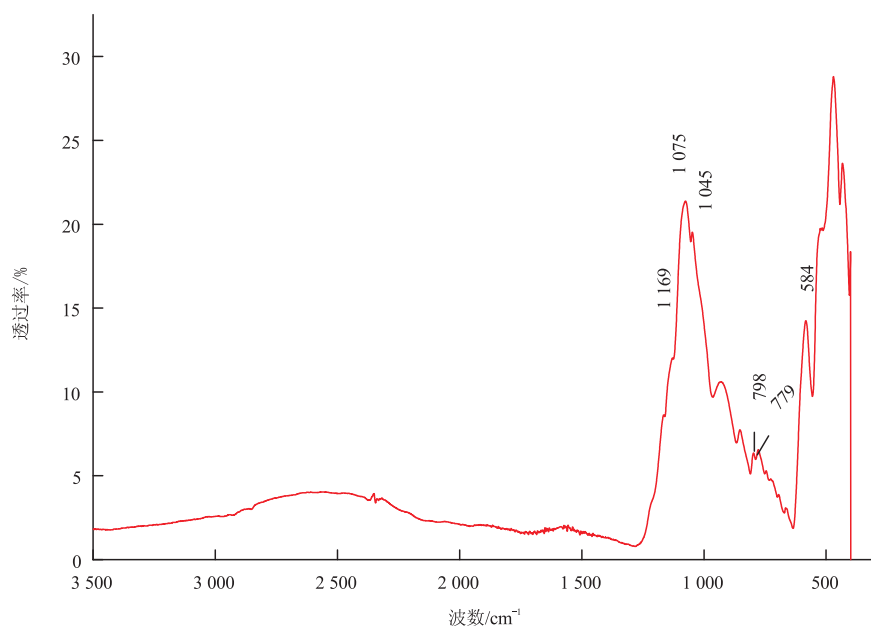


图 6 样品的红外光谱

Fig. 6 Infrared spectrum of the sample

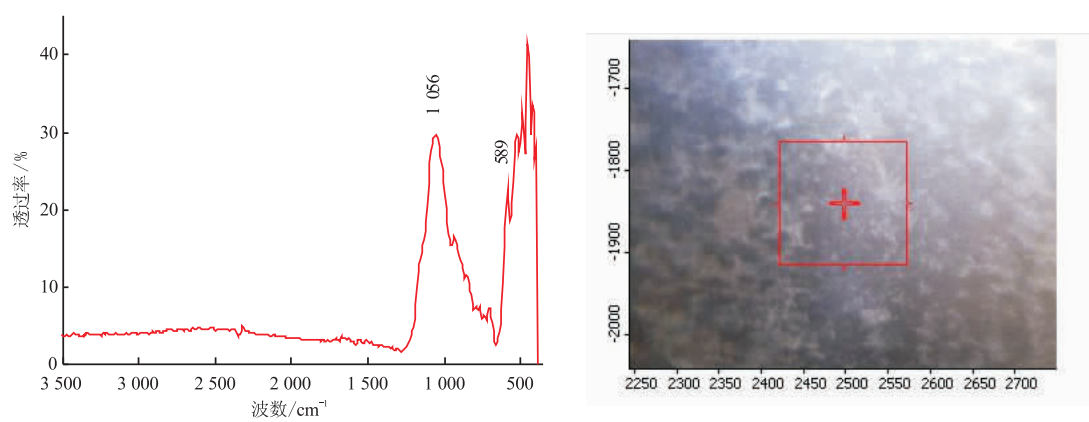


图 7 紫色部分显示硬玉的红外光谱

Fig. 7 The purple parts showing typical infrared spectrum of jadeite

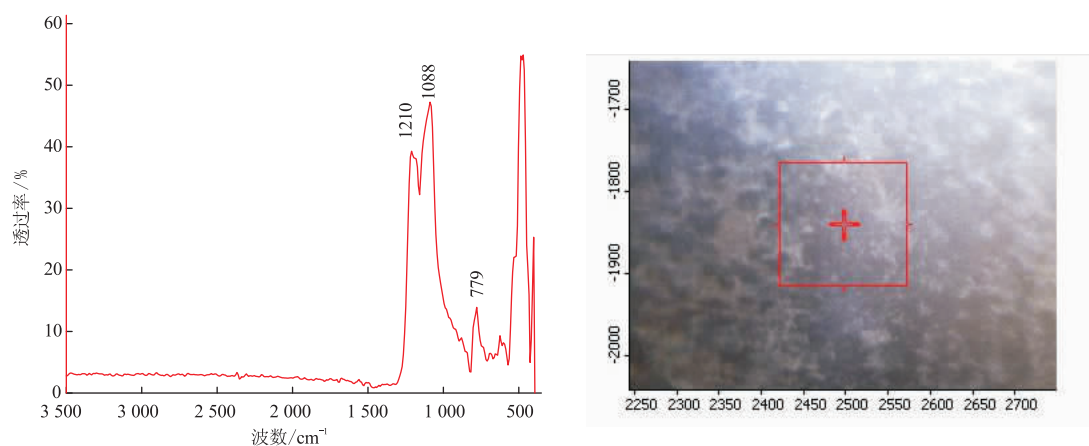


图 8 白色部分显示石英的红外光谱

Fig. 8 The white parts showing typical infrared spectrum of quartz

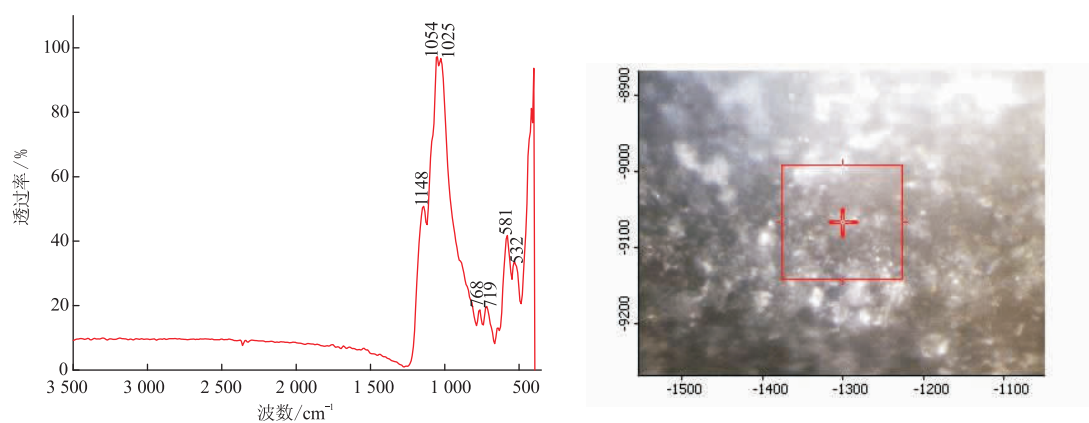


图 9 紫色硬玉中夹杂的细小白点显示长石的红外光谱

Fig. 9 The tiny white spots surrounded by purple jadeite showing infrared spectrum of albite

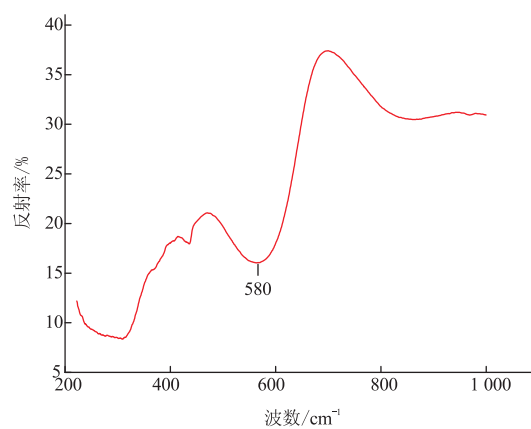


图 10 样品的紫外-可见吸收光谱

Fig. 10 UV-Vis spectrum of sample



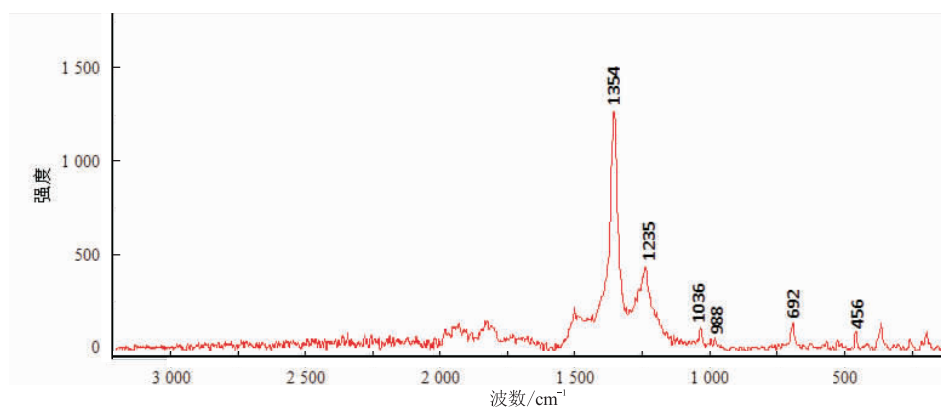


图 11 石英中包裹体的拉曼光谱

Fig. 11 Raman spectrum of inclusions in quartz

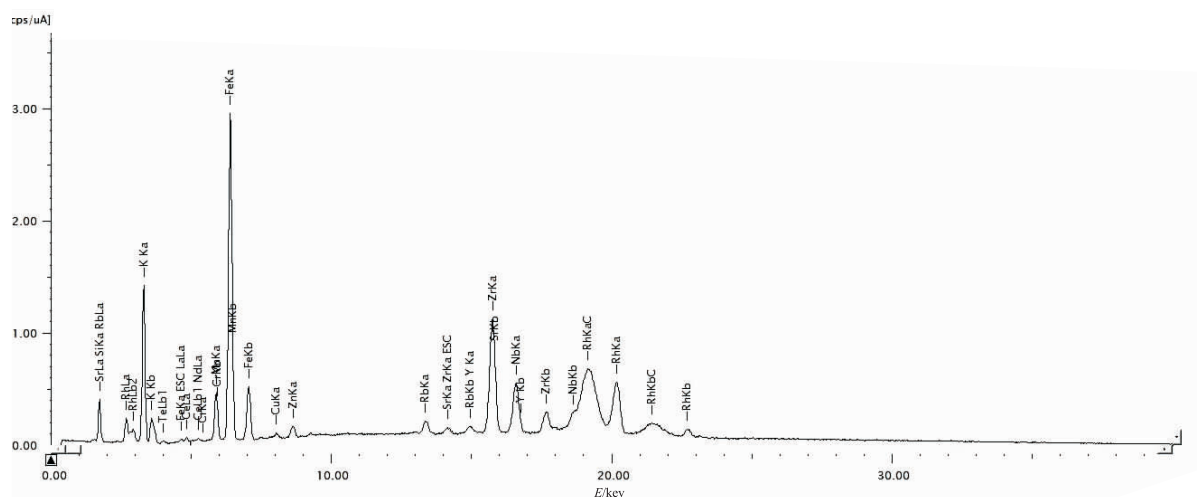


图 12 样品的能量色散型 X 荧光光谱

Fig. 12 Energy dispersive X-ray fluorescence spectrum of the sample

# 铝硼锆钙石 (Painite) 的宝石学特征测试分析

郭 杰<sup>1</sup>, 廖任庆<sup>1</sup>, 郑秋菊<sup>2</sup>

(1. 深圳技师学院珠宝学院, 广东 深圳 518116; 2. 深圳百泰投资控股集团有限公司  
检测中心, 广东 深圳 518083)

**摘 要:** 针对客户提供的 4 颗无法确定品名的样品, 进行全面宝石学特征的测试分析, 结果表明: 样品折射率超出折射仪测量范围, 强玻璃光泽, 二色性明显, 可见光区有典型吸收光谱, LW 紫外灯下惰性, SW 下为中~强度黄绿色荧光。放大可见明显刻面棱重影、裂隙、矿物及流体包体。密度为  $3.89 \pm 0.02 \text{ g/cm}^3$ , 摩氏硬度为 7~8, 贝壳状断口。红外光谱指纹区特征峰为 413、424、461、505、523、555、604、681、714、743、824、 $1\,306 \text{ cm}^{-1}$ , 与铝硼锆钙石一致, 官能团区泛频峰数量多, 较为复杂, 推测与水的吸收峰有关。785nm 激发光源下,  $1\,500 \text{ cm}^{-1}$  以下有较强荧光包,  $1\,590$ 、 $1\,625$ 、 $2\,252 \text{ cm}^{-1}$  三个位置较强的拉曼峰。在 532nm 激发光源下, 180、219、303、349、378、396、434、466、536、576、589、617、653、717、789、810、848、988、 $1\,323 \text{ cm}^{-1}$  与 RRUFF 谱库中的铝硼锆钙石一致。光致发光测试, 在 405 nm 激发光源下, 可见 786 nm 处发光光谱带并伴有 710 nm 的肩峰, 在 532 nm 激发光源下, 可见 796 nm 发光光谱带并伴有 710、703、694、611 nm 的肩峰, 具体成因机制尚待进一步研究。紫外可见测试, 在 400~650 nm 有一宽吸收带, 并伴有 385、423、550 nm 叠加峰, 推测与样品中含有微量 Ti、V、Fe 有关。EDS 能谱测试, 样品主量元素 Ca、Zr、Al、O 与铝硼锆钙石化学式一致, 但 B 元素未测定参与分析, 主量元素质量分数与理论值有一定偏差。综合分析判定, 该批样品为少见的铝硼锆钙石。

**关键词:** 铝硼锆钙石; 红外光谱; 拉曼光谱; EDS 能谱; 光致发光光谱; 谱学特征

## Gemological Characteristics of Painite

GUO Jie<sup>1</sup>, LIAO Renqing<sup>1</sup>, ZHEN Qiuju<sup>2</sup>

(1. Shenzhen Institute of Technology, Shenzhen 518116, China; 2. Testing Center,  
Shenzhen Batar Investment Holding Group Co., Ltd., Shenzhen 518083, China)

**Abstract:** The customer provided 4 samples that could not be accurately identified and named, this paper for the customer's identification needs, a comprehensive gemological characteristics of the test analysis, the test results are as follows. The refractive index of the samples is beyond the measuring range of the refractometer. The samples have strong glass luster and obvious dichroism. The samples have typical absorption spectrum in the visible light region. The samples are inert under LW ultraviolet lamp and moderate to strong yellow green fluorescence under SW. They can be enlarged to ob-

serve obvious faceted prism, cracks, minerals and fluid inclusions. The density of the samples is  $3.89 \pm 0.02 \text{ g/cm}^3$ , and the Mohs hardness of the samples is 7~8. The shell fracture can be observed by the samples. The characteristic peaks in the infrared fingerprint region of the samples are 413, 424, 461, 505, 523, 555, 604, 681, 714, 743, 824,  $1\,306 \text{ cm}^{-1}$ , which are consistent with Painite. The number of overtone frequency peaks in the functional group area is more complex, which is supposed to be related to water vibration. Under 785 nm excitation light source, the samples have strong fluorescence package below  $1\,500 \text{ cm}^{-1}$  and strong Raman peaks at  $1\,590$ ,  $1\,625 \text{ cm}^{-1}$  and  $2\,252 \text{ cm}^{-1}$ . Under 532 nm excitation light source, the test results showed that 180,219,303,349,378,396,434,466,536,576,589,617,653,717,789,810,848,988,  $1\,323 \text{ cm}^{-1}$  were consistent with Painite in RRUFF database. The results of photoluminescence test showed that under 405 nm excitation light source, 786 nm emission band with 710 nm shoulder peak was visible. Under 532 nm excitation light source, the test results were 796 nm emission band with 710, 703, 694, 611 nm shoulder peaks. The specific mechanism needs to be further studied. The results of UV visible test show that the samples have a wide absorption band in the range of 400—650 nm, accompanied by superposition peaks of 385, 423 nm and 550 nm, which may be related to the trace Ti, V and Fe in the samples. EDS results show that the main elements of the samples are Ca, Zr, Al and O, which are consistent with the chemical formula of painite. However, boron element was not determined to participate in the analysis, so the mass fraction of major elements in EDs test results deviated from the theoretical value. According to comprehensive analysis, the samples are painite, a rare gem variety.

**Key words:** painite; Infrared Spectrum; Raman Spectrum; EDS Energy Spectrum; Spectral Characteristics

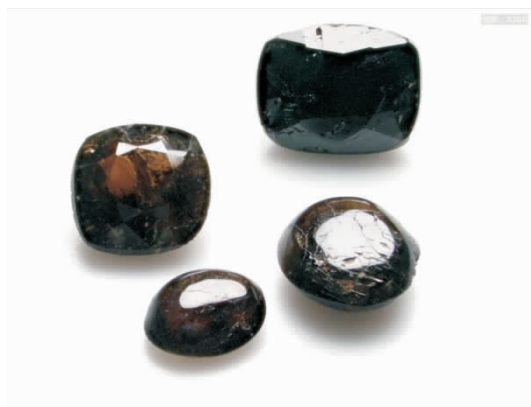


图1 铝硼锆钙石样品 20×  
(左上 CP1,右上 FP2,左下 FP1,右下 CP2)

Fig. 1 Appearance of painite magnification: 20×

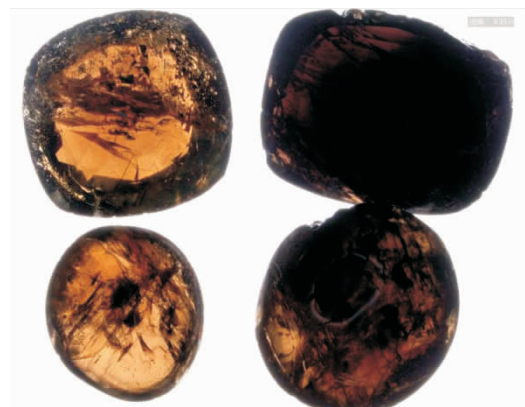


图2 铝硼锆钙石样品 30×  
(左上 CP1,右上 FP2,左下 FP1,右下 CP2)

Fig. 2 Appearance of painite magnification: 30×

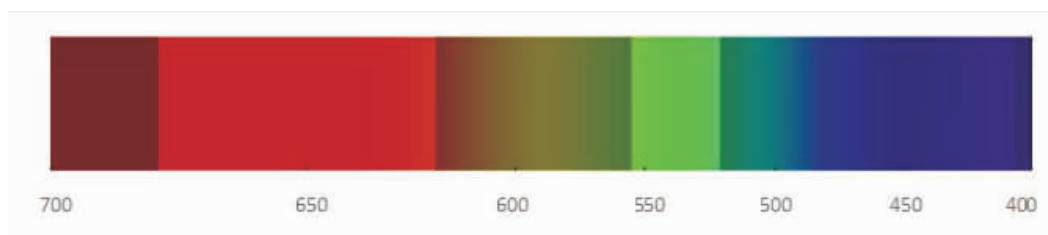


图 3 手持分光镜吸收光谱图(FP2)

Fig. 3 Absorption spectrogram of hand spectroscopy(FP2)

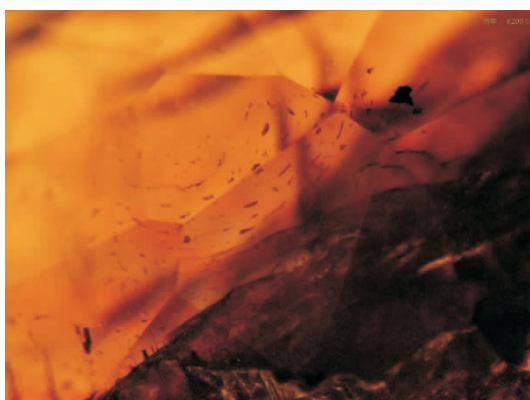


图 4 样品 CP1 中流体包裹体 200×

Fig. 4 Fluid Inclusions in sample CP1 200×

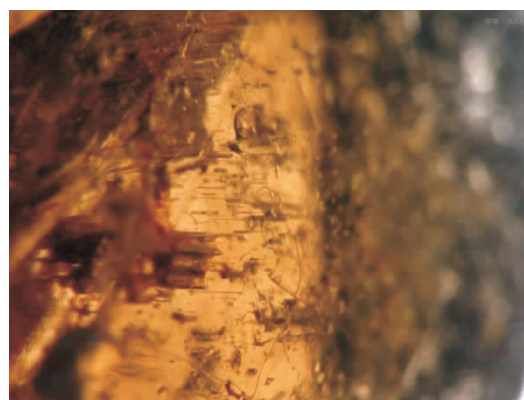


图 5 样品 CP1 中气液两相包裹体 200×

Fig. 5 Gas Liquid two phase inclusions in sample CP1 200×

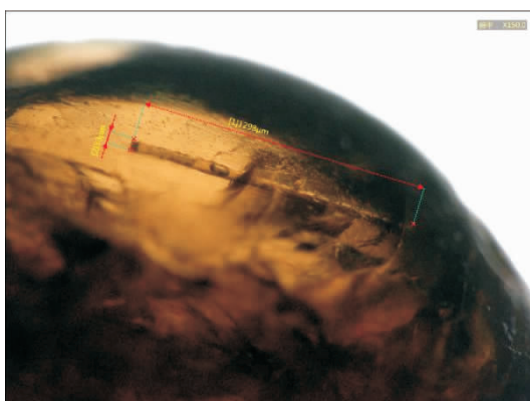


图 6 样品 FP1 中的气液两相包裹体 150×

Fig. 6 Gas-liquid two phase inclusions in sample FP1 150×

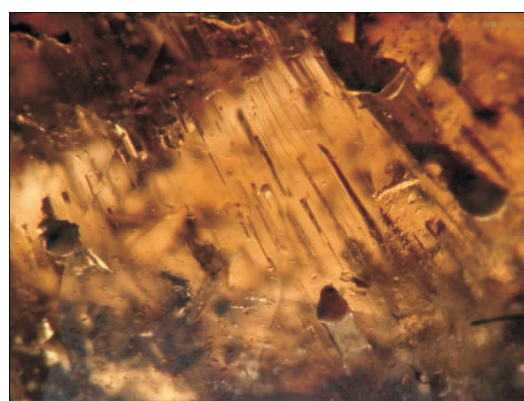


图 7 样品 FP1 中的定向管状晶体包裹体 200×

Fig. 7 Directional tubular crystal inclusions in sample CP1 200×



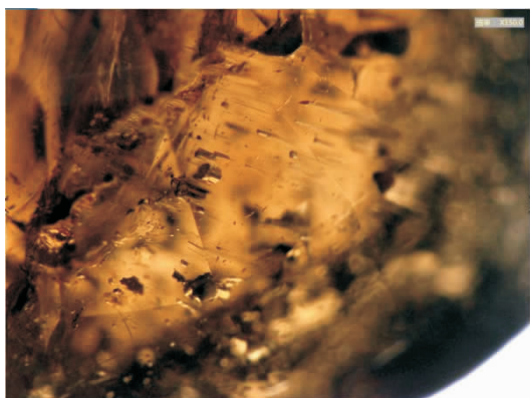


图 8 样品 FP1 中的定向管状晶体包裹体 150×  
Fig. 8 Directional tubular crystal inclusions in sample  
FP1 (Magnification: 150×)

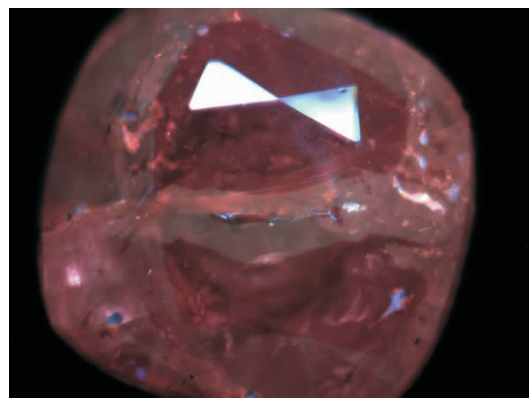


图 9 样品 CP1 在 DiamondView™ 下呈现的红色荧光  
Fig. 9 Red fluorescence of sample CP1 in DiamondView™

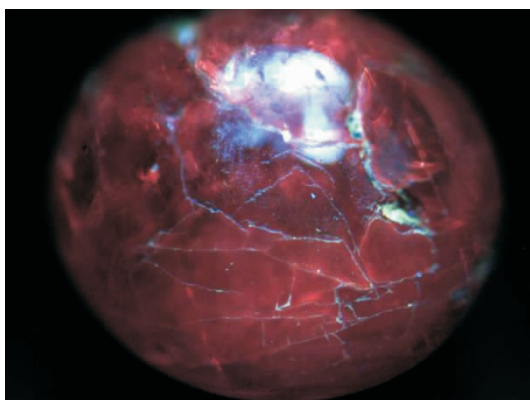


图 10 样品 CP2 在 DiamondView™ 下呈现的红色荧光  
Fig. 10 Red Fluorescence of sample CP2 in  
DiamondView™

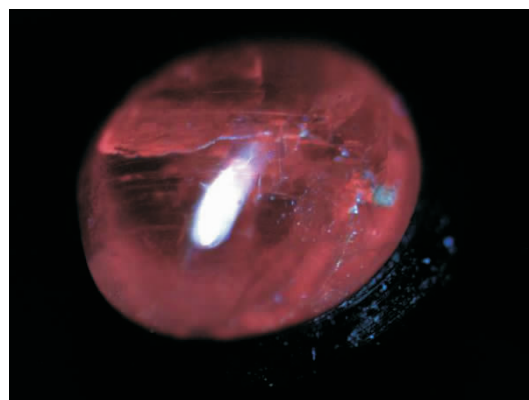


图 11 样品 FP1 在 DiamondView™ 下呈现的红色荧光  
Fig. 11 Red Fluorescence of sample FP1 in  
DiamondView™

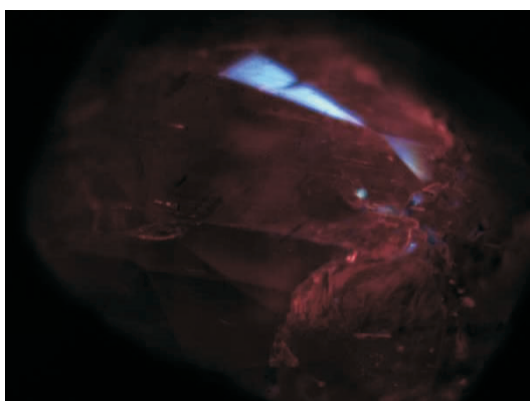


图 12 样品 FP2 在 DiamondView™ 下呈现的红色荧光  
Fig. 12 Red fluorescence of sample FP2 in DiamondView™



图 13 样品 FP2 的贝壳状断口 150×  
Fig. 13 Conchoidal fracture of sample FP2 150×

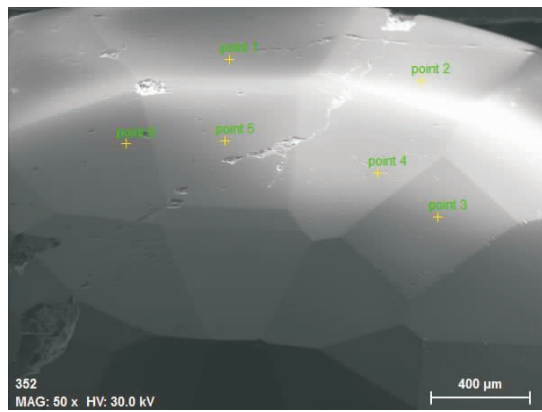


图 14 样品 CP1 的 EDS 选点位置图

Fig. 14 EDS point selection diagram of sample CP1

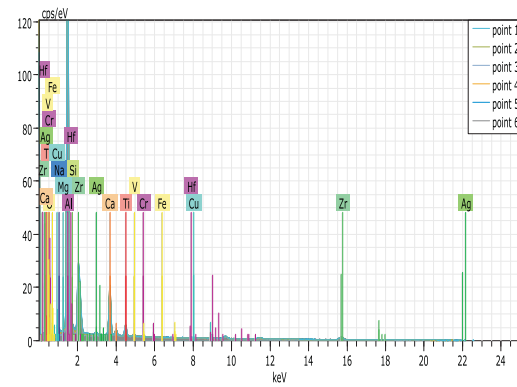


图 15 样品 CP1 的 EDS 全部选点测试图谱

Fig. 15 EDS spectrum of sample CP1

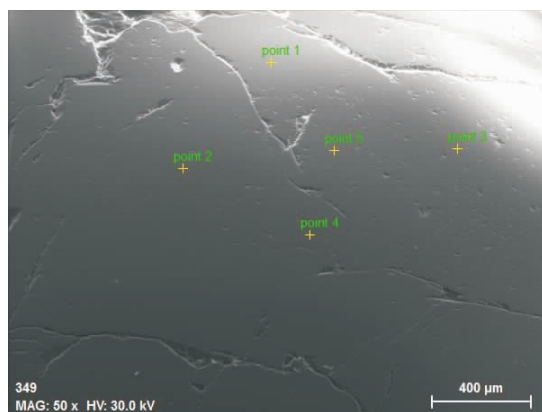


图 16 样品 CP2 的 EDS 选点位置图

Fig. 16 EDS point selection diagram of sample CP2

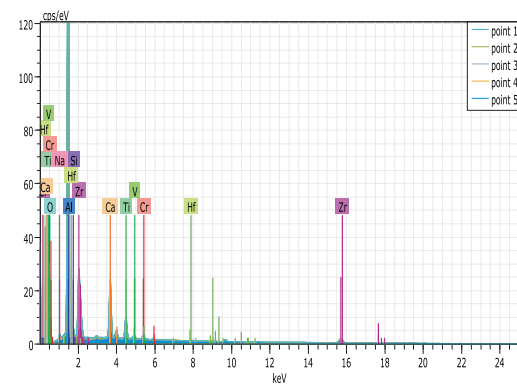


图 17 样品 CP2 的 EDS 全部选点测试图谱

Fig. 17 EDS spectrum of sample CP2

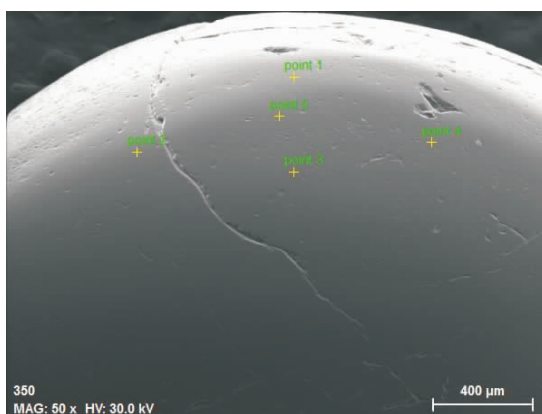


图 18 样品 FP1 的 EDS 选点位置图

Fig. 18 EDS point selection diagram of sample FP1

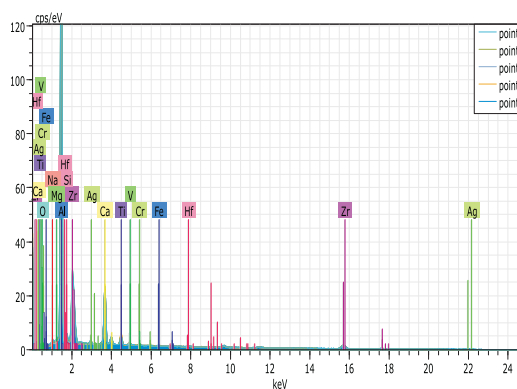


图 19 样品 FP1 的 EDS 全部选点测试图谱

Fig. 19 EDS spectrum of sample FP1

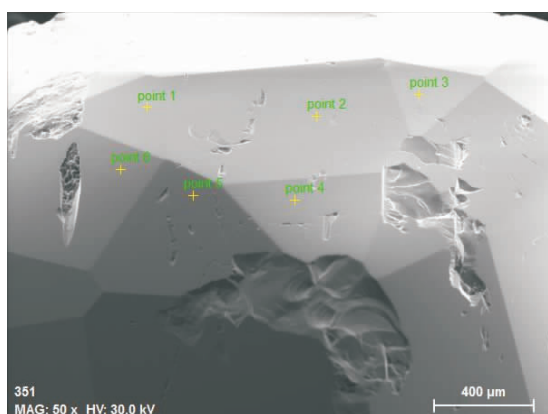


图 20 样品 FP2 的 EDS 选点位置图

Fig. 20 EDS point selection diagram of sample FP2

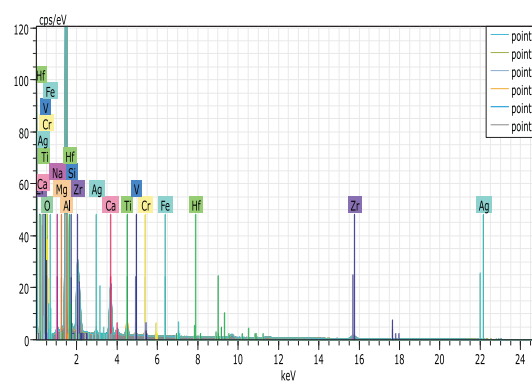


图 21 样品 FP2 的 EDS 全部选点测试图谱

Fig. 21 EDS spectrum of sample FP2

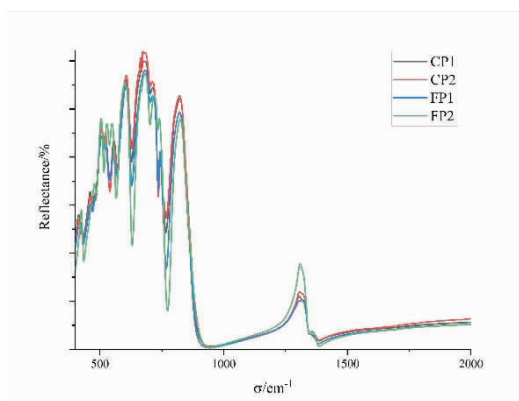


图 22 样品的漫反射红外图谱

Fig. 22 Diffuse light test results of samples CP1, CP2 and FP1 and FP2 under Fourier transform infrared spectrometer

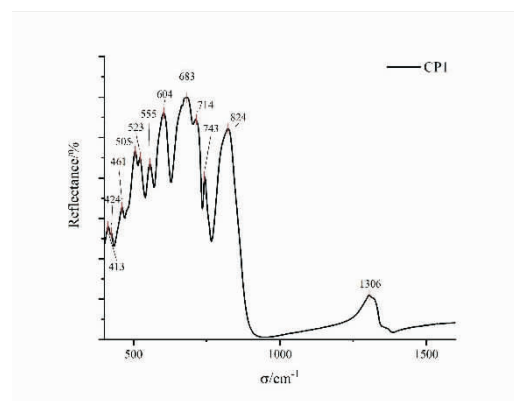


图 23 样品 CP1 的漫反射红外图谱

Fig. 23 Diffuse light test results of samples CP1 under Fourier transform infrared spectrometer

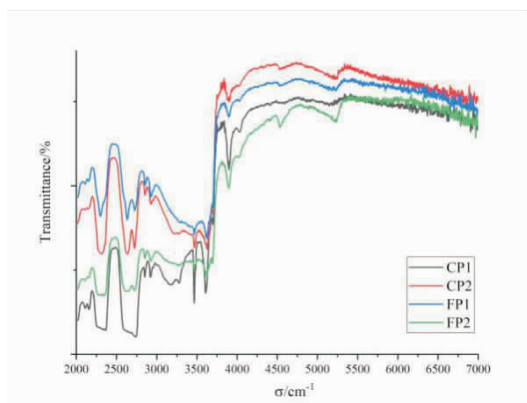


图 24 样品 CP1、CP2 和 FP1、FP2 红外透射图谱

Fig. 24 Transmission light test results of sample CP1, CP2 and FP1, FP2 under Fourier transform infrared spectrometer

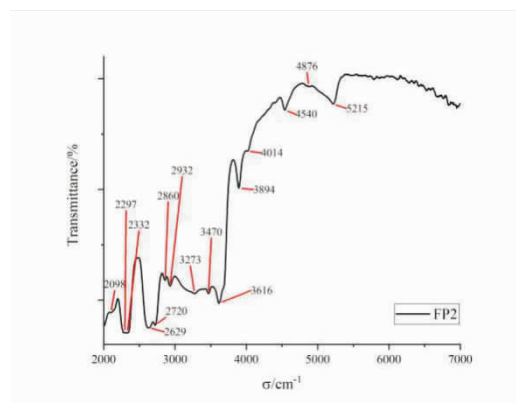


图 25 样品 FP2 红外透射图谱

Fig. 25 Transmission light test results of sample FP2 under Fourier transform infrared spectrometer

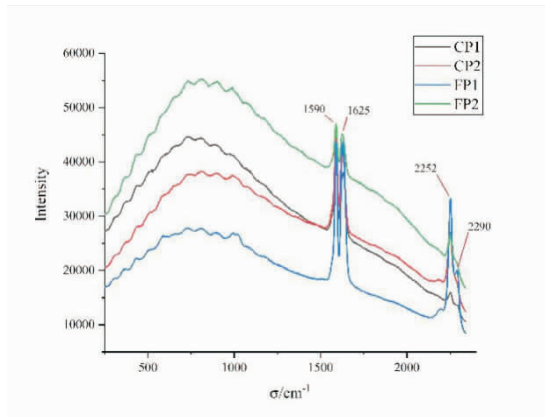


图 26 样品 CP1、CP2 和 FP1、FP2 在 785nm 光源下拉曼图谱(未经校准图谱)

Fig. 26 Sample CP1, CP2 and FP1, FP2 Raman spectra tested with 785nm wavelength laser light sources (original spectral test results not calibrated by baseline)

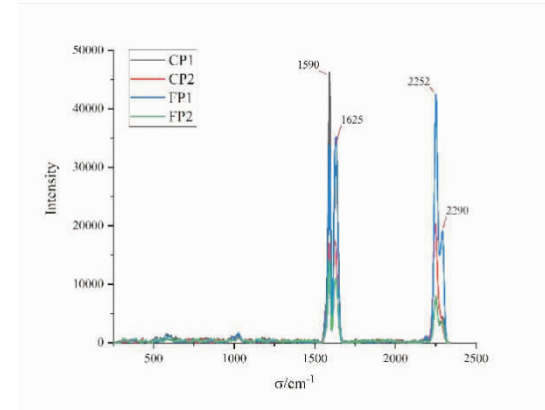


图 27 样品 CP1、CP2 和 FP1、FP2 在 785nm 光源下拉曼图谱(基线校准后图谱)

Fig. 27 Sample CP1, CP2 and FP1, FP2 Raman spectra tested with 785nm wavelength laser light sources (baseline-calibrated spectra)

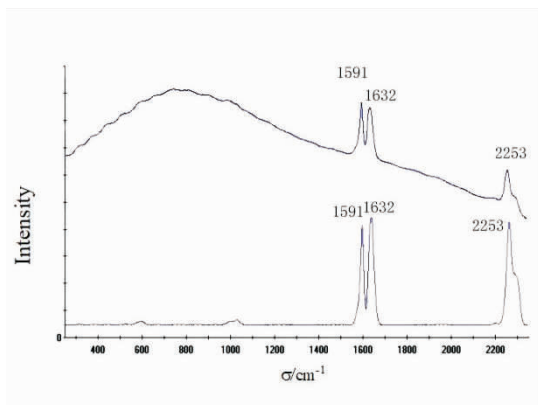


图 28 样品 CP2 在 785nm 光源下拉曼图谱(上图为原始图谱,下图为基线校准后图谱)

Fig. 28 Sample CP2 Raman spectrum tested By 785nm wavelength laser light source (above is the original spectral test results that have not been calibrated by the baseline, and the following image is the spectral test results that have been calibrated by the baseline)

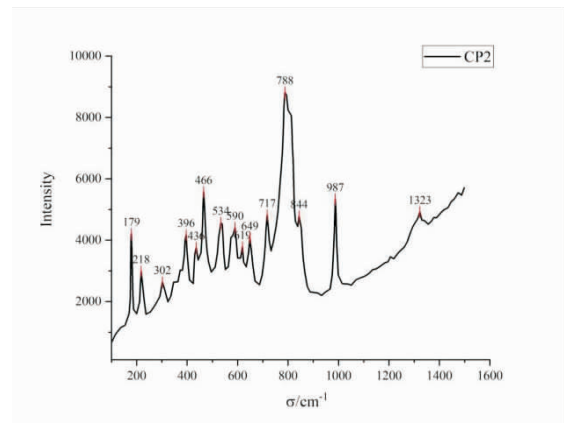


图 29 样品 CP2 在 532 nm 光源下拉曼图谱(未经基线校准)

Fig. 29 Sample CP2 Raman spectrum tested by 532nm wavelength laser light source (original map not calibrated by baseline)

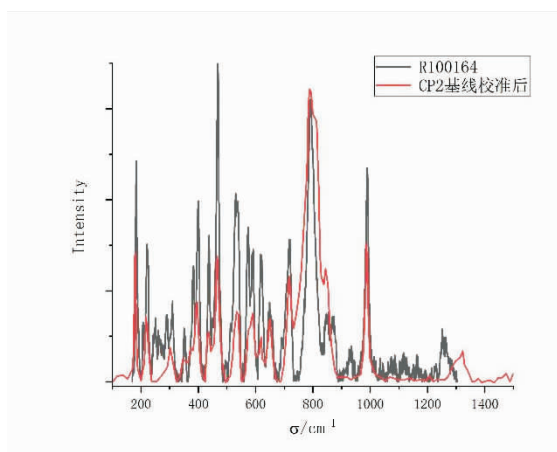


图 30 样品 CP2 在 532nm 光源下拉曼图谱(未经基线校准)和 RRUFF 数据库中 R100164 数据比较

Fig. 30 Comparison of Raman spectra of sample CP2 under 532 nm laser source (the spectral test results that have been calibrated by the baseline) and R100164 data in RRUFF database

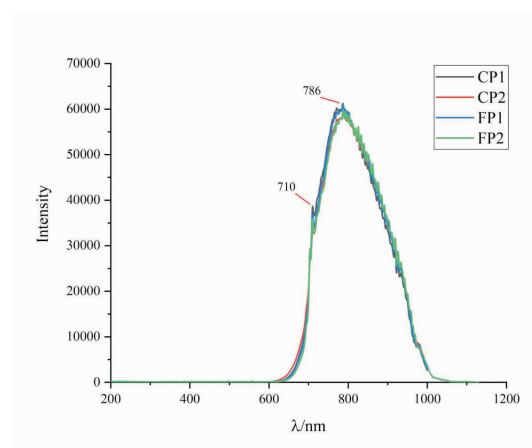


图 31 样品 CP1、CP2 和 FP1、FP2 在 405 nm 光源下光致发光图谱

Fig. 31 Photoluminescence spectra of samples CP1, CP2 and FP1, FP2 under 405 nm light source

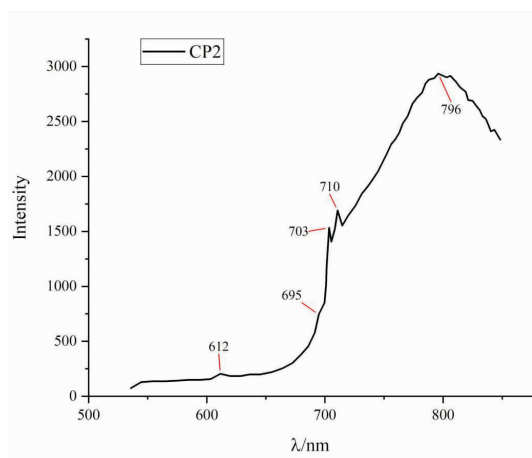


图 32 样品 CP2 532 nm 光源下光致发光图谱

Fig. 32 Photoluminescence spectra of samples CP2 under 532 nm light source

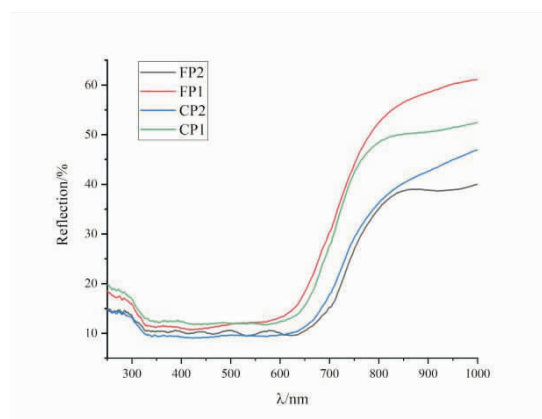


图 33 样品 CP1、CP2 和 FP1、FP2 紫外~可见光谱图 (250~1 000 nm, 测试条件 1)

Fig. 33 UV-Vis spectra of samples CP1, CP2 and FP1, FP2 (250~1 000 nm, test condition 1)

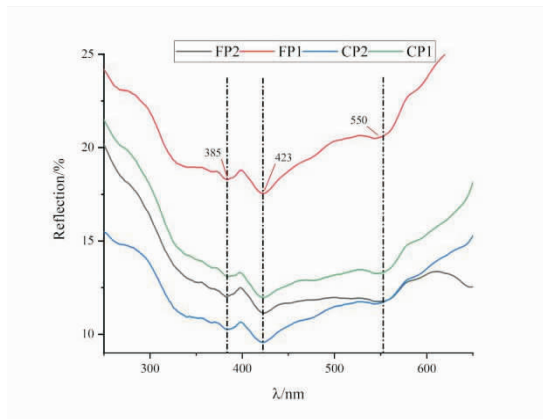


图 34 样品 CP1、CP2 和 FP1、FP2 紫外~可见光谱图  
(250~650 nm, 测试条件 2)

Fig. 34 UV-Vis spectra of samples CP1, CP2 and FP1, FP2(250~650 nm, test condition 2)

# 墨西哥红蓝料琥珀的宝石学特征

赵彤<sup>1</sup>, 苏小鹏<sup>1</sup>, 王雅玫<sup>1,2</sup>, 李妍<sup>1,3</sup>

(1. 中国地质大学珠宝学院, 湖北 武汉 430074; 2. 中国地质大学珠宝检测中心, 广东 广州 510145; 3. 湖北省珠宝工程技术研究中心, 湖北 武汉 430074)

**摘要:**近年来,墨西哥琥珀在市场上的占有量越来越大,但墨西哥琥珀中的红蓝料由于形成条件的限制却很稀少。红蓝料琥珀作为琥珀的品种之一,其表层通常具有一层褐红色的氧化皮层,内层琥珀在紫外光下具有蓝绿色荧光,因此红蓝料琥珀也被称为“红皮蓝珀”。由于蓝珀的蓝色荧光在黑色背景下才能完美展现,红皮即可充当黑色背景的作用,使得红蓝二色集于一块琥珀,增加了墨西哥琥珀的美感和价值。文章旨在通过宝石学常规测试、显微放大观察、傅里叶红外光谱和光致发光光谱等测试手段,对墨西哥红蓝料琥珀的宝石学特征和谱学特征进行研究,并与墨西哥黑皮料琥珀的特征进行对比研究。墨西哥红蓝料琥珀内部颜色包括黄色、金色、褐红色等。抛光面呈树脂光泽,红皮常呈微透明,内部为半透明—微透明;红蓝料琥珀的相对密度在 1.05 左右,折射率(点测)为 1.54。长波紫外线下内部显示较强的蓝色荧光,红皮部分荧光强度较弱,甚至无荧光。黑皮料琥珀与红蓝料琥珀的基础宝石学特征并无太大差异;墨西哥红蓝料琥珀内部包裹体繁杂。表层的红皮厚度不均,且黑色点状包裹相对聚集;红外光谱显示墨西哥红蓝料外层红皮部分的含氧基团  $C=O$  的  $1723\text{ cm}^{-1}$  及  $C-O$  的  $1250\sim 1030\text{ cm}^{-1}$  吸收峰均强于内层部分, $C=O$  与  $-CH_3$  的强度比约为  $4/5$ ,内部约为  $2/5\sim 1/2$ ,说明红蓝料琥珀的氧化主要发生表层,并且红蓝料琥珀内部氧化程度高于黑皮料内部。含氧基团  $C=O$  是使红蓝料琥珀呈现深邃红色的生色团;光致发光光谱结果表明红蓝料琥珀的外层红皮部分和内层的发光中心不同,外层以  $562, 506\text{ nm}$  为发光中心,内层大多以  $467, 472\text{ nm}$  为发光中心。光致发光光谱显示出随着氧化程度的增加,发光中心逐渐红移,且红皮部分荧光强度明显低于内层。黑皮料琥珀内部具  $489, 466\text{ nm}$  两个宽发光中心,其内部的荧光强度较红蓝料琥珀内部更高。 $C=O$  对墨西哥红蓝料琥珀红皮部分的荧光起到了淬灭作用。本文为墨西哥红蓝料琥珀的鉴别提供了依据,有助于墨西哥红蓝料琥珀与其他产地、其他品种琥珀的区分。

**关键词:**红蓝料琥珀;墨西哥;宝石学特征;谱学特征

## Gemmological Characteristic of Mexican Red Blue Amber

ZHAO Tong<sup>1</sup>, SU Xiaopeng<sup>1</sup>, WANG Yamei<sup>1,2</sup>, LI Yan<sup>1,3</sup>

(1. Gemmological Institute, China University of Geosciences, Wuhan 430074, China;

收稿日期:2020-09-30

基金项目:国家重点研发计划项目(2018YFF0215400);中国地质大学(武汉)珠宝检测技术创新中心开放基金 CIGTXM-02-202001

作者简介:赵彤(1997—),女,硕士研究生,主要从事琥珀宝石学的研究工作。

通讯作者:李妍(1987—),女,副教授,主要从事宝石学材料及先进制造材料加工方向研究。E-mail: yanli@cug.edu.cn

- 
2. *Gem Testing Center, China University of Geosciences, Guangzhou 510145, China;*  
 3. *Hubei Engineering Research Center of Jewelry, Wuhan 430074, China)*

**Abstract:** In recent years, Mexican amber has gained more and more market share, but the Mexican red blue amber is scarce due to the formation condition. The predecessors' research on Mexican red blue amber is basically blank. Red blue amber as one of the varieties of blue amber, its surface often has a maroon layer of oxide, the inner layer of amber with blue fluorescence under ultraviolet light. Since the blue fluorescence of the blue amber can only be perfectly displayed on a black background, the red skin can act as a black background, making the red and blue colours collected in a piece of amber, increasing the beauty and value of Mexican amber. This article aims to study the gemmological and spectroscopy characteristics of Mexican red blue amber and compare it with Mexican amber burying in the surrounding black rock by gemmological routine methods, microscopic observation, infrared spectroscopy and photoluminescence spectroscopy. Mexican red blue amber internal colours include yellow, gold, maroon, etc. The surface is resinous luster. The red skin of Mexican red and blue amber is often slightly transparent, and its interior is translucent to slightly transparent. The relative density of red blue amber was about 1.05 and the refractive index was 1.54. Under long-wave UV, the inside shows strong blue fluorescence, and the red skin has weak fluorescence intensity, even no fluorescence. The basic gemmological characteristics of Mexican amber burying in the surrounding black rock and red blue amber are not much different. Mexican red blue amber has complex inclusions. The thickness of red skin is uneven, and it is composed of black dots wrapped and flowing. FTIR spectra shows red part of Mexican red blue amber has absorption peak of C=O in  $1\,723\text{ cm}^{-1}$  and C—O in  $1\,250\text{--}1\,030\text{ cm}^{-1}$  which is stronger than the inner part. The absorption intensity ratio of the C=O peak and  $\text{—CH}_3$  peak of the red blue amber's red part is about  $4/5$ , and the inner part is about  $2/5\sim 1/2$ . Specification of red blue amber oxidation occurs mainly on the surface, and inner part of red blue amber's oxidation degree is higher than the inner part of amber burying in the surrounding black rock. C=O makes deep maroon of red blue amber material surface; The luminescence centers of red part are located at 562 nm and 506 nm, while the inner part mostly emits 467 nm and 472 nm center. As the degree of oxidation increases, the luminescent center gradually shifts to red spectra region, and the fluorescence intensity is significantly decreased. The inner part of amber burying in the surrounding black rock has two wide luminescence centers of 489 nm and 466 nm. The fluorescence intensity inside amber burying in the surrounding black rock is higher than that of red blue amber inside. C=O quenches the fluorescence of Mexican red blue amber. This paper provides reference for the identification of Mexican red blue amber, and helps to distinguish Mexican red blue amber from other producing areas and varieties of amber.

**Key words:** red blue amber; Mexico; gemmological characteristic; spectroscopy characteristic





图 1 墨西哥红蓝珀琥珀

Fig. 1 Mexican red blue amber

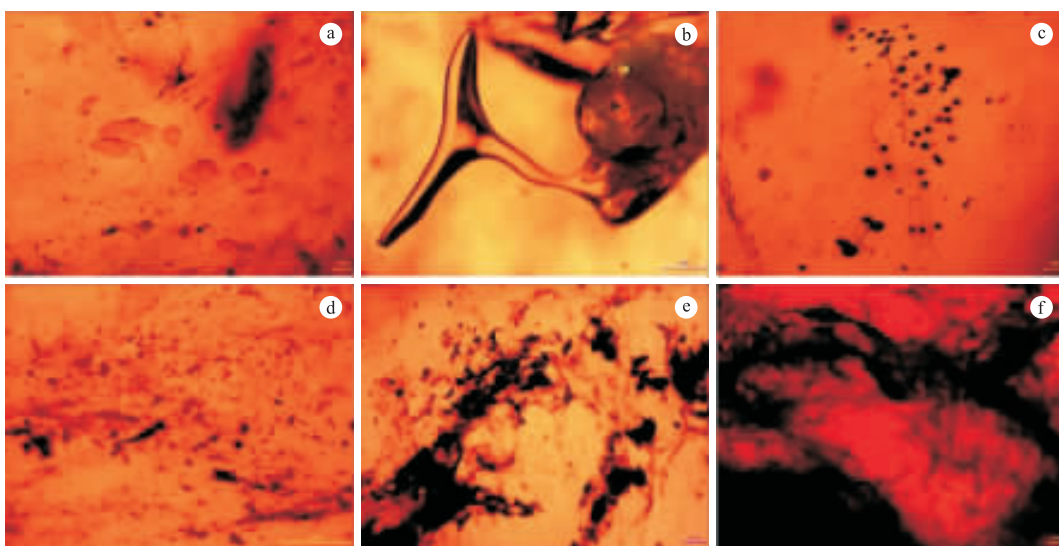


图 2 红蓝料琥珀样品中的包裹体:

(a) 盘状包裹体; (b) 气液两相包裹体; (c) 黑色圆点状包裹体; (d) 植物碎屑包裹体; (e) 黑色有机质包裹体; (f) 繁杂絮状暗色有机质包裹体

Fig. 2 Internal inclusions in red blue amber samples;

(a) disc-like inclusions; (b) gas-liquid two-phase inclusion; (c) black dot-like inclusions; (d) plant debris inclusions; (e) black organic inclusions; (f) miscellaneous flocculent dark organic inclusion

# 萤石的宝石学特征及荧光特性研究

穆宏赫<sup>1</sup>, 林静韬<sup>2</sup>, 李妍<sup>2,3</sup>, 卢勒<sup>2</sup>

(1. 中国科学院上海硅酸盐研究所, 上海 200000; 2. 中国地质大学珠宝学院, 湖北 武汉 430074;  
3. 湖北省珠宝工程技术研究中心, 湖北 武汉 430074)

**摘要:** 萤石, 又称为“氟石”, 主要化学成分为氟化钙( $\text{CaF}_2$ ), 因在紫外线、阴极射线照射下发出荧光而得名。国内外研究曾经探讨过变色萤石的变色效应和萤石的热释光性, 本研究主要针对性地研究萤石的荧光特性, 选取了 3 块不同颜色的天然萤石样品和 5 块合成氟化钙样品, 分别对萤石样品的宝石学特征进行测试和研究, 并采用电感耦合原子发射光谱仪、傅里叶红外光谱仪和激光拉曼光谱仪对萤石样品进行测试, 对萤石样品的各类光谱进行总结分析, 通过紫外-可见吸收光谱测试和荧光光谱测试, 对样品的荧光特性进行重点分析。前期实验测试显示, 萤石样品所含的杂质元素主要有铈(Ce)、镝(Dy)、镧(La)、锶(Sr)、钇(Y)。通过成分分析和紫外-可见吸收光谱确定荧光光谱的激发波长, 得到萤石样品的吸收光谱中显示  $\text{Ce}^{3+}$  的发射峰以及可能为  $\text{Tb}^{3+}$  的发射峰。通过高斯函数拟合最终得到萤石样品主要具有在 316 nm 和 336 nm 附近的发射峰以及在 427 nm 附近的谱峰, 萤石样品的紫外-可见吸收光谱和荧光光谱的对比验证了 316 nm 和 336 nm 附近的发射峰为主要的发光中心所产生的。

**关键词:** 萤石; 宝石学特征; 荧光特性; 稀土元素离子

## Gemmological and Fluorescence Characteristic of Fluorite

MU Honghe<sup>1</sup>, LIN Jingtao<sup>2</sup>, LI Yan<sup>2,3</sup>, Lu Ren<sup>2</sup>

(1. Shanghai Institute of Ceramics, Shanghai 200000, China; 2. Gemmological Institute, China University of Geosciences, Wuhan 430074, China; 3. Hubei Engineering Research Center of Jewelry, Wuhan 430074, China)

**Abstract:** Fluorite, also known as fluorspar, is made from calcium fluoride ( $\text{CaF}_2$ ), which is famous because of its fluorescence under ultraviolet and cathodic rays. Previous research has studied the discoloration effect and thermoluminescence property of fluorite, however, this research tries to specifically investigate the fluorescence characteristics of fluorite. This research chose three different colours of fluorite and five synthetic calcium fluoride crystal samples, the gemmological characteristics of fluorite samples were studied via inductively coupled atomic emission spectrometer, Fourier transform infrared spectrometer (FT-IR) and laser Raman spectrometer to summarize the spectral

收稿日期: 2020-09-30

作者简介: 穆宏赫(1997—), 女, 硕士研究生, 主要从事材料科学与工程方向研究。

通讯作者: 卢勒(1960—), 男, 教授, 主要从事宝石学方向研究。E-mail: renlu.cc@gmail.com

characteristics of fluorite samples, and to analyze the fluorescence characteristics of the samples through UV-Vis spectra and fluorescence spectra test. The results of previous experiments show that the impurity elements in fluorite samples mainly include cerium (Ce), dysprosium (Dy), lanthanum (La), strontium (Sr) and yttrium (Y). The excitation wavelength of the fluorescence spectra was determined by component analysis and UV-Visible absorption spectrum, and the emission peaks of  $Ce^{3+}$  and  $Tb^{3+}$  were obtained. The emission peak at 316 nm and 336 nm and the spectral peak at 427 nm were found by gaussian function fitting. The comparison of UV-Vis absorption spectrum and fluorescence spectrum of fluorite samples verified that the emission peak at 316 nm and 336 nm was caused by the main luminescence center.

**Key words:** fluorite; gemological characteristic; fluorescence characteristic; rare earth element ion

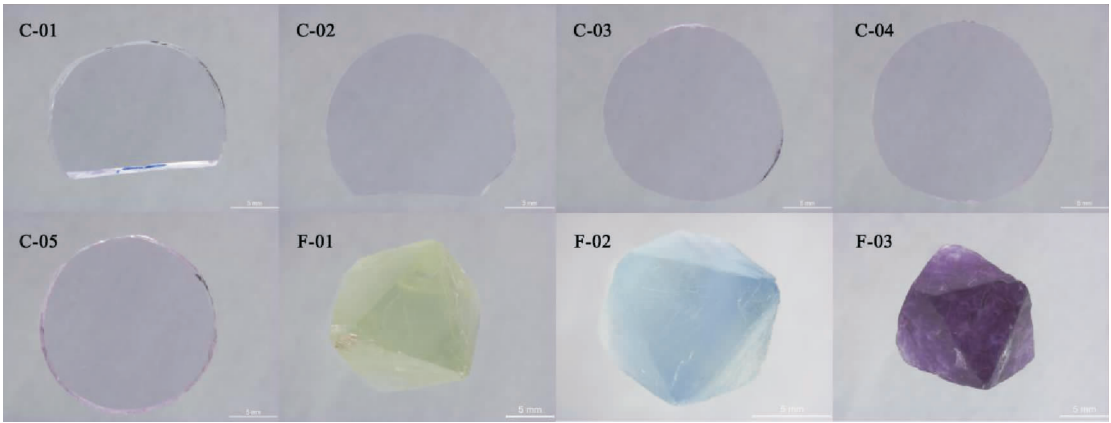


图 1 样品显微拍照  
Fig. 1 Micrographs of samples

表 1 样品的基本性质  
Table 1 Basic properties of samples

样品编号	颜色	折射率	相对密度	偏光镜
F-01	绿色	1.434	3.174	全暗,异常消光不明显
F-02	蓝色	1.433	3.172	有明暗变化的异常消光现象
F-03	紫色	1.434	3.177	有明暗变化的异常消光现象,异常消光明显

表 2 样品的荧光特征  
Table 2 Fluorescence characteristics of samples

样品编号	体色	荧光特征	
		LW	SW
C-01	绿色	强蓝紫色荧光	蓝色荧光
C-02	蓝色	强蓝色荧光	弱蓝色荧光
C-03	紫色	惰性	

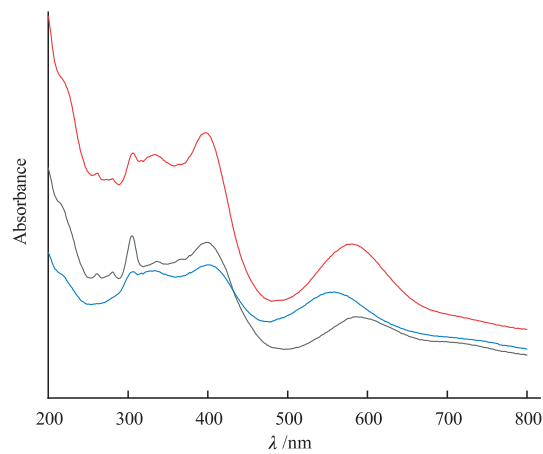


图3 紫外-可见吸收光谱

Fig. 3 UV-Vis spectra

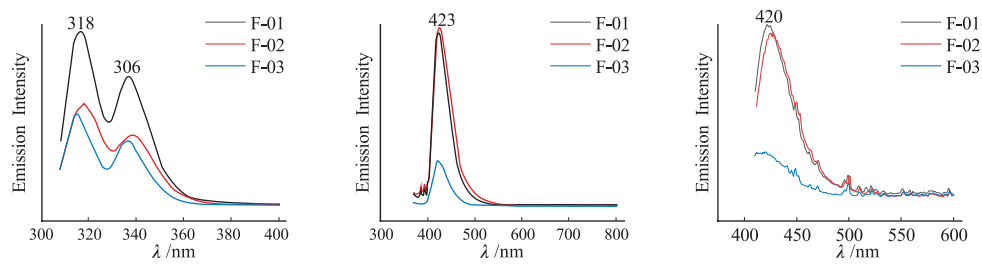


图4 萤石样品的荧光光谱(左为 305EX、中为 350EX、右为 400EX)

Fig. 4 Fluorescence spectra of fluorite samples (Left: 305EX, Middle: 350EX, Right: 400EX)

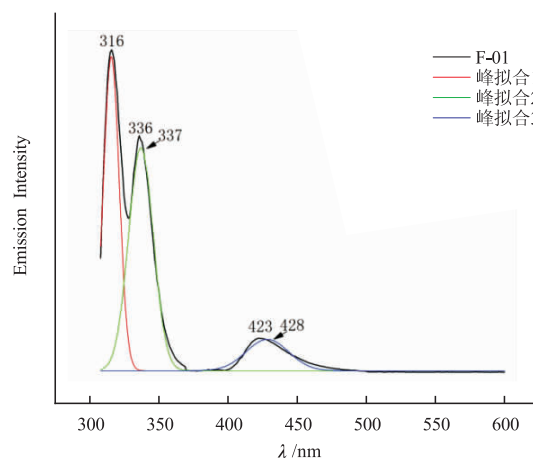


图5 萤石样品 F-01 荧光光谱的高斯拟合结果

Fig. 5 Gaussian fitting of fluorescence spectra of fluorite sample F-01

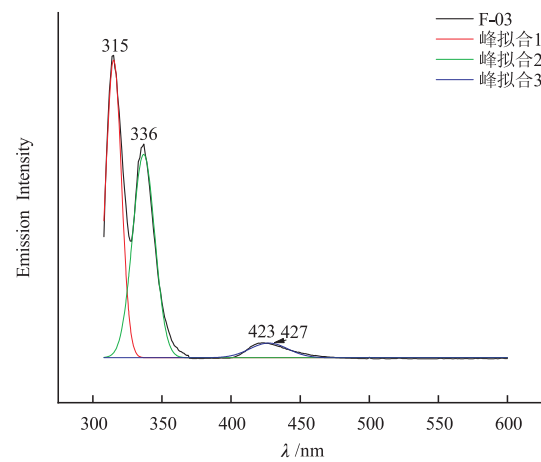


图 6 萤石样品 F-02 荧光光谱的高斯拟合结果  
Fig. 6 Gaussian fitting of fluorescence spectra of fluorite F-02

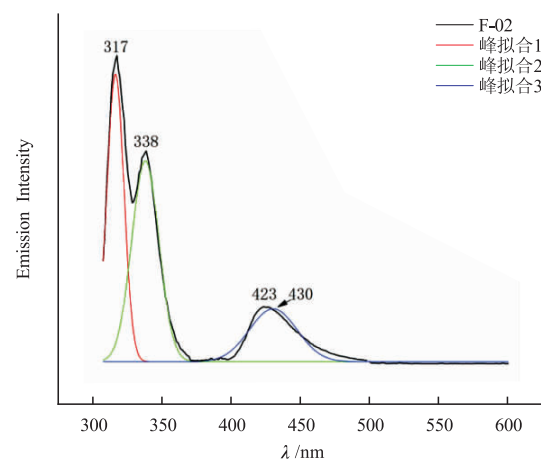


图 7 萤石样品 F-03 荧光光谱的高斯拟合结果  
Fig. 7 Gaussian fitting of fluorescence spectra of Fluorite F-03

# 寿山金狮峰田石石皮的谱学特征

郑金字<sup>1</sup>, 陈 涛<sup>1</sup>, 姚春茂<sup>1</sup>, 周征宇<sup>2,3</sup>, 李梦阳<sup>1</sup>, 徐 行<sup>1</sup>

(1. 中国地质大学珠宝学院, 湖北 武汉 430074; 2. 同济大学海洋与地球科学学院, 上海 200092; 3. 同济大学宝石及材料工艺实验室, 上海 200092)

**摘 要:**田黄作为“印石之帝”是图章石市场中最为重要的一个品种,随着资源不断地枯竭,与田黄成因相近的掘性田石品种——金狮峰田石逐渐受到关注。金狮峰田石产自福建寿山乡的金狮公山矿脉,具有黑色石皮,可见“沙星”;石肉颜色丰富,多见黄色、红色和白色。采用红外光谱仪和拉曼光谱仪研究分析其谱学特征。利用红外光谱对样品进行测试,红外反射法测试结果呈现典型高岭石族矿物特征峰,高频区可见地开石特征;为了进一步分析其矿物类型,使用溴化钾粉末压片透射法对样品进行测试,图谱表征主要组成矿物为无序地开石;石皮的官能团区可见大量包络峰,指示其矿物组成较为复杂,选用曲线拟合的图谱分析方法对高频区域进行分峰拟合,拟合结果显示除地开石以外,还具有较弱的高岭石和珍珠陶石的特征吸收峰位。对石皮进行拉曼光谱测试,图谱可见黄铁矿的特征拉曼位移,还具有无定形碳(Amorphous Carbon)的弥散状拉曼峰。黄铁矿的存在导致外皮呈现“沙星”,无定形碳导致石皮的黑色,长期的风化、流水搬运、微生物以及土壤掩埋等次生作用导致石皮的矿物成分较基体更为复杂。综上所述,金狮峰田石主要由无序地开石组成,含少量高岭石和珍珠陶石。无定形碳的产生可能与生物有关,可能存在极微量的叶蜡石。

**关键词:**田黄;金狮峰;石皮;分峰拟合;红外光谱;拉曼光谱

## Spectroscopic Characteristic of Weathering Skin of Seal Stone from Jinshifeng Field from Shoushan

ZHENG Jinyu<sup>1</sup>, CHEN Tao<sup>1</sup>, YAO Chunmao<sup>1</sup>, ZHOU Zhengyu<sup>2,3</sup>,  
LI Mengyang<sup>1</sup>, XU Xing<sup>1</sup>

(1. *Gemmological Institute, China University of Geosciences, Wuhan, 430074, China;*  
2. *Ocean and Earth Science School, Tongji University, Shanghai 200092, China;*  
3. *Laboratory of Gem and Technological Materials, Tongji University, Shanghai 200092, China*)

**Abstract:** As the “empire of the seal stone”, Tianhuang stone is a significant species in the seal stone. Stone from Jinshifeng, which is a variety of excavated stone formed simi-

收稿日期:2020-09-30

作者简介:郑金字(1996—),男,硕士研究生,主要从事宝石学和谱学研究。

通讯作者:陈涛(1979—),女。教授,主要从事粘土矿物学和宝石学的研究工作。E-mail:summerjewelry@163.com

lar with Tianhuang stone, is drawing consumer's eyes. Seal stone from Jinshifeng field originates from the lode of Jinshigong mountain located in Shoushan county, Fujian Province. The appearance characteristics of the stone are black weathering skin and flash points on the surface. The inside matrix is colourful that rich in yellow, red and white. Data was collected using two high spectral resolution Fourier transform infrared spectrometer and Raman spectrometer. The samples were tested by FTIR and the results of specular reflection method were shown that the characteristic absorption peaks of kaolinite group minerals, and the high frequency region had the characteristics of dickite. For the purpose of analyzing minerals, transmission method using KBr method was necessary. Disordered dickite was founded in the spectra and envelope peaks appeared in functional group region indicated that it is made of more minerals. The solution was then assayed for identifying minerals using the curve fitting method. The results shown weak peaks of kaolinite and nacrite besides dickite. Using Raman spectrometer, we were able to find sharp Raman shift of pyrite and dispersion envelope peaks of amorphous carbon (a-C) peaks. The existence of pyrite and a-C lead to the phenomenon of flash points and black weathering skin respectively. Secondary actions such as weathering, running water transported, microbial action and soil burial etc. made the minerals component of the weathering skin more complex. The investigation of spectroscopic characteristics of seal stone from Jinshifeng field has shown that it is made of disordered dickite and contains a small quantity of kaolinite and nacrite. There is a possibility that the formation of a-C is relative to biological action. We speculated that the pyrophyllite may exist in weathering skin according to the spectra of FTIR.

**Key words:** Tianhuang; Jinshifeng; weathering skin; curve fitting; FTIR; Raman spectrum



图1 金狮峰田石样品

Fig. 1 Seal stone sample from Jinshifeng field



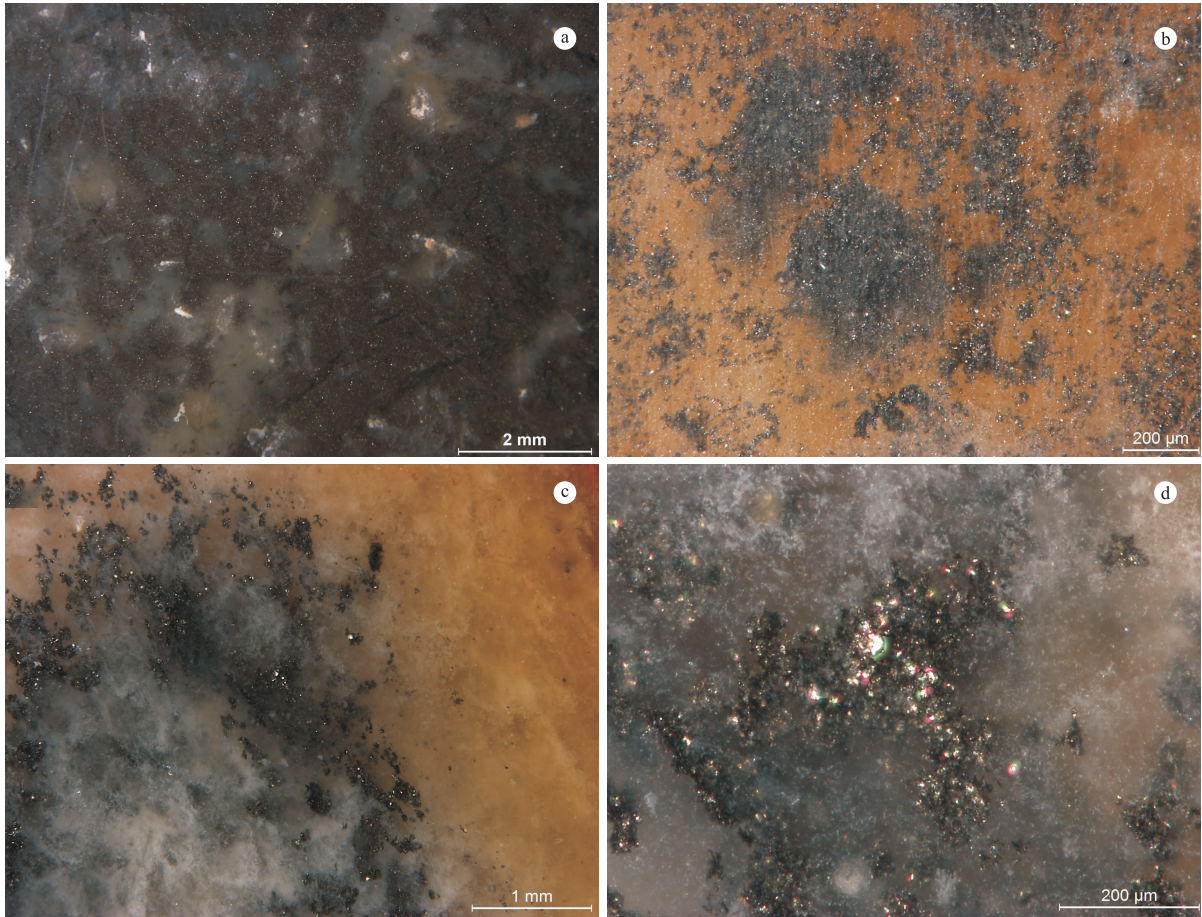


图 2 金狮峰田石的石皮特征图

Fig. 2 Characteristics of weathering skin of seal stone from Jinshifeng field

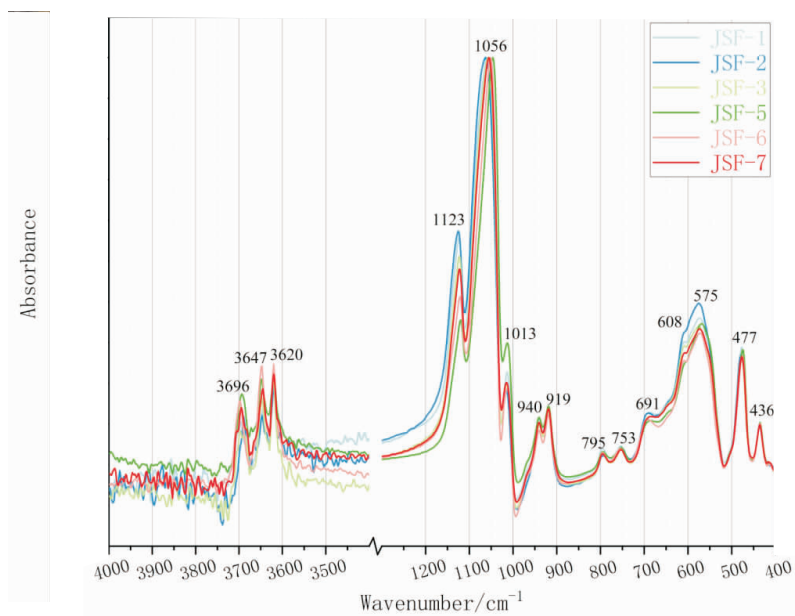


图3 金狮峰田石的红外反射光谱

Fig. 3 FTIR reflectance spectra of seal stone from Jinshifeng field

(图谱经 K-K 转换)

(The spectra are processed by Kramers—Kronig transformation)

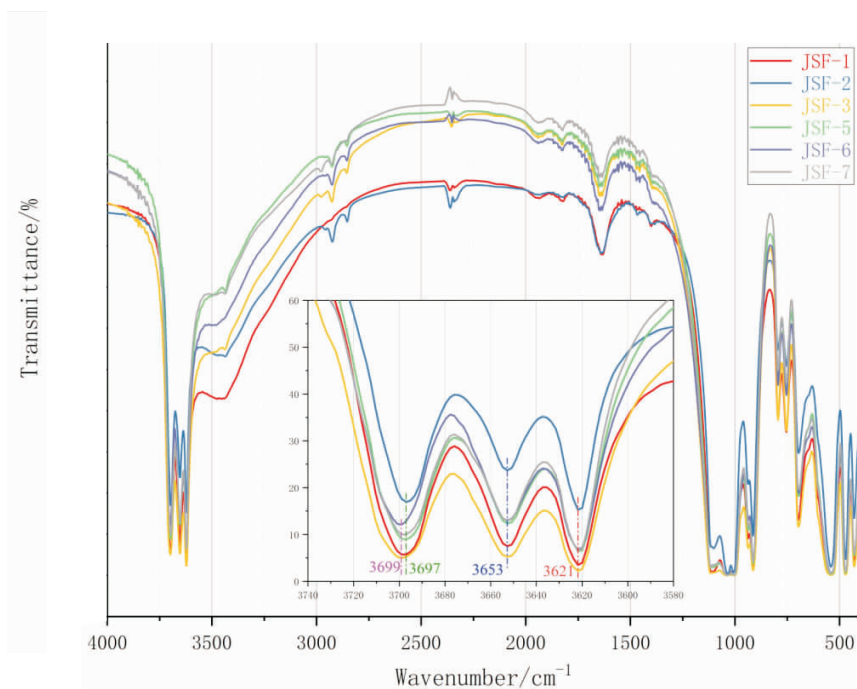


图4 金狮峰田石的红外透射光谱

Fig. 4 FTIR transmittance spectra of seal stone from Jinshifeng field

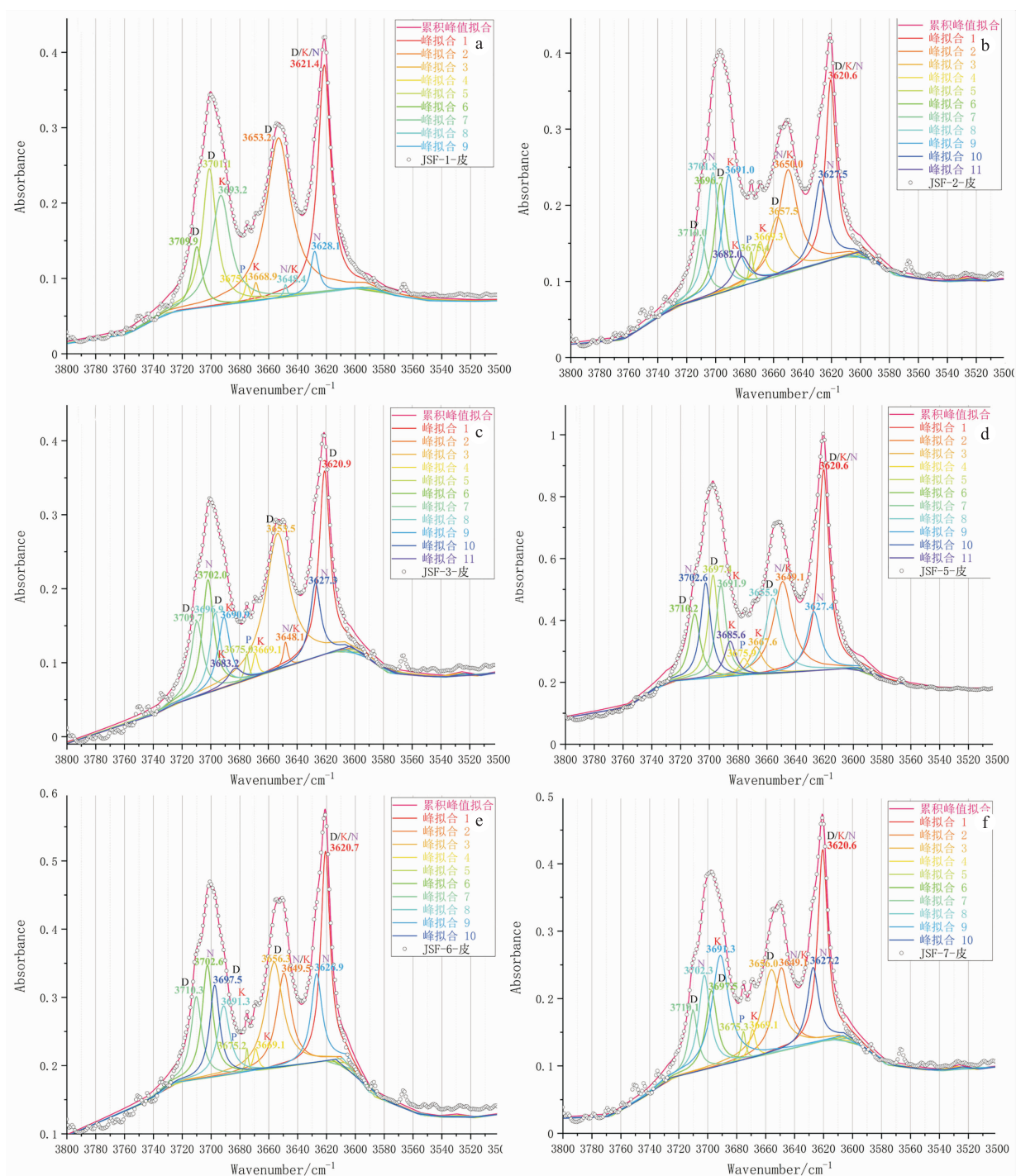


图 5 金狮峰田石石皮红外光谱高频区的分峰拟合

Fig. 5 The curve fitting of FTIR high frequency region of weathering skin of seal stone from Jinshifeng field

(D:地开石;K:高岭石;N:珍珠陶石;P:叶蜡石)

(D: dickite; K: kaolinite; N: nacrite; P: pyrophyllite)

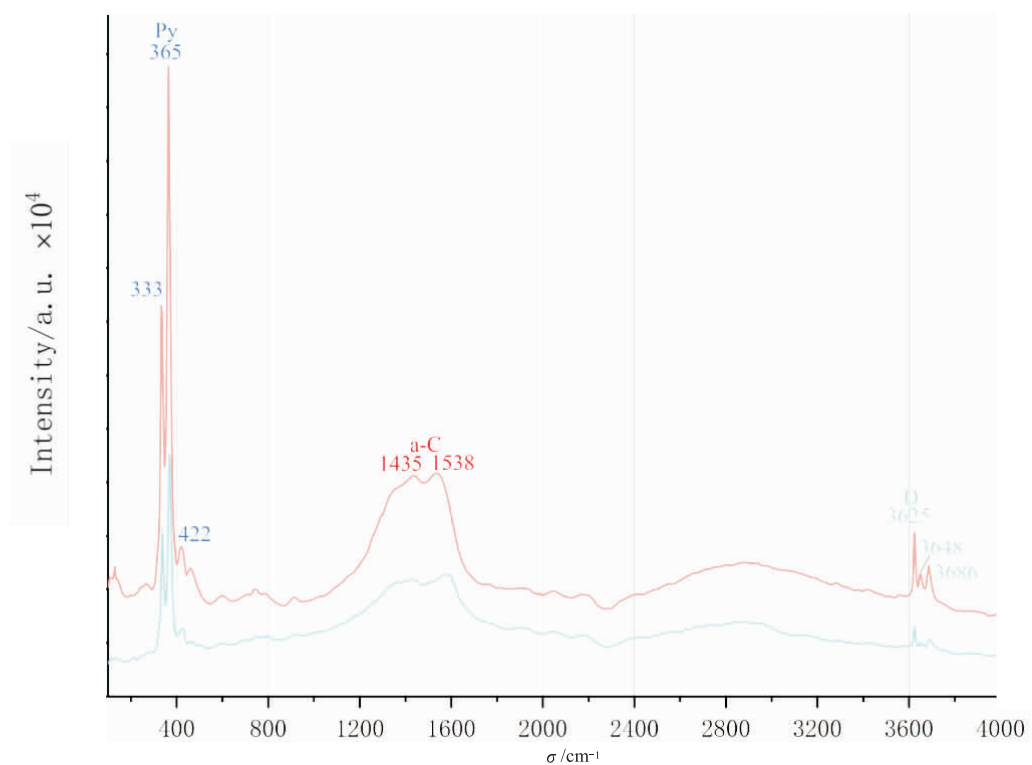


图 6 金狮峰田石黑色石皮的拉曼图谱

Fig. 6 Raman spectra of black weathering skin of seal stone from Jinshifeng field

(Py: 黄铁矿; a-C: 无定形碳; D: 地开石)

(Py: Pyrite; a-C: amorphous carbon; D: dickite)

# 浙江省遂昌县好川墓地绿松石料珠的 宝石学特征及工艺评价

姜 炎, 杨明星

(中国地质大学珠宝学院, 湖北 武汉 430074)

**摘 要:**浙江省遂昌县好川墓地是浙西南地区一处较完整的新石器时代遗址, 时代为良渚文化晚期至夏末商初, 是浙江省继河姆渡文化、马家浜文化、良渚文化之后确立的又一支考古学文化, 填补了浙西南地区无史前文明的空白。好川墓地入选 1997 年全国十大考古发现, 2013 年被国务院核定为第七批全国重点文物保护单位。在好川墓地的出土随葬品中, 有五件绿松石料珠较为特殊, 遂昌本地及周边并无绿松石出土, 五件料珠的发现证明当时的好川先民与矿源地或相关文化区曾进行过实际的物质交流。五件料珠为国家三级文物, 经浙江省文物局准予行政许可(浙文物许准字[2019]第 6 号)批准, 由中国地质大学(武汉)珠宝学院承担 5 件出土绿松石的成分鉴定和研究工作。

此次研究的 5 件绿松石料珠来源于好川墓地 M52 号墓, 均为鼓形饰珠, 中有对钻小孔, 发掘时在朱红色漆痕旁呈排状分布, 可能是容器口沿部位的镶嵌或漆类物质粘附的装饰物。作为珍贵的国家文物, 具有不可复制性和唯一性, 必须采取无损鉴定方法。故对于本次的研究样品的测试采取了宝石学的常规测试法和大型仪器无损鉴定法。主要通过常规宝石学测试、超景深显微镜、红外光谱以及 X 射线荧光光谱对料珠进行鉴定, 从而确定料珠的成分、抛磨工艺, 对玉料可能来源及当时好川地区先民的玉料加工水平进行研究。红外光谱采用反射法测试, 可见 5 件样品均有绿松石特征峰, 证明 5 件料珠基底均为较纯净的绿松石。XRF 数据中显示微量元素钡的含量较高, 与湖北十堰及周边地区出产绿松石的特征较为相似, 可作为判断 5 件绿松石料珠玉料来源的一个可能证据, 为接下来进一步玉料来源问题的研究奠定基础。通过显微照相相对 5 件绿松石料珠进行观察, 能够对当时先民的玉石加工工艺水平进行评价。5 颗样品表面均有若干不同程度的蚀坑, 侵蚀程度较浅, 证明绿松石本身致密程度较佳, 且土中埋藏条件较好; 5 件样品均可见定向的抛磨痕迹, 和一定数量的抛磨小面, 并没有完全细磨平整, 留下粗磨面, 证明当时的好川文化先民已经具有加工打磨长宽不大于 1 厘米料珠的能力; 加工珠形的方式是将不规则玉料原料分多个小面打磨, 直至成为一个桶珠形状, 但可能尚未具备弧面打磨及抛光的能力; 钻孔形状较规整, 近圆形, 有抛磨痕迹, 指出好川墓地当时已具备一定程度的玉料加工能力。

**关键词:**好川墓地; 好川文化; 料珠; 绿松石; 加工

收稿日期: 2020-09-30

基金项目: 国家社科基金“基于产源视角下浙江安吉龙山 107 号墓(八亩墩)出土绿松石研究”(20BKG30)项目

作者简介: 姜炎(1996 —), 女, 硕士研究生, 主要从事绿松石文化研究。

通讯作者: 杨明星(1966 —), 男, 教授, 主要从事宝石学、宝石检测和玉文化方面的教学与研究工作。E-mail: yangm@cug.edu.cn



## Jade Characteristic and Technological Evaluation of Turquoise Material Beads of M52 Tomb in Haochuan Cemetery, Suichang County, Zhejiang Province

JIANG Yan, YANG Mingxing

*(Gemmological Institute, China University of Geosciences, Wuhan 430074, China)*

**Abstract:** The Haochuan Cemetery in Suichang County, Zhejiang Province is a relatively complete Neolithic site in southwestern Zhejiang. The period is from the late Liangzhu Culture to the late summer and early Shang Dynasty, after the Hemudu Culture, Majiabang Culture, and Liangzhu Culture in Zhejiang Province. The discovery of this archaeological culture fills the void of no prehistoric civilization in southwestern Zhejiang. The Haochuan Cemetery was selected as one of the top ten archaeological discoveries in the country in 1997 and was approved by the State Council as the seventh batch of national key cultural relics protection units in 2013. Among the burial objects unearthed in the Haochuan Cemetery, there are five turquoise beads that are quite special. There is no turquoise unearthed in and around Suichang. The discovery of the five beads proves the communication between the ancestors of Haochuan and the mineral origin or related culture at that time. The district has conducted actual material exchanges. The five pieces of material beads are national third-level cultural relics, which were approved by the Zhejiang Provincial Cultural Relics Bureau (Zhejiang Cultural Relics License [2019] No. 6), and the identification of components of the five unearthed turquoises were undertaken by the Gemmological Institute of China University of Geosciences (Wuhan).

The five turquoise beads in this study came from tomb M52 in the Haochuan Cemetery. They are all drum-shaped beads drilled with small holes. They were arranged in rows beside the vermilion lacquer marks during excavation. They may be decorative objects embedded or adhered around the mouth of a container. As precious national cultural relics, they are non-reproducible and unique, and non-destructive identification method must be adopted. Therefore, the conventional test method of gemmology and the non-destructive identification method of large-scale equipment were adopted for the test of these research sample. Tests were done mainly through conventional gemmological tests, ultra-depth-of-field microscope, infrared spectroscopy and X-ray fluorescence spectroscopy to identify the beads, so as to determine the composition of the beads, the polishing process, the possible source of the jade and the processing levels of the ancestors in the Haochuan area at that time. Infrared spectroscopy was tested by reflection method, and it can be seen that all five samples have characteristic peaks of turquoise, which proves that the base of the five beads is pure turquoise. XRF data shows that the content of trace element barium is relatively high, which is similar to the characteristics of turquoise produced in Shiyan, Hubei and surrounding areas. It can be used as a possible evidence to identify the source of the five turquoise beads and jade materials for the



next step, which lays the foundation for research. Observing the pieces of turquoise beads through photomicrography can evaluate the jade processing level of the ancestors at that time. The five samples have several corrosion pits of different degrees on the surface, and the erosion degree is relatively shallow, which proves that the turquoise itself is more dense and the buried conditions in the soil are better; the five samples have visible directional polishing marks, and they are obvious. A certain number of polished small faces were not completely finely ground, leaving a rough surface, which proves that the ancestors of the Haochuan Culture at that time already had the ability to process and polish material beads with a length and width of no more than 1 cm; the method of processing beads is to grind the irregular turquoise material into multiple small surfaces until it becomes a barrel bead shape, but it may not have the ability to grind and polish the arc surface; the shape of the hole is relatively regular, nearly circular, with polishing marks, which shows that the Haochuan Cemetery already had a certain degree of jade processing capacity.

**Key words:** Haochuan Cemetery; Haochuan Culture; material bead; turquoise; process

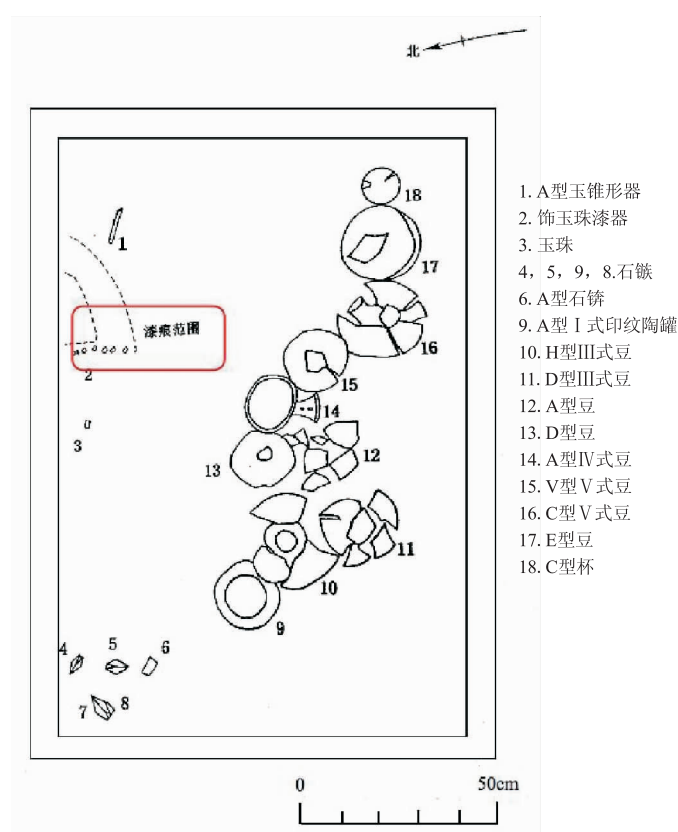




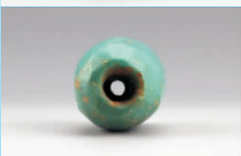
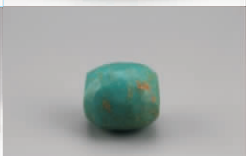
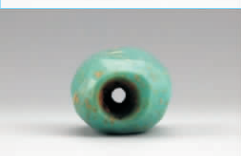

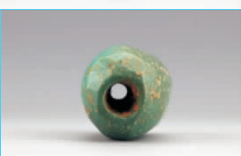
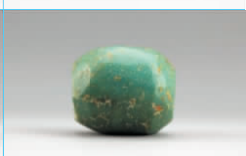


图 1 好川墓地 M52 平面图

Fig. 1 Planform of M52 Haochuan Cemetery

表 1 好川墓地五件绿松石料珠的基本特征

Table 1 Basic characteristics of five turquoise beads in Haochuan Cemetery

	尺寸/cm	重量/g	光泽	形状	图片	
M52 : 2	直径 0.5—0.7、 长 0.9	0.50	油脂光泽	鼓形		
M52 : 3	直径 0.8、 长 0.9	0.95	油脂光泽	鼓形		
M52 : 4	直径 0.8、 长 1.0	0.90	油脂光泽	鼓形		
M52 : 5	直径 0.6—0.7、 长 0.9	0.54	油脂光泽	鼓形		
M52 : 8	直径 0.9、 长 1.0	1.10	油脂光泽	鼓形		

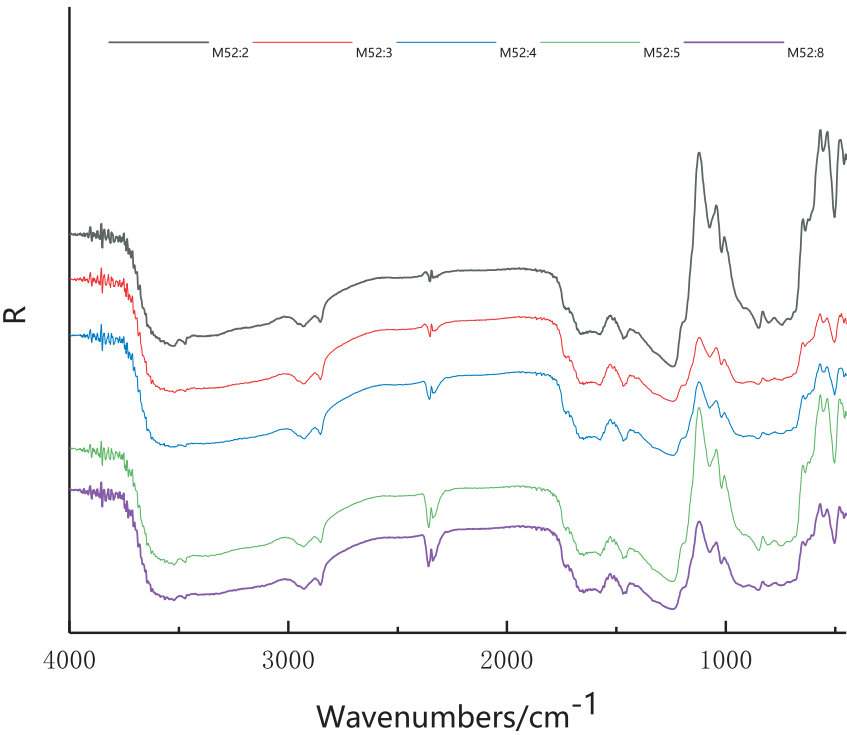


图 2 好川墓地出土五件绿松石料珠的红外光谱

Fig. 2 Infrared spectra of five turquoise beads unearthed from the Haochuan Cemetery

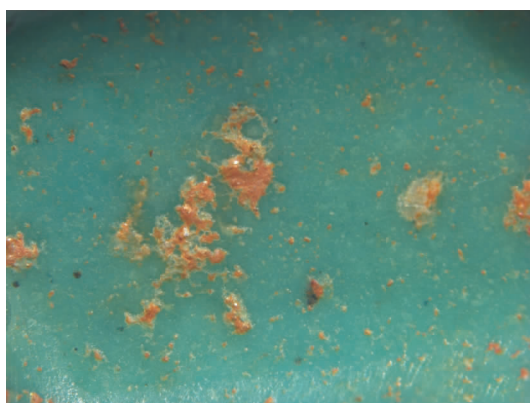


图3 样品 M52 : 2 表面蚀坑  
Fig. 3 Surface pit of sample M52 : 2



图4 样品 M52 : 8 表面抛光面  
Fig. 4 Polished surface of sample M52 : 8

# The Glory of Turquoise from Neolithic to Bronze Age in Persia

Bahareh Shirdam, Yang Mingxing, Andy H. Shen

*(Gemmological Institute, China University of Geosciences, Wuhan 430074, China)*

Turquoise is an opaque, blue-to-green gem-material that has not only attracted people's attention due to its beauty and vivid colour but also its divine place in different civilizations. Originally called "Piruzeh" in Persian language, the spiritual value of turquoise in Persian culture is to the point that even its name carries the meaning of victorious, triumphant and prosperous. In Persian literatures, turquoise has been celebrated by poets, and various legends and beliefs are associated with it (Vinogradov, 1966).

This article conducts a review on turquoise deposit and their distribution in the Iranian plateau, comparing it with the distribution of turquoise artifact discovered in prehistoric archeological sites, to stimulate possible trade routes for turquoise trade. Studying the obtained turquoise artifact from excavations, offers some insight into the status of turquoise, development and progression of crafting, inlay and bead industry in prehistoric culture and its very first civilizations.

## TURQUOISE DEPOSITS IN THE IRANIAN PLATEAU

As a country extraordinarily rich in natural resources of copper, lead and silver, as well as metamorphic rocks and semi-precious stone such as turquoise, archeological sites in Iran suggest an early interest in these resources and developing new technologies to exploit them (Helwing 2004).

Turquoise is a mineral at the top of the porphyry-epithermal systems (Momenzadeh 2004). The Nishapur, Baghu, Meyduk and Sar Cheshmeh ancient turquoise mines are all located in the alternation zones of porphyry-epithermal systems with Cu, Au mineralization. Turquoise mining in Iran (Fig. 1) has been discontinuously continued from prehistoric to the present time.

The most important, best known and long living mine is the Neyshabur turquoise mine. But some other mines have been producing turquoise in west of Kerman, south of Damghan, and southeast of Tabas. Turquoise from Kerman area is well known in the history and archaeology of Iran. The term of "Kerman turquoise" is applied to turquoise from both Sar Cheshmeh and Meyduk porphyry copper deposits.



Fig. 1 Distribution of archeological sites, active and inactive ancient turquoise mines.

Ancient-Active Turquoise Deposit (Blue): 1-Neyshabur Mine, 2-Baghu Mine, 3-Meyduk Mine  
 Ancient-Inactive Turquoise deposit (Red): 1-Gazu Mine, 2-Runiz Mine, 3-Sar Cheshmeh Mine

Table 1 Archeological sites with evidence of using turquoise ornaments

Period	Chronology (cal B. C. )	Location	Province
Neolithic	7500	Tape Ali Kosh	Ilam
	7000	Tape Mohamad-Djaffar	Ilam
	6000 – 7000	Tal-e Atashi	Kerman
	6000	Tape Rahmat Abad	Fars
	5200	Tape Zagheh	Qazvin
Chalcolithic	4800	Tape Pardis	Tehran
	4600	Tape Sialk	Isfahan
	4360	Tape Borj	Razavi Khorasan
	4500 – 3800	Tape Yahya	Hormozgan
	4300	Tal-i-Iblis	Kerman
	4100 – 4 500	Tal-e Bakun	Fars
Bronze Age	3800 – 3400	Tape Yahya	Hormozgan
	3500	Tape Hesar	Semnan
	2800	Shahr-i Sukhte	Sistan & Baluchestan
	2800 – 2300	Jiroft	Kerman
	2600 – 2200	Susa IV	Khuzestan
	1800	Tal-e Malyan	Fars

## TURQUOISE DISCOVERIES FROM ARCHEOLOGICAL EXCAVATIONS

In spite of the transitional period from pre pottery Neolithic in Ali-Kosh to pottery Neolithic in Mohamad-Djaffar, the large number of turquoise artifacts discovered from burials in both phases, suggests the importance of this mineral in their traditions.

The distribution of turquoise deposits in the Iranian plateau and ancient sites from which turquoise has been discovered, is demonstrated in Fig. 1. A visual comparison of these data suggests a significant distance between Neolithic sites (particularly in Ali-Kosh, Mohamad-Djaffar and Zagheh sites) and turquoise deposits, and therefore the necessity of transport route and trade to explain the presence of turquoise ornaments (Fig. 2).

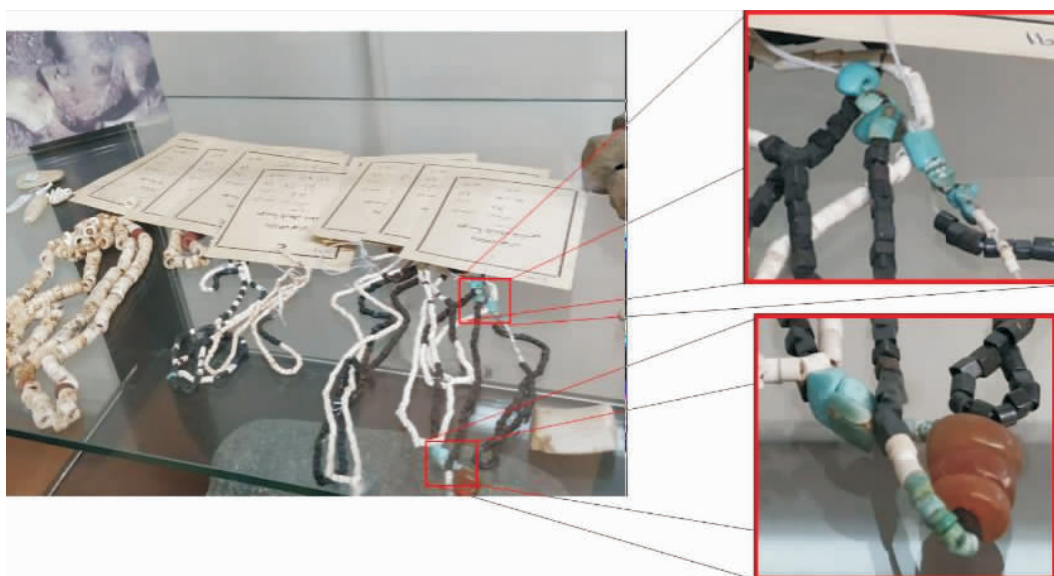


Fig. 2 Turquoise ornament from Tape Zagheh site, exhibits in Archeology Museum of University of Tehran, photo by B. Shirdam

### The Chalcolithic

This era is marked by a decrease in the use of local chlorite for bead making and a significant increase in the use of turquoise (Beale, 1973). While some ancient communities have moved closer to the ore deposits in the chalcolithic, material culture found in Sialk and Pardis (Chalcolithic sites far from turquoise deposits), not only suggest a local development of different industries but also indicate the extension of contacts towards eastern areas, due to the presence of turquoise discoveries in excavated layers.

### The Bronze Age

Turquoise production peaked during the Bronze Age. Excavators unearthed many differ-

ent types of artifacts inlaid with turquoise, significantly in Jiroft archeological site. Workshops for bead production have been found at several sites from the early 3rd millennium BC, like Tappeh Hesar, Susa, Shahdad, Tal-i Malyan and Shahr-i Sokhta. At the latter, carnelian and turquoise were used in addition to lapis lazuli (Foglini & Vidale, 2000; Casanova, 1995). Bead-makers of this era were professional craftsmen, and some of them carried the tools of their trade with them at all times, even into the grave, as some burials from Shahdad demonstrate (Hakemi, 1997). Another characteristic of this period is the growing utilization of inlay technology; as observed in Fig. 3, turquoise has





Fig. 3 A turquoise inlaid on chlorite vase from Jiroft, exhibits in the Archaeology Museum of Jiroft

been inlaid on a chlorite vase from Jiroft's great civilization.

Around the same time, flint drills were discovered in big numbers in Shahr-i Sokhtae. A comparative study between the turquoise waste found in the archeological site's layers and turquoise beads discovered in burials indicate that turquoise came to the towns in the form of finished products, in contrast to lapis lazuli which was manufactured at the place (because of the larger number of extracted lapis waste) (Tosi 1973).

## REFERENCES

- Vinogradov V. , Lopatin S. V. , Mamedov E. D. (1966). The Turquoise of the Kyzyl-Kum. *Soviet Anthropology and Archeology*, 4(4), 11–28.
- Helwing B. (2004). Early towns in Iran, Persian antiques Splendor; Mining crafts and archaeology in ancient Iran, Deutsches Bergbau-Museum Bochum, Bochum.
- Momenzadeh M. , Hajisoltan A. , Momenzadeh M. (2004). Metallic mineral resources of Iran. mined in ancient times; A brief review, Persian Antiques splendor; Mining crafts and archaeology in ancient Iran. Deutsches Bergbau-Museum Bochum, Bochum.
- Garazhian E. , Lotfi F. (2014). Turquoise in prehistoric Iranian plateau; Rural cultures and the beginning of urbanization. *Honar va Fan Journal*. 3(3), 45–66.
- Hole F. , Flannery K. V. , Neely J. A. (1969). *Prehistory and human ecology of the deh luran plain*. University of Michigan Press, Michigan.
- Beale T. (1973). *Early trade in highland Iran: a view from a source area*. *World Archaeology* (5), 133–148.
- Foglini L. , Vidale M. (2000). *Reconsidering the lapis lazuli working areas of Shar-i Sokhta*. Proceedings of the First International Congress on the Archaeology of the Ancient Near East, Roma, 471–482.
- Casanova M. (1995). *La fabrication des perles de lapis-lazuli*. Les pierres précieuses de l'Orient ancien, Paris, 45–46.
- Hakemi A. (1997). *Shahdad: Archaeological excavations of a bronze age center in Iran*. Istituto Italiano per il Medio ed Estremo Oriente Roma IsMEO, Roma.
- Tosi M. (1973). The cultural sequence of Shahr-i Sokhta. *Bulletin of the Asia Institute*, (3), 64–80.

# 中国某公司合成粉色—红色系钻石的 宝石学特征研究

张传政<sup>1</sup>, 李建军<sup>2</sup>, 程佑法<sup>2</sup>, 范春丽<sup>2</sup>, 王礼胜<sup>1</sup>

(1. 河北地质大学, 河北 石家庄 050031; 2. 山东省计量科学研究院, 山东 济南 250014)

**摘 要:** 本文主要采用宝石显微镜、Diamond View™(钻石观测仪)、显微红外光谱仪、紫外-可见分光光度计、光致发光光谱仪、X 射线荧光光谱仪对 6 颗切磨为圆明亮型的中国某公司生产的经改色处理为粉—红色系列的高压高温(HPHT)合成钻石进行测试研究。研究表明: 样品内部含有针柱状、不规则或点状包裹体并可见清晰的颜色分区现象; 荧光颜色为红色—橙红色; 部分样品生长结构呈典型“黑十字”, 可见立方体、菱形十二面体、八面体的生长分区; 紫外-可见光谱具(N-V)心、GR1 心或 595 nm 等吸收峰, 红外光谱可见 1 450 cm<sup>-1</sup> 吸收峰, PL 光谱可见(N-V)心、GR1 心、3H 心、588 nm 等峰值特征。综合基础宝石学特征及光谱分析, 该批次样品为经辐照处理加退火处理的复合工序处理所产生的 Ib 型粉色—红色高温高压合成钻石。

**关键词:** 粉色—红色; 辐照处理; 退火处理; 合成钻石; 宝石学特征

## Gemmological Characteristic of Pink-Red Synthetic Diamond Produced by a Chinese Company

ZHANG Chuanzheng<sup>1</sup>, LI Jianjun<sup>2</sup>, CHENG Youfa<sup>2</sup>, FAN Chunli<sup>2</sup>, WANG Lisheng<sup>1</sup>

(1. Hebei GEO University, Shijiazhuang 050031, China; 2. Shandong Institute of Metrology, Jinan 250014, China)

**Abstract:** This study focuses on the basic gemmological characteristics and spectral characteristics of pink-red high temperature and high pressure (HPHT) synthetic diamonds produced by a Chinese company. It is expected that this research can provide theoretical basis for the future research of pink-red diamonds, and provides theoretical support for the identification of HPHT synthetic diamonds. This article uses gem microscope, DiamondView™, micro-infrared spectrometer, Ultraviolet-visible spectrophotometer, Photoluminescence spectrometer, X-ray fluorescence spectrometer to study 6 round cutting bright HPHT synthetic diamonds that have been colour-treated to pink-red produced by a Chinese company. The results showed that the sample contains needle, columnar, irregular or point inclusions and clear colour partitions phenomenon; the

收稿日期: 2020-09-30

作者简介: 张传政(1991—), 女, 硕士研究生, 矿物学、岩石学、矿床学专业。

通讯作者: 李建军(1976—), 男, 国家黄金钻石制品质量监督检验中心研究员, 主要从事珠宝玉石、钻石的检测与研究工作。E-mail: geoli@vip.sina.com

fluorescence showed red-orange colour under the Diamond View<sup>TM</sup>; the growth structure of cube, rhombic dodecahedron and octahedron can be clearly seen from the sample H-01—H-03, and showed the typical "dark cross" phenomenon. It is speculated that the growth structure image observed with different diamond cutting direction has obvious difference; The ultraviolet-visible spectrum showed 260 nm wide absorption band and (N-V) center, GR1 center or 595 nm absorption peak; The infrared spectrum showed the absorption peak of 1 131, 1 330, 1 344, and 1 450  $\text{cm}^{-1}$ ; The PL spectrum showed (N-V) center, GR1 center, 3H center, 588 nm and 886 nm characteristic peaks. Based on the basic gemmology-cal characteristics and spectrum analysis, this batch of experimental samples are type Ib pink-red HPHT synthetic diamonds produced by irradiation and annealing treatment.

**Key words:** pink-red; irradiation treatment; annealing treatment; synthetic diamond; gemmological characteristic

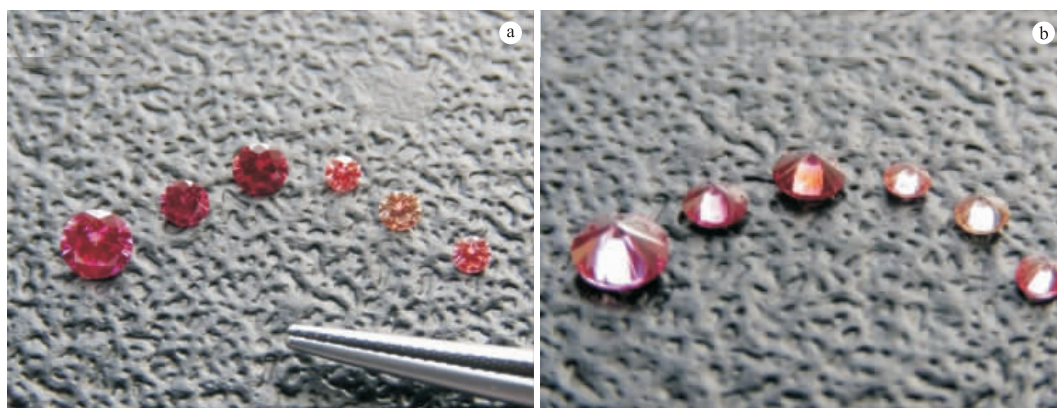


图1 实验样品(从左至右依次为 H-01,H-02,H-03,H-04,H-05,H-06)

Fig. 1 Test samples (from left to the right: H-01,H-02,H-03,H-04,H-05,H-06)

a. 台面方向;b. 亭部方向

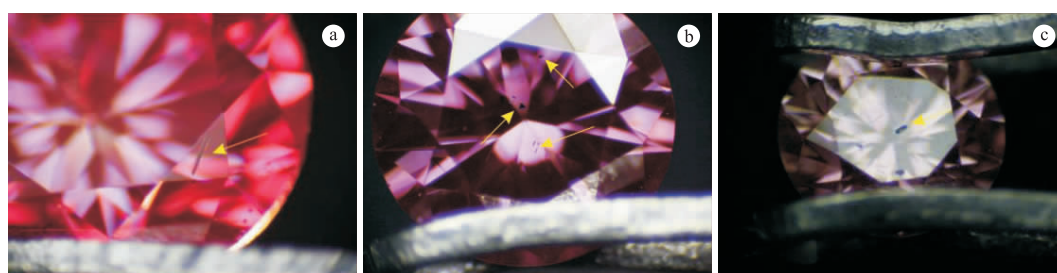


图2 部分样品包裹体特征

Fig. 2 Inclusion characteristics of samples

a. 样品 H-01; b. 样品 H-02; c. 样品 H-04

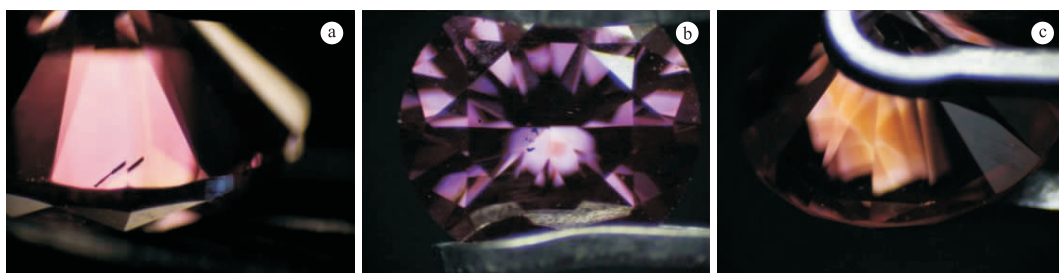


图 3 部分样品颜色分区现象

Fig. 3 Colour partitioning phenomenon of samples

a. 样品 H-01; b. 样品 H-02; c. 样品 H-04

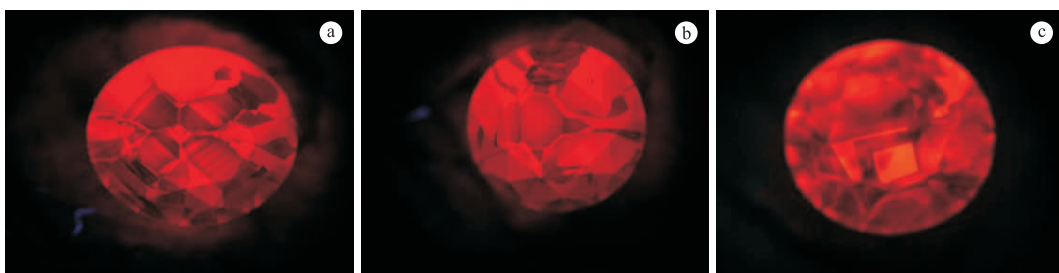


图 4 部分样品生长结构荧光图像

Fig. 4 Fluorescence images of growth structure in samples

a. 样品 H-01; b. 样品 H-02; c. 样品 H-05

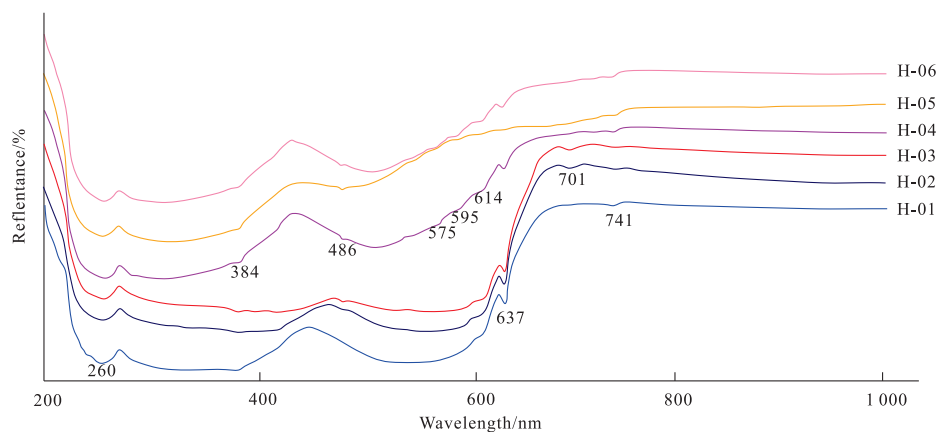


图 5 样品的紫外-可见光谱

Fig. 5 Ultraviolet-visible spectra of the samples

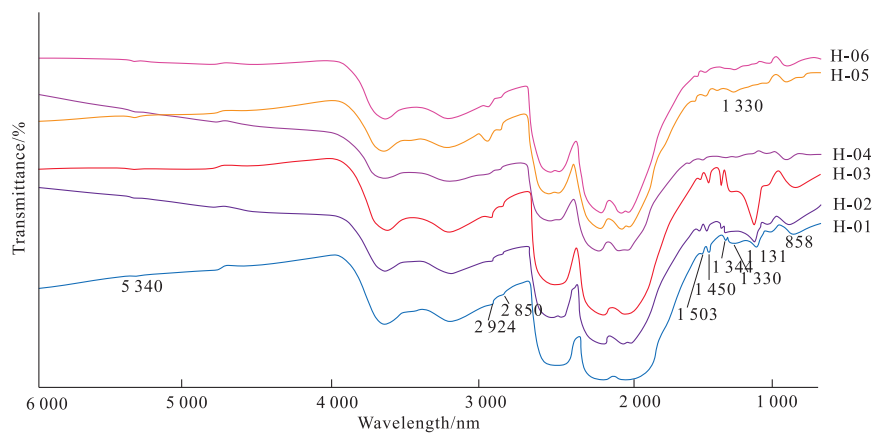


图 6 样品的红外光谱

Fig. 6 Micro-infrared spectra of the samples

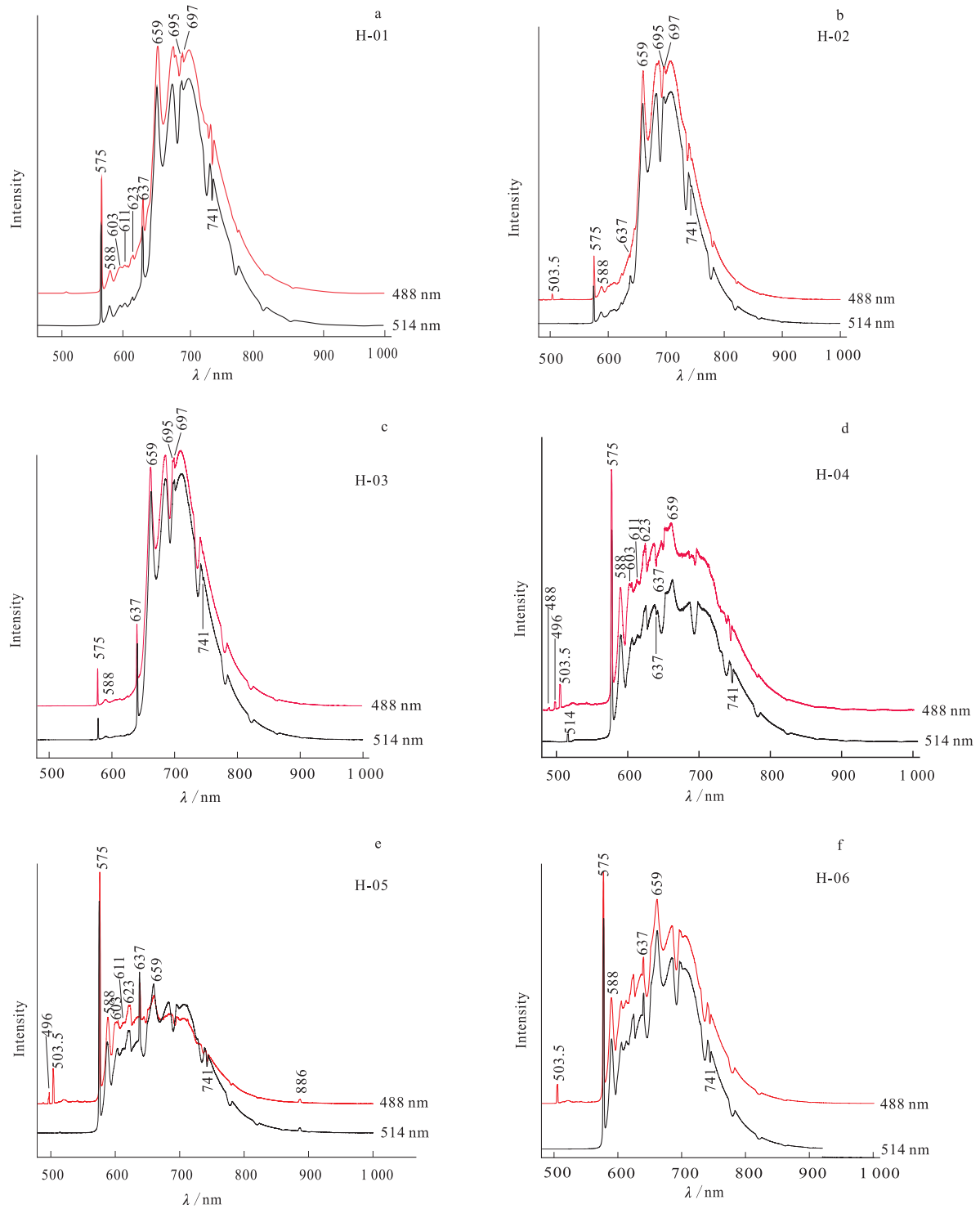


图7 样品的光致发光光谱

Fig. 7 Photoluminescence spectra of the samples

# 水热法合成蓝绿色绿柱石的宝石学及光谱学特征

张嘉麟, 张倩, 裴景成, 黄伟志

(中国地质大学珠宝学院, 湖北 武汉 430074)

**摘要:**针对新出现在市场上的一种水热法合成蓝绿色绿柱石,运用 LA-ICP-MS、红外光谱、拉曼光谱、紫外-可见光谱进行系统研究,旨在获得其宝石学及谱学特征,探讨颜色成因,为检测机构鉴定该合成宝石提供参考数据。结果表明,样品折射率为 1.570~1.576,与天然绿柱石相近,内部含特征的水波纹状生长纹理,可作为主要鉴定特征之一。LA-ICP-MS 分析表明,该合成绿柱石化学成分相对单一,主要致色元素为 Cr、Ti,还含有微量的 V,碱金属含量极低。紫外-可见光谱主要显示 Cr 的吸收峰,结合 LA-ICP-MS 测试,认为其蓝绿色调主要由 Cr 和 Ti 共同导致。其中绿色调主要由 Cr 致色,微量的 V 可能也对绿色调有所影响。Ti 则致紫色,与绿色叠加形成样品具有的蓝绿色调,具体的致色机理有待进一步研究。在 2 000~4 000  $\text{cm}^{-1}$  的红外光谱中,以 3 700  $\text{cm}^{-1}$  为中心的宽吸收带吸收强烈,归属于两种类型通道水的基频振动及其耦合;2 449、2 615、2 746、2 813、2 885、2 983  $\text{cm}^{-1}$  处吸收峰,均为  $\text{Cl}^-$  引起;3 108、3 299  $\text{cm}^{-1}$  的较强吸收峰由  $\text{NH}_4^+$  所致。在 4 000~8 000  $\text{cm}^{-1}$  的近红外吸收光谱中,为合成绿柱石通道水的合频和倍频振动区。其中,Ⅰ型水的合频振动所致的 5 275  $\text{cm}^{-1}$  处强吸收峰、伴随 5 106、5 455  $\text{cm}^{-1}$  处较强吸收峰,及Ⅰ型水倍频振动所致的 7 143  $\text{cm}^{-1}$  强吸收峰,可作为样品是水热法合成绿柱石的重要鉴定特征,且对于鉴定较厚的刻面宝石尤为重要。天然绿柱石中相应的这两处吸收峰强度较弱甚至不存在。样品的拉曼光谱和标准绿柱石的拉曼光谱一致。685  $\text{cm}^{-1}$  峰的半高宽为 7.1~7.3  $\text{cm}^{-1}$ ,小于 8.5  $\text{cm}^{-1}$ ,可作为水热法合成绿柱石的又一鉴定特征。

**关键词:**合成绿柱石;水热法;紫外-可见光谱;红外光谱;拉曼光谱

## Gemmological and Spectroscopic Characteristic of Synthetic Blue-Green Beryl by Hydrothermal Method

ZHANG Jialin, ZHANG Qian, PEI Jingcheng, HUANG Weizhi

(Gemmological Institute, China University of Geosciences, Wuhan 430074, China)

**Abstract:** This paper analyzed a new blue-green hydrothermal synthetic beryl appears on the market, the systematic research is conducted by using LA-ICP-MS, IR spectrum, Raman spectrum, UV-Vis absorption spectrum, to obtain the gemmological and spectroscopic characteristics, and to analyze the causes of colour, and provide reference data for testing institutions to identify such synthetic gems. The results show that the re-

收稿日期:2020-09-30

作者简介:张嘉麟(1998—),女,学士,主要从事宝石学的学习和研究。

通讯作者:裴景成(1974—),男,副教授,主要从事彩色宝石及产地教学及研究工作。E-mail:peijc@cug.edu.cn



fractive index of the sample is 1.570–1.576, which is similar to natural beryl. All samples have the characteristic water ripple growth texture inside, which can be used as one of the main identification characteristics of this synthetic beryl. LA-ICP-MS analysis showed that the chemical composition of this synthetic beryl is relatively simple, the main chromogenic elements are Cr and Ti, and trace amounts of V, and the alkali metal content is extremely low. The UV-Vis spectrum mainly shows the absorption peak of Cr, combined with the LA-ICP-MS test results, it is believed that the blue-green tone is mainly caused by Cr and Ti. The green tone is mainly caused by Cr, the trace amounts of V may also affect the green tone. Titanium causes the purple colour, superimposed with green to form the blue-green hue of the sample, the specific colour mechanism needs to be further studied. In the infrared spectrum of 2 000–4 000  $\text{cm}^{-1}$ , the broad absorption band centered at 3 700  $\text{cm}^{-1}$  absorbs strongly, which belongs to the fundamental frequency vibration and coupling of two types of channel water. Peaks at 2 449, 2 615, 2 746, 2 813, 2 885, 2 983  $\text{cm}^{-1}$  are caused by  $\text{Cl}^-$ ; The strong absorption peaks of 3 108  $\text{cm}^{-1}$  and 3 299  $\text{cm}^{-1}$  are caused by  $\text{NH}_4^+$ . In the near infrared absorption spectrum of 4 000–8 000  $\text{cm}^{-1}$ , it is the combined frequency and frequency doubling vibration area of the channel water in synthetic beryl. Among them, the strongest absorption peaks at 5 275  $\text{cm}^{-1}$ , accompanied by the stronger absorption peaks at 5 455  $\text{cm}^{-1}$  and 5 106  $\text{cm}^{-1}$  caused by the combined frequency vibration of type I water, and the strong absorption peak at 7 143  $\text{cm}^{-1}$  caused by frequency doubling vibration of type I water can be used as an important identification features of hydrothermal synthetic beryl, and is particularly important for the identification of thick faceted gemstones. The corresponding absorption peaks in natural beryl are weak or even absent. The Raman spectrum of the sample is basically the same as that of standard beryl. The half-height width of the 685  $\text{cm}^{-1}$  peak is 7.1–7.3  $\text{cm}^{-1}$ , less than 8.5  $\text{cm}^{-1}$ , which can be used as another identification feature of this hydrothermal synthetic beryl.

**Key words:** synthetic beryl; hydrothermal method; UV-Vis spectrum; IR spectrum; Raman spectrum



图1 水热法合成蓝绿色绿柱石样品

Fig. 1 Hydrothermal synthetic blue-green beryl samples





图 2 部分样品内部观察到沿愈合裂隙面  
分布大量流体包裹体

Fig. 2 A large number of fluid inclusions distributing  
along the fracture surface

表 1 水热法合成蓝绿色绿柱石样品的化学成分

Table 1 Chemical compositions of hydrothermal synthetic blue-green beryl samples  $w_B/\%$

成分	BH-1	BH-2	BH-3	BH-4
$\text{Al}_2\text{O}_3$	19.238	19.586	19.279	19.580
$\text{SiO}_2$	66.627	66.245	66.739	65.879
$\text{BeO}$	13.469	13.558	13.378	13.936
$\text{TiO}_2$	0.434	0.428	0.426	0.430
$\text{Cr}_2\text{O}_3$	0.152	0.146	0.156	0.128
$\text{V}_2\text{O}_3$	—	0.006	—	—
$\text{Na}_2\text{O}$	0.007	0.005	0.008	0.005

注：—表示该元素的质量分数低于仪器检出限

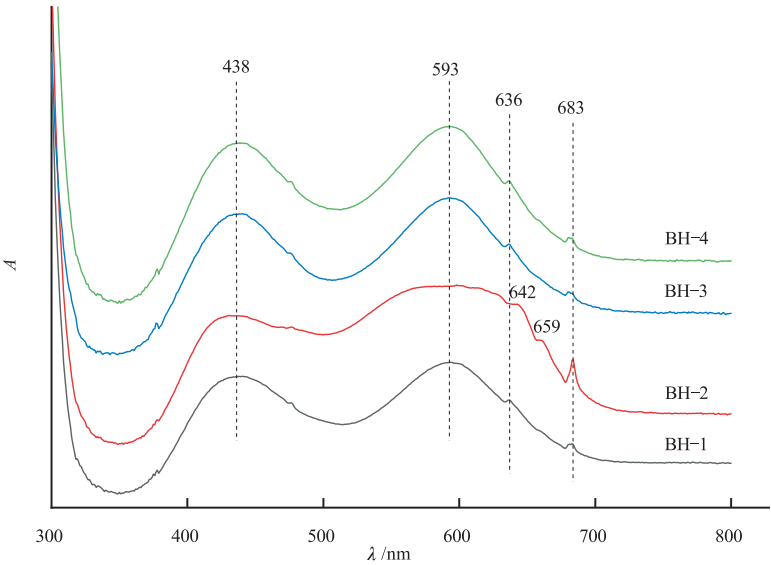


图 3 水热法合成蓝绿色绿柱石样品的紫外-可见吸收光谱

Fig. 3 UV-Vis spectra of hydrothermal synthetic blue-green beryl samples

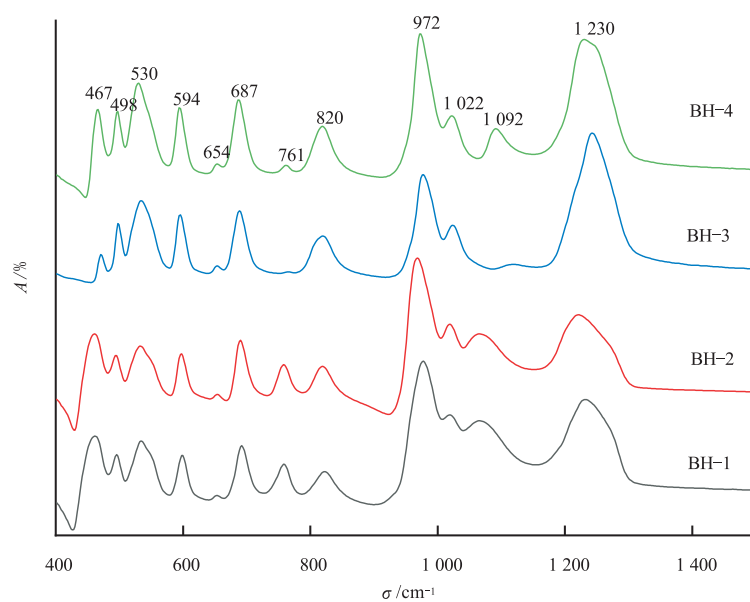


图4 水热法合成蓝绿色绿柱石样品的红外吸收光谱( $400\sim1\,500\text{ cm}^{-1}$ )

Fig. 4 IR spectra of hydrothermal synthetic blue-green beryl samples( $400-1\,500\text{ cm}^{-1}$ )

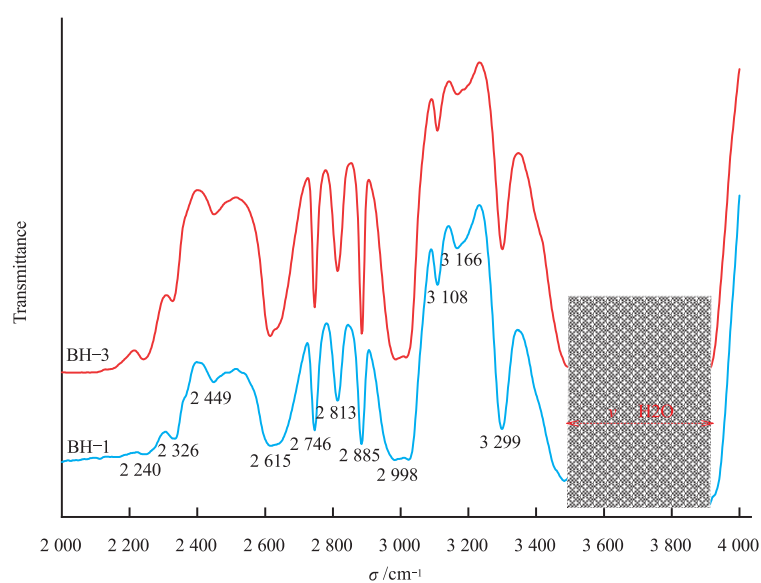


图5 水热法合成蓝绿色绿柱石样品的红外吸收光谱( $2\,000\sim4\,000\text{ cm}^{-1}$ )

Fig. 5 IR spectra of hydrothermal synthetic blue-green beryl samples( $2\,000-4\,000\text{ cm}^{-1}$ )

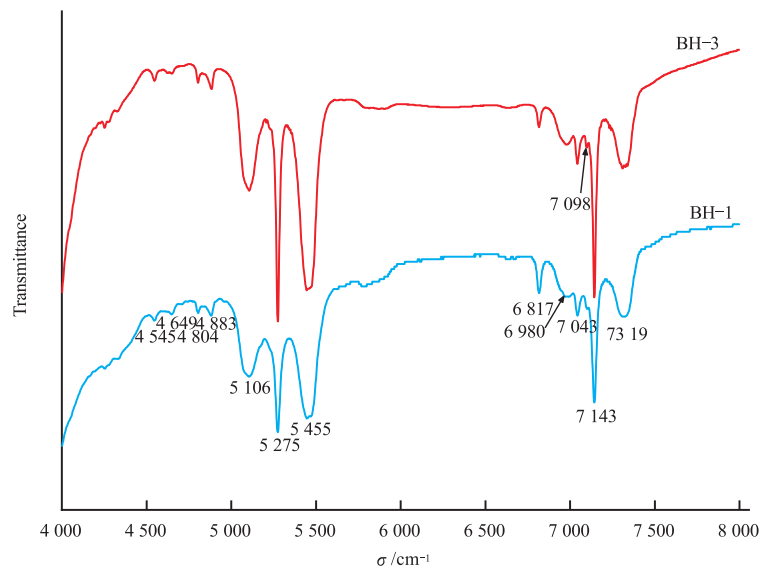


图6 水热法合成蓝绿色绿柱石样品的红外吸收光谱(4 000~8 000 cm<sup>-1</sup>)

Fig. 6 IR spectra of hydrothermal synthetic blue-green beryl samples(4 000—8 000 cm<sup>-1</sup>)

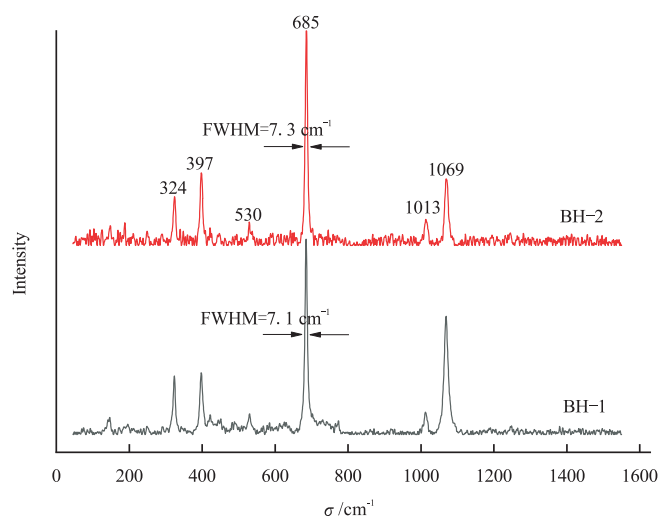


图7 水热法合成蓝绿色绿柱石样品的拉曼光谱

Fig. 7 Raman spectra of hydrothermal synthetic blue-green beryl samples

# 合成水晶晶簇的鉴定特征

代会茹<sup>1</sup>, 周丹怡<sup>2</sup>, 宋中华<sup>2</sup>, 苏 隽<sup>2</sup>, 李海波<sup>2</sup>, 陆太进<sup>2</sup>, 马永旺<sup>1</sup>

(1. 国家珠宝玉石质量监督检验中心北京实验室, 北京 100013; 2. 自然资源部珠宝玉石首饰管理中心, 北京 100013)

**摘 要:** 近日, 国家珠宝玉石质量监督检验中心(简称 NGTC)接收到一种合成水晶晶簇, 其与天然水晶晶簇具有十分相似的晶体形态、晶面花纹及蚀像特征, 并具有与天然水晶晶簇极其相似的指纹状、雾状气液包裹体等特征。NGTC 宝石学家赴东海水晶市场进行实地调研, 并对样品进行了一系列宝石学测试, 包括显微镜观察、发光图像观察、红外吸收光谱测试等。测试结果显示, 样品的红外吸收光谱为其合成成因提供了诊断性依据。样品中的无色晶体没有天然无色水晶所特有的  $3\,379$ 、 $3\,484\text{ cm}^{-1}$  和  $3\,595\text{ cm}^{-1}$  吸收峰, 而出现了合成无色水晶的特征峰  $3\,432$ 、 $3\,294$ 、 $3\,194$ 、 $3\,585\text{ cm}^{-1}$  吸收峰。绿色水晶颗粒缺失天然绿水晶和辐照处理绿水晶特有的  $4\,455\text{ cm}^{-1}$  吸收峰。因此该类样品应定名为合成水晶。

**关键词:** 合成水晶晶簇; 红外光谱; 鉴定特征

## Identification Characteristic of Synthetic Rock Crystal Cluster

DAI Huiru<sup>1</sup>, Zhou Danyi<sup>2</sup>, SONG Zhonghua<sup>2</sup>, SU Jun<sup>2</sup>,  
LI Haibo<sup>2</sup>, LU Taijin<sup>2</sup>, MA Yongwang<sup>1</sup>

(1. *Beijing Laboratory of National Gemstone Testing Center, Beijing 100013, China;*  
2. *National Gems & Jewelry Technology Administrative Center, Beijing 100013, China*)

**Abstract:** Recently, National Gemstone Testing Center (NGTC) received a kind of synthetic rock crystal cluster, whose crystal morphology, striations and etchings are very similar to those of natural rock crystal cluster, and whose internal inclusion characteristics are fingerprint like and foggy, which are more likely to be present in natural quartz. NGTC gemmologists went to Donghai crystal market for research, and conducted gemmological tests on the samples, including microscopic observation, DiamondView™ fluorescence imaging and infrared absorption spectrum, etc. The results show that the infrared absorption spectrum provides a diagnostic evidence for the origin of the sample. The colorless crystal on the cluster has no IR absorption peaks at  $3\,379$ ,  $3\,484$ ,  $3\,595\text{ cm}^{-1}$ , which are characteristic IR absorptions of natural rock crystal quartz. But the IR absorption peaks at  $3\,585$ ,  $3\,432$ ,  $3\,294\text{ cm}^{-1}$  and  $3\,194\text{ cm}^{-1}$  appear, which matches the IR absorption features of synthetic rock crystal quartz. And the IR absorption spectrum of green crystal lacks the absorption band at  $4\,455\text{ cm}^{-1}$ , which appears in the IR ab-

sorption spectrum of natural and irradiation treatment green quartz. Therefore, this kind of sample should be named synthetic rock crystal.

**Key words:** synthetic rock crystal cluster; infrared spectrum; identification characteristic



图1 合成水晶晶簇

Fig. 1 Synthetic rock crystal cluster

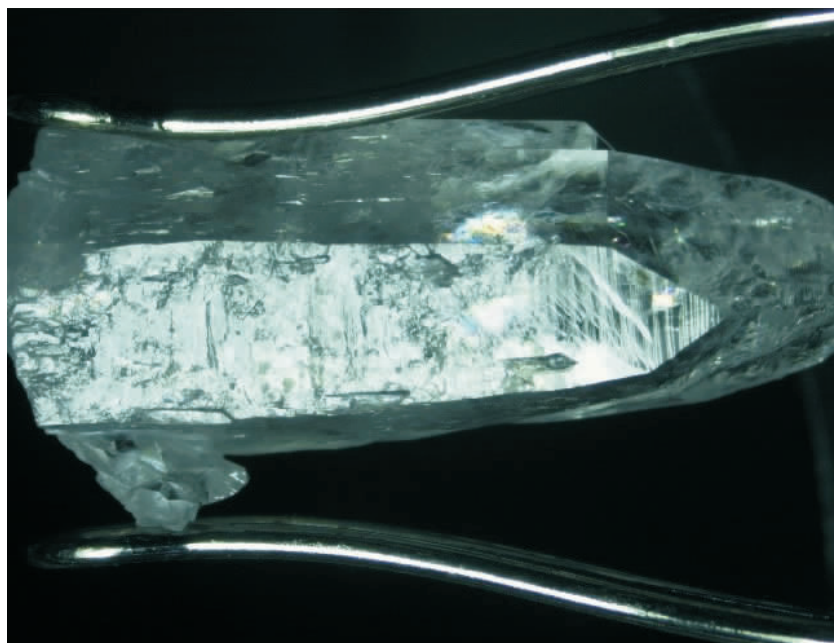


图2 无色晶体的表面条纹和蚀像

Fig. 2 Striations and etchings on the colorless crystal



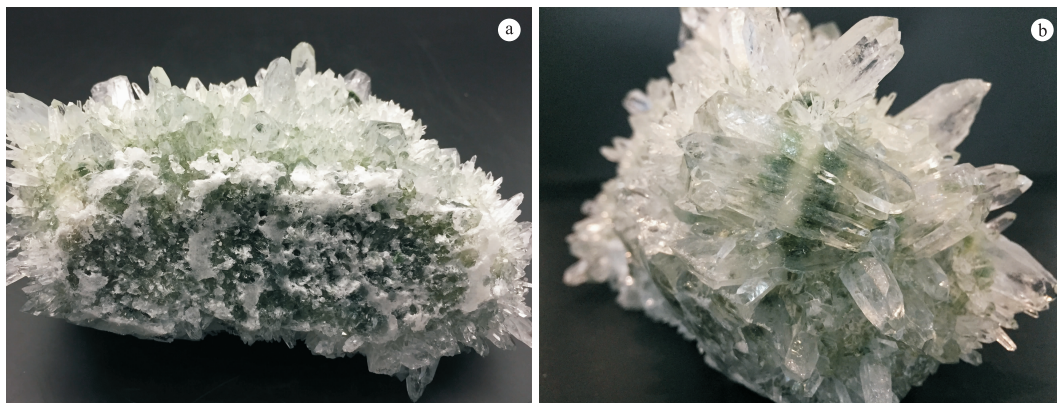


图3 绿色水晶颗粒组成的基底(a)和晶簇侧面的一组平直色带(b)

Fig. 3 The green substrate of the cluster is composed of many green quartz particles(a), and a group of colour band in the side of the cluster(b)

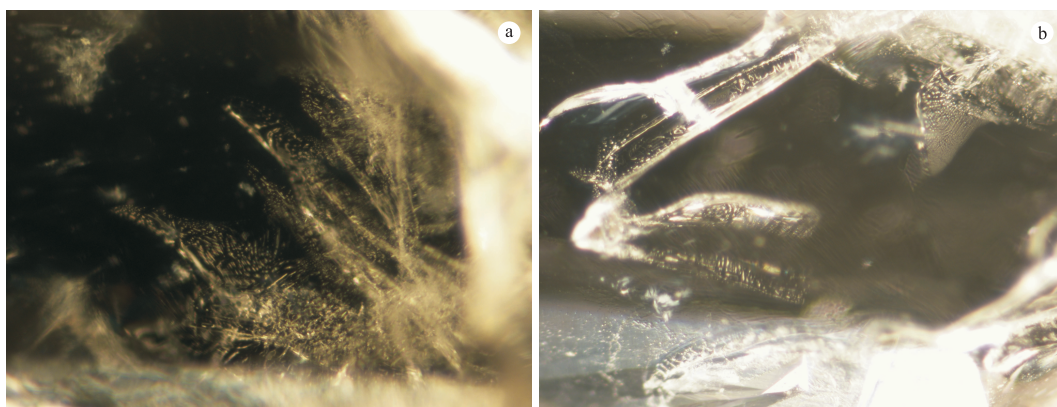


图4 无色晶体内部的指纹状、雾状气液包裹体

Fig. 4 Fingerprint like and foggy gas-liquid inclusions in the colorless crystals



图5 无色晶体在 DiamondView™下的荧光特征

Fig. 5 Fluorescence characteristics of the colorless crystal under DiamondView™

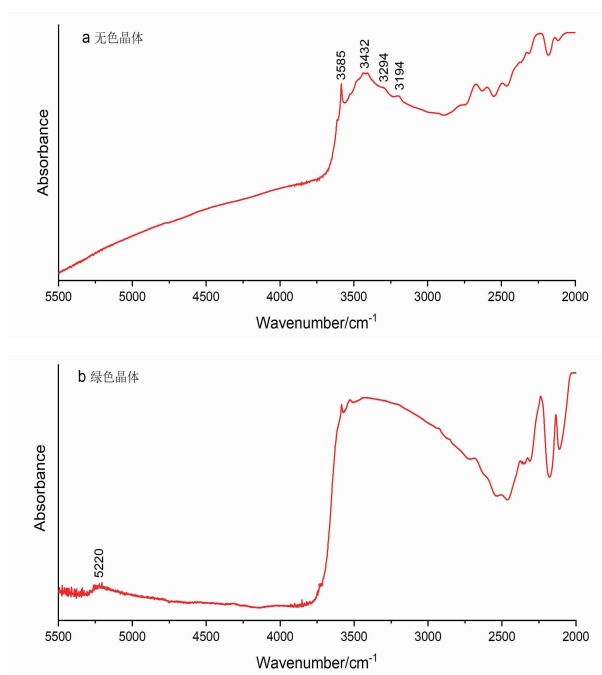


图 6 无色水晶晶体(a)与绿色水晶晶体(b)的红外吸收光谱  
Fig. 6 Infrared absorption spectra of colorless crystal (a) and green crystal (b)



# 3D 打印技术在首饰设计创客教育中的应用探索

姜婷煜<sup>1</sup>, 杨金凤<sup>1</sup>, 李妍<sup>1,2</sup>, 何萌<sup>1,3</sup>

(1. 中国地质大学珠宝学院, 湖北 武汉 430074; 2. 湖北省珠宝工程技术研究中心, 湖北 武汉 430074; 3. 湖北工业大学  
土木建筑与环境学院, 湖北 武汉 430068;)

**摘要:**随着智能化时代的到来,教育创新越来越受到重视,3D 打印技术与创客教育的融合已经成为中小学以及高等教育的重要教学模式,3D 打印技术的快速发展以及快速成型“设计即生产”的理念,可以增强学生在学习过程中的深度体验与参与,打造虚实结合的教育应用创新服务平台,锻炼学生的创造性思维和跨学科思维,促进创造式学习模式的发展。3D 打印技术与首饰设计创客教育的融合为首饰制作和教育教学带来了新的发展,文章从创意首饰、智能穿戴首饰和文创产品等方面分析了 3D 打印技术在首饰设计创客教育的应用方向。

就 3D 打印技术在创客教育的未来发展方向来说,宏观环境的 PEST 分析表明,3D 打印技术在社会环境政策、经济增长以及技术环境等方面都拥有许多优势,为其在创客教育中的发展提供了良好的条件,在教育需求方面,通过 SWOT 模型分析,对教育方案提出改革建议,从而把握优势、规避劣势、回避威胁、抓住机会,制定出更完善的创客教育方案。综合首饰设计创客教育的市场需求和教育需求,将 3D 打印技术和智能穿戴等数字技术融入到创客教学中有着很好的发展前景,文章从创客社交空间和创客文化氛围建设、创客通识教育和创客特色建设、网络平台搭建和社会资源共享等方面详细阐述了创客教育未来发展和努力的方向。随着新兴科学技术的快速发展,以创客教育为理念和以 3D 打印为主要技术的创新教学模式推动着首饰设计专业人才发展和创新复合型人才的培养,3D 打印技术在创客教育中的应用也还需要不断完善,以期最终能够实现将创意直接应用于实践的教育教学模式,促进行业的发展。

**关键词:** 3D 打印技术; 创客教育; 首饰设计; 人才培养

## Application Exploration of 3D Printing Technology in Jewelry Design Maker Education

JIANG Tingyu<sup>1</sup>, YANG Jinfeng<sup>1</sup>, LI Yan<sup>1,2</sup>, HE Meng<sup>1,3</sup>

(1. Gemmological Institute, China University of Geosciences, Wuhan 430074, China;

收稿日期: 2020-09-30

基金项目: 湖北省珠宝工程技术研究中心—高分辨率高导热铜复合材料激光选区熔融增材制造关键技术, 项目编号 CIGTXM-03-202003

作者简介: 姜婷煜(1997—), 女, 本科, 主要从事宝石学材料及先进制造加工方向的学习和研究。

通讯作者: 李妍(1987—), 女, 副教授, 主要从事宝石学材料及先进制造材料加工方向的研究工作。E-mail: yanli@cug.edu.cn

---

2. *Hubei Engineering Research Center of Jewelry, Wuhan 430074, China*; 3. *School of Civil, Environmental Engineering & Architecture, Hubei University of Technology, Wuhan 430068, China*)

**Abstract:** With the advent of the intelligent era, more and more attention has been paid to educational innovation. The integration of 3D printing technology and maker education has become an important teaching model for primary and secondary schools as well as higher education. With the rapid development of 3D printing technology and fast prototyping, “design is production” concept enhances students’ in-depth experience and participation in the learning process, create an educational application innovation service platform that combines virtual and reality, exercises students’ creative thinking and interdisciplinary thinking, and promotes the development of creative learning mode. This integration of 3D printing technology and jewelry design maker education has brought new development to jewelry making and education and teaching. This article analyzes the application of 3D printing technology in jewelry design maker education from creative jewelry, smart wearable jewelry, cultural and creative products ,etc.

In terms of the future development direction of 3D printing technology in maker education, the PEST analysis of the macro environment shows that 3D printing technology has many advantages in terms of social environmental policy, economic growth, and technological environment. This provides good conditions for 3D printing technology in maker education development. Regarding the educational needs of 3D printing technology, the SWOT analysis model is used to propose reform suggestions to the educational program, so as to grasp advantages, avoid disadvantages and threats, seize opportunities, and formulate a more complete maker education program. Integrating the market demand and educational needs of jewelry design maker education, integrating digital technologies such as 3D printing technology and smart wearing into maker teaching has a good development prospect. This article elaborates on the future development and efforts of maker education from the aspects of maker social space and maker cultural atmosphere construction, maker general education and maker characteristic construction, network platform construction and social resource sharing. With the rapid development of emerging science and technology, the innovative teaching model based on the concept of maker education and 3D printing as the main technology promotes the cultivation of jewelry design professionals and innovative compound talents. The application of 3D printing technology in the maker education also needs to be continuously improved, with the hope that the education and teaching model that directly applies creativity to practice will eventually be realized and promote the development of the industry.

**Key words:** 3D printing technology; maker education; jewelry design; talent development

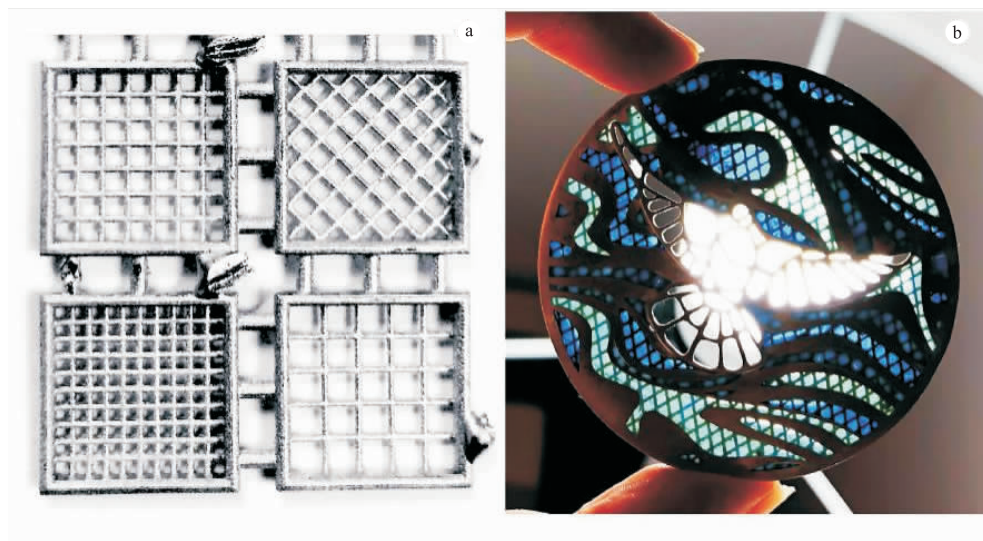


图1 小单元支撑线条样片(a)和笔者设计的小单元支撑线条珐琅片(b)

Fig. 1 The sample of the small cell supporting line (a) and the design of the enamel of the supporting line (b)



图2 *Thumb Brace* 拇指支架功能(a)和 *Thumb brace* 拇指支架外观(b)

Fig. 2 The function of CMC care Thumb Brace(a) and the outlook of CMC care Thumb Brace(b)



图3 创客教育活动现场和青少年3D打印文创  
产品创意首饰作品

Fig. 3 Maker education activities and youth 3D printing  
cultural and creative products creativity  
jewelry works

# 面向智能首饰的大规模个性化的 生产模式研究

李星枰<sup>1</sup>, 李妍<sup>1,2</sup>, 潘瑞琪<sup>1</sup>

(1. 中国地质大学珠宝学院, 湖北 武汉 430074; 2. 湖北省珠宝工程技术研究中心, 湖北 武汉 430074)

**摘要:** 首饰长久以来被认为是佩戴在人身上的装饰物, 而当代首饰设计越来越强调首饰与佩戴者的关系。考虑到可穿戴智能设备与用户关系密切, 生产商逐渐重视将设计形态学及美学融入可穿戴设备中, 许多珠宝公司也开始尝试生产智能首饰。市场上的个性化珠宝首饰生产以小型工作室提供的高端定制服务为主, 多数大规模生产的首饰形制和材料多具有相似性。随着物联网发展和云计算热潮的到来, 市场竞争更为激烈, 用户需求不断趋向个性化和多样化, 千篇一律的共性产品越来越难满足用户的个性需求, 这迫使生产商转变生产经营模式, 更好地在市场中赢得竞争。目前, 多数生产制造业的公司逐渐表现出个性化、小批量的特点, 这正是大规模个性化的表现, 而这一模式同样适用于珠宝首饰行业。大规模个性化生产模式可以充分发挥互联网优势, 更高效、更具象的收集用户个性化产品需求。它打破原有的单一且封闭运行的传统生产模式, 使设计、制造、销售等环节能够更加紧密高效地协作。同时, 可穿戴设备呈现出高度专业化、复杂化的特点, 需要人体健康大数据支撑和专家知识库, 来指导模型的动态演变预测与优化, 提高多维度定制产品的设计效率。本文运用大规模个性化的理论和策略, 根据可穿戴设备行业的特点, 着重分析生产进程中用户与公司交流互动的方式, 探讨如何将用户需求更好地纳入智能首饰生产过程。最后根据珠宝首饰市场的发展趋势和用户需求, 提出了一种以用户需求为导向的智能首饰大规模个性化设计模式, 旨在探究通过智能设计和仿真与制造网络协同实现更高效且成本可控的产品与服务解决方案。

**关键词:** 大规模个性化; 智能首饰; 用户需求; 生产流程

## Mass Personalized Manufacturing Mode for Smart Jewelry

LI Xingping<sup>1</sup>, LI Yan<sup>1,2</sup>, PAN Ruiqi<sup>1</sup>

(1. *Gemmological Institute, China University of Geosciences, Wuhan 430074, China;*

*2. Hubei Engineering Research Center of Jewelry, Wuhan 430074, China)*

**Abstract:** Jewelry has been regarded as a kind of ornament worn on human body in a long time, while the relationship between jewelry and wearer is more and more emphasized in contemporary jewelry design. Considering wearable intelligent devices are closely related to users, manufacturers have paid more attention to integrating design mor-

收稿日期: 2020-09-30

基金项目: 高分辨率高导热铜复合材料激光选区熔融增材制造关键技术(项目编号 CIGTXM-03-202003)

作者简介: 李星枰(1997—), 女, 本科, 主要从事宝石学材料及先进制造材料加工方向的学习和研究。

通讯作者: 李妍(1987—), 女, 副教授, 主要从事宝石学材料及先进制造材料加工方向研究工作。E-mail: yanli@cug.edu.cn

phology and aesthetics into wearable devices, and many jewelry companies have begun to try to produce smart jewelry. In the market, most personalized jewelries are produced by small studios based on high-end customized services, and the jewelry style and materials of large scale producing are similar. With the advent of internet of things (IOT) and cloud computing booming, market competition is becoming fierce and the individualization and diversification of user needs is increasing, it makes manufacturers try to change production and management mode in order to win the market competition better. Most companies of manufacturing industry has increasingly featured personalization and small batches, which shows the trend of mass personalization, and this mode is also applicable to the jewelry industry. The mass personalization production mode can utilize the advantages of the Internet well and collect the user's individual needs more efficiently and concretely. It breaks the single and closed conventional production mode, and makes the design, manufacturing, sales and other link processes more closely and efficiently cooperated. Meanwhile, wearable devices are highly specialized and complex, and it needs big data on human health and expert knowledge to support and guide the prediction and optimization of the models dynamic evolution, and improve the design efficiency of multi-dimensional customized products. According to the characteristics of wearable devices industry, this paper focuses on the analysis of the interaction ways between users and companies in the production process based on the theory and strategy of mass personalization, and discusses how to integrate the user needs into the smart jewelry production process better. Finally, according to the development trend of jewelry market and the needs of users, a mass personalized jewelry design mode based on users' demand is proposed. This research tries to explore a more efficient and cost controllable product and service solution through intelligent design, simulation and manufacturing network collaboration.

**Key words:** mass personalization; smart jewelry; user's need; production process



图1 针对手部矫形的智能康复产品(CMC care Thumb Brace)

Fig. 1 Smart rehabilitation products for hand orthosis (CMC care Thumb Brace)



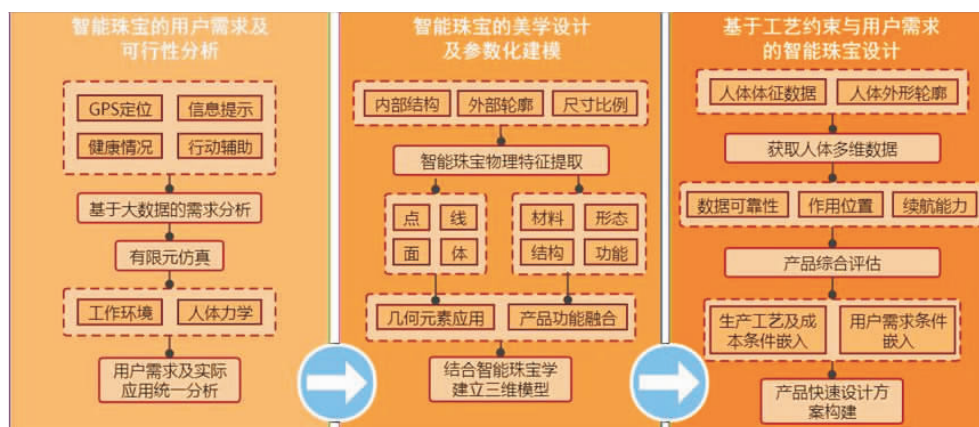


图2 大规模个性化生产中功能-美学-工艺多维数据共生联动体系

Fig. 2 Symbiotic and linked system of function-aesthetics-technics multi dimensional data in mass personalized production

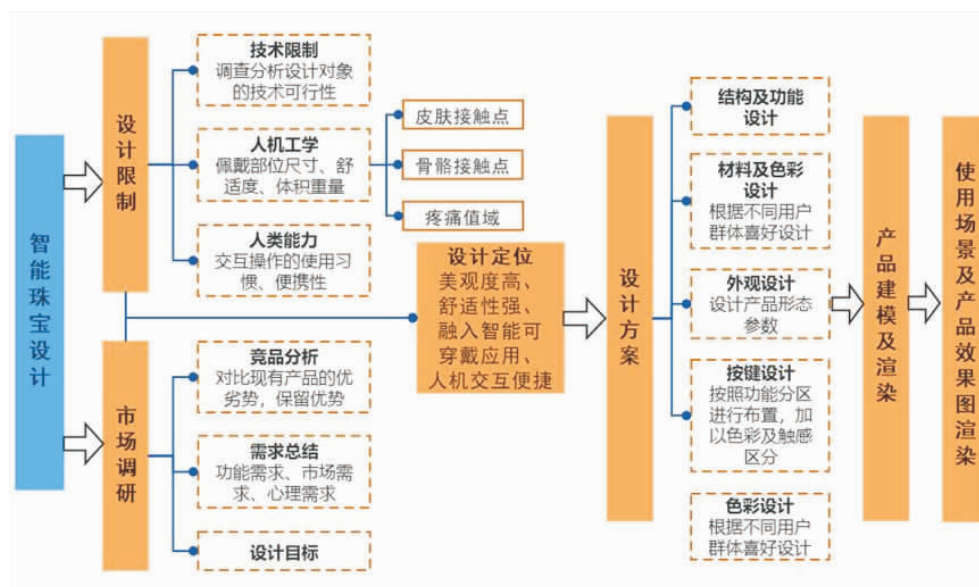


图3 大规模个性化智能珠宝的设计流程思维导图

Fig. 3 Design process mind map of mass personalized intelligent jewelry



# 辽代契丹文化中的融合与包容 ——以金属工艺纹样为例

文尚佳, 卢 韧, 刘艺苗

(中国地质大学珠宝学院, 湖北 武汉 430074)

**摘 要:**内蒙古文博及考古研究机构联合推出的“契丹印象—辽代(公元916年—1125年)文物精品展”近日在广东省博物馆展出。展品中的金属锤揲、錾刻、鎏金工艺风格多样,纹饰种类丰富。不少作品使用了两种极具异域风格的纹样:一个是源自印度神话的摩羯(摩伽罗),另一个是源于以色列犹太文化的大卫之星(即六芒星)。其以契丹人对金属饰品的加工工艺及纹样设计为载体,展示了辽代契丹文化与至少四类不同民族文化的交流与融合。通过对饰品纹样的溯源,可以还原辽代时期各民族(文明)之间文化流通的真相,同时也体现出契丹族对外来文化的包容性。

摩羯(摩伽罗)纹样源自印度神话,是由多种动物组合而成的生物形象,头为鳄鱼或大象,身体为鱼、蛇或其他爬行动物,四肢为大象腿或鳄鱼爪。建立于印度北部洛马斯里希洞穴的巴拉巴佛窟(公元前350年,见图1),其石门(图2)上雕刻的纹样被认为是最早的摩羯纹证据,彼时摩羯纹为鳄首象身(图3)。公元100年至200年首次出现鱼身摩羯形象(图4)。中国文化中的“文鱼”与摩羯纹是非常类似的形象。战国时期(公元前475年—前221年)即有“文鱼”的文字记载,《山海经—西山经》中:“泰器之山,观水出焉,西流注于流沙。是多文鳐鱼,状如鲤鱼,鱼身而鸟翼,苍文而白首赤喙……”。三国时期(公元220年—280年)的曹植(公元192年—232年)所著《洛神赋》中同样有描述“腾文鱼以警乘,鸣玉鸾以偕逝”。与此同时,前人研究认为摩羯的概念是在三国时期随佛教佛经传入中国,吴地康居国僧人康僧会译《弥兰经》云:“海有神鱼,其名摩羯,触败其船,众皆丧身,弥兰骑板,仅而获免”。至东晋时期(公元317年—420年),著名画家顾恺之(公元348年—409年)将曹植所著《洛神赋》画出,画中的文鱼已是龙首(亦有说象首,见图5),可见摩羯纹已经与汉人文化融合并开始演变。隋唐时期(公元581年—790年)大致演化出两类摩羯纹:一类是龙首鱼身也称鱼龙纹,另一类是龙首鱼身、加翅膀或其它生物。在庞大的唐文化体系下摩羯纹也逐渐融入契丹族的文化之中。

此次契丹印象展中摩羯造型的展品有金银首饰、金银铜器物和陶瓷器物。赤峰市喀喇沁旗哈达沟门窑藏出土的摩羯纹金花银盘被认为是唐代(公元618年—907年)的工艺精品(图6)。用捶揲的工艺将摩羯纹突显出来,再用錾刻工艺雕刻细节,乃一件非常典型的龙首鱼身形象。通辽市科尔沁左翼后旗吐尔基山辽墓出土的摩羯形金耳坠,是捶揲金片后焊接而成,整体造型立体感极强,两侧似双翼似鱼鳍并錾刻有云纹和细密曲线(图7)。另有耳饰直接将摩羯造型抽象化,把两个U形金片焊在一起(图8)。还有的耳饰将金属片简单捶揲錾刻后再焊接,龙首、鱼鳍、鱼鳞和戏珠都被完整的刻画出来,造型灵动(图9)。图10所示耳坠中的龙首、鱼鳞、鱼背鳍和似羽翼似鱼鳍的两侧,还有花苞形的龙珠都用金属工艺细致入微地錾刻出来。单从这些耳饰就可知辽代的摩羯纹种类之多风格变化之大,与同时期印度摩羯纹(公元850年—925年)已大相径庭(图11)。

由于唐代疆土其后分成北宋与辽,所以辽代墓常能见唐代摩羯纹文物。虽然唐代有摩羯纹文物出土,但辽代的相关文物数量如此之多引人深思。前人曾提出:“若辽代摩羯是完全袭自唐代,那么在汉人

收稿日期:2020-09-30

作者简介:文尚佳(1987—),女,博士研究生,主要从事珠宝首饰、宝石学方向研究。

通讯作者:卢韧(1960—),男,教授,主要从事宝石学方向研究。Email:renlu.cc@gmail.com

集中的辽南京(现北京市郊)和西京(现山西大同)地区,应该是出土摩羯物较多的地区,何以事实恰恰相反,偏是上京(今赤峰)和东京(今通辽)地区偏多。”因此笔者认为这可能与契丹族的渔猎文化有关。契丹辽地主要以草原和山林(包括沼泽、河涂)为主,因此形成了极富特色的渔猎和畜牧文化。尤其在冬季的凿冰捕鱼,逐渐成为契丹族的习俗活动并传承至今,而特殊的文化习俗推动了摩羯纹在辽文化中的盛行。

如果说摩羯纹体现了辽代契丹文化对唐朝文化的继承、对北宋汉人文化的融合以及对自身渔猎文化的发扬,那么这件通辽市奈曼旗陈国公主墓出土的“辽代阿拉伯文鏤花铜盆”(图 12)中的大卫之星纹饰则显示出契丹人强大的交流能力与文化包容性。宗教符号大卫之星起源于犹太教。公元 476 年至公元 1500 年传到伊斯兰教,又称所罗门之印。这个符号最初常见于宗教建筑,之后在生活器物上也常能见到。图 13 是被认为现存最古老的完整手抄希伯来圣经(公元 1008 年)中,有关大卫之星的一页。另有一件来自阿拉伯的鏤刻大卫之星铜碗现存于大都会博物馆(图 14),被认为是公元 1100 年至 1199 年的物件,与辽代同期。因此可以推测,笔者所见“辽代阿拉伯文鏤花铜盆”应是成品由波斯地区流入契丹。此外,本次“契丹印象”展中具有标识性的琥珀璆珞,制作材料来自西方的“琥珀之路”,纹样和造型却承自佛教文化,同样是契丹对多元文化的包容与融合的写照。

辽代契丹人生活在一个有着独特历史地位的地理环境和文明时代当中,是中华民族漫长繁衍中的一个重要分支,创造了辉煌灿烂的古代文明。在统治北方广袤富饶草原的两百多年中,契丹人前承袭强盛大唐,后与繁荣北宋并肩,在保持自己文化独特性的同时,多方位与佛教文化、汉人习俗、西域波斯文化乃至北部欧陆文明交流、融合,对外来文化展现出极高的包容性。尼采曾说:“他们吸收了其他民族的活生生的文化。唯有他们走得如此之远,原因在于他们懂得在其他民族止步的地方,继续前行”。今人无法回到过去,但通过研究文物工艺、纹饰的“变与不变”,足以感受大辽帝国开放包容的草原文明,以及辽帝国在中外文化交流、草原丝绸之路中的重要地位。

**关键词:** 契丹;辽代;摩羯;大卫之星

## Fusion and Embrace in the Khitan Culture of Liao Dynasty: Symbolism in Metalwork

WEN Shangjia, LU Ren, LIU Yimiao

(*Gemmological Institute, China University of Geosciences, Wuhan 430074, China*)

**Abstract:** The repoussé, chased, and gilded crafts from the “Khitan Impression-Exhibition of Cultural Relics of the Liao Dynasty (907—1125 A. D.)” are diverse in style and rich in patterns. Many metalwork crofts used two exotic patterns, of which is the Makara derived from Indian mythology, and the other is the Star of David which is derived from Israel (Jewish culture). Metalwork crafts worked as a carrier of at least four cultures’ fusion (Khitan/Liao, Han/North-Song, Israel /Jewish and India/Buddhism). All these clues can give us opportunities to restore the truth of the cultural circulation among the ethnic groups in the Liao Dynasty through the trace-ability of patterns. At the same time, it shows how inclusive the Khitan are with other cultures.

The Makara from Indian mythology is a combination of animals: whose head is crocodile or elephant, whose bodies is fish, or snake or other kinds of reptiles, and with elephant legs or crocodile claws. Its earliest image appeared in the Lomas Rishi Cave (Fig. 1) (350 B. C.) in northern India (Fig. 2, Fig. 3). Then, between 100 and 200

A. D. , Makara first appeared with a fish-shaped body (Fig. 4). The Chinese mythical creature Wen-yao fish is very similar to Makara. And it was documented in Shan-hai Ching-Xi-shan Ching during the Warring States period (475-221 B. C. ). And there is also a description in the poem *Ode to the Nymph of the Luo River* by Cao Zhi (192–232 A. D. ), who is a poet in the Three Kingdoms Period (220–280 A. D. ). At the same time, it is widely believed that the concept of Makara was introduced into China with the introduction of buddhist scriptures during this period . By the Eastern Jin Dynasty (317–420 A. D. ), the famous painter Gu Kaizhi (348–409 A. D. ) painted the story of *Ode to the Nymph of the Luo River* (Fig. 5). At that time, the Wen-yao fish in this painting had owned a dragon head. It can be seen that Makara has been evolved with the enhancement of local culture impact. After the fusion, Makara has been changed into two categories during the Sui and Tang Dynasties (581–790 A. D. ). One with a dragon head and the fish body is also known as the dragon-fish pattern, and the other is a combination of dragons, fish, bird wings, or other creatures. The Makara pattern also gradually entered the Khitan culture under the huge multiculturalism of the Tang Dynasty.

Many items in this exhibition used Makara's shapes, including gold and silver jewelry, metal products, and ceramics. The repoussé and chased parcel-gilt silver bowls with Makara and flower patterns unearthed from the Hadagoumen kiln of Kalaqin Banner, Chifeng is considered to be a handicraft of the Tang Dynasty (618–907 A. D. ), and it is a typical dragon-fish pattern craft (Fig. 6). The Makara gold earrings were unearthed from the Liao Tomb of Tuerji Mountain, Horqin Zuoyinghouqi, Tongliao. It had a strong sense of three-dimensionality and was welded by gold pieces after hammered. On both sides there are parts like fins and wings with engraved moire and delicate curves (Fig. 7). Some earrings directly welded two U-shaped gold pieces together to form an abstract Makara image (Fig. 8). There are also earrings by simply repoussé and chased the metal pieces and then welded them. The dragon head, fins, scales, and beads(sacred pearl) are fully revealed, and the shape is lively (Fig. 9). In Fig. 10, the dragon head, fish scales, fish fin, both sides of the earring, as well as the flower bud-shaped sacred pearl are all made extremely refined. From these earrings you can understand the Liao Dynasty Makara pattern variety, style changes greatly. It is quite different from the Indian Makara pattern (Fig. 11) of the same period (850–925 A. D. ).

Because of the secession of the Tang Dynasty, the territory was divided into Northern Song Empire and Liao Empire. Therefore, there were Makara relics of the Tang Dynasty occasionally unearthed from the tombs of the Liao Dynasty. Wu Di pointed out in *Makara Prints and Their Cultural Meaning in the Liao Dynasty*: That if Makara in the Liao Dynasty is completely inherited from the Tang Dynasty, then the place where the Han ethnic group lives in Liao Nanjing (now the suburbs of Beijing) and Xijing (now Shanxi Datong) should unearth more Makara artifacts. However, many artifacts were unearthed in Shangjing (now Chifeng) and Dongjing (now Tongliao). The Khitan's preference of Makara may be derived from their special culture. Their land is mainly grassland and mountain forest (including some swamps and rivers), which froms their very specific fishing, hunting, and animal husbandry customs and culture. Especially in

the cold winter, it is necessary for ice fishing. This gradually became a custom activity of Khitan people and has been passed down to this day.

The Star of David (Magen/ Mogen David) originated in Judaism and then spread to Islam (476—1500 A. D. ), also known as the Seal of Solomon, is often found in decorations on religious buildings. Fig. 14 is the complete manuscript of the Hebrew Bible that is considered the oldest (1008 A. D. ) in existence, and this is a page about the Star of David. The bronze bowl chased with the Star of David is now in the Metropolitan Museum of Art (Fig. 13), date 1100—1199 A. D. Fig. 14 is a copper basin chased with Arabic and a Star of David motif from the Liao Dynasty. It can be inferred that this handicraft may have been made before it was imported into Khitan.

No dynasty is as special as Liao Dynasty. The Khitan people ruled the northern grasslands in the Liao Dynasty for nearly two hundred years. Their special geographical location and ethnic characteristics enable them to maintain their own cultural uniqueness while also being extremely tolerant of other cultures. Another strong evidence is that the most popular Yingluo Necklace in the “Khitan Impression” is made of gemstones from the west, while the patterns and shapes are from Buddhist culture. “They invariably absorbed other living cultures. The very reason they got so far is that they knew how to pick up the spear and throw it onward from the point where others had left it”. Although we cannot travel back to the past, we can still focus on the “variation and immutability” of the symbolism in metalworks, and get close to the majestic and inclusive grassland civilization of the Liao Empire.

**Key words:** Khitan; Liao Dynasty; Makara; Star of David



图1 巴拉巴佛窟全视图, Colin Mackenzie 1814 年绘

Fig. 1 General view of the cave temples in the Barabar Hills, Gaya (Bihar, 1814), painted by Colin Mackenzie



图2 巴拉巴佛窟正面

Fig. 2 The facade of Lomas Rishi cave, Barabar Hills

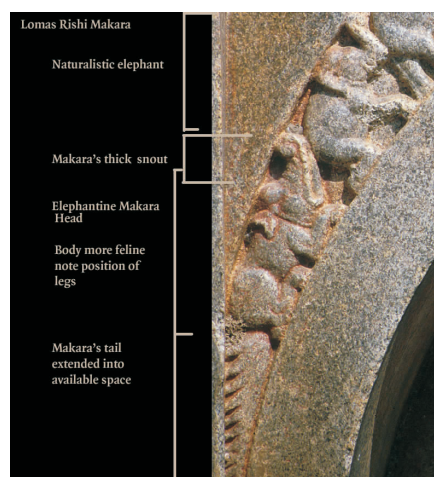


图3 左门楣摩竭雕刻细节

Fig. 3 A closer view of the Makara on the left of the lintel



图4 鱼身摩竭

Fig. 4 Makara first appeared as a fish body



图5 截取自故宫博物院《洛神赋图》卷,晋,顾恺之(宋摹),绢本

Fig. 5 Taken from the "Nymph of the Luo River" volume, this painting is a Song-dynasty (960–1279 A. D.) copy of an original attributed to Gu Kaizhi





图6 摩羯错金银花盘细节  
Fig. 6 Repoussé and chased gilded silver bowls with Makara and flower patterns



图7 摩羯形金耳坠  
Fig. 7 Makara-shaped gold earrings



图8 辽代摩羯形金耳坠  
Fig. 8 Golden earrings in the form of Makara, Liao Dynasty



图9 摩羯形耳坠  
Fig. 9 Pair of Makara earrings, Liao Dynasty



图10 辽代摩羯形金耳坠  
Fig. 10 Golden earrings in the form of Makara, Liao Dynasty



图11 印度摩羯形黄金装饰品  
Fig. 11 Golden earring in the form of Makara

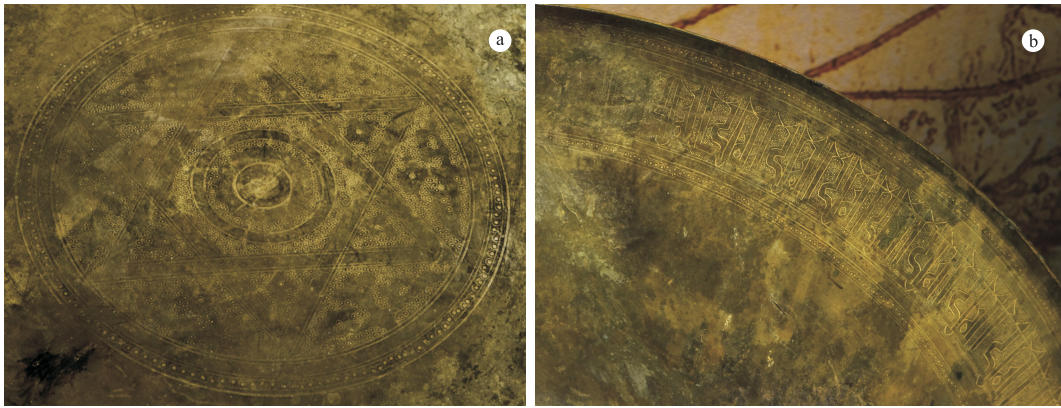


图 12 通辽市奈曼旗陈国公主墓出土阿拉伯文字及大卫之星镌花铜盆细节

Fig. 12 Detail of a bronze pot with Arabic engravings on the inner rim and Star of David at inner bottom unearthed from the tomb of Princess Chen in Naiman Banner, Tongliao



图 13 莱宁格勒手抄本

Fig. 13 The manuscript of the Hebrew Bible



图 14 镌刻大卫之星花纹铜碗

Fig. 14 The bronze bowl chased with the Star of David



# 初探首饰日用之中的价值旨归 ——以乌木首饰为例

曾义平

(长沙理工大学设计艺术学院, 湖南 长沙 410000)

**摘 要:** 首饰是一种与人类活动密切链接的物质文化, 在构建社会礼仪秩序的同时, 也成为人与自身、与他人、与自然对话的媒介。不离日用又高于日用的艺术价值, 是首饰最吸引人的地方。作者通过近五年乌木首饰设计制作经历, 并以商业首饰从业者、学院派艺术首饰教师双重身份, 试图从不同的维度思考首饰日用之中的价值旨归。

**关键词:** 传统首饰; 当代首饰; 价值; 日用; 唤醒

## Preliminary Exploration of the Spiritual Value of Ebony Jewelry in Daily Use

ZENG Yiping

(Changsha University of Science & Technology, Changsha 410000, China)

**Abstract:** Jewelry is a kind of material culture closely connected with human activities. It not only constructs the social etiquette order, but also acts as a medium for people to talk with themselves, others and nature. Inseparable from the daily value but higher than the daily artistic value is the most attractive point of jewelry. Through nearly five years of jewelry design and making experience, the author, as a commercial jewelry practitioner and an academic art jewelry teacher, tries to explore the value of jewelry in daily use from different perspectives.

**Key words:** traditional jewelry; contemporary jewelry; value; daily use; arouse



图1 碎片人生系列首饰

Fig.1 *Fragments of Life* jewelry series



图2 止语系列首饰

Fig.2 *Introspection* jewelry series



图3 一见倾心系列首饰

Fig.3 *Love at First Sight* jewelry series



图4 停云系列首饰

Fig. 4 *Resting Clouds* jewelry series

# 从应用型技术本科的角度构想 珠宝专业本科人才培养模式改革

刘衍宇, 赵靖娜, 吴 璠, 杨天畅, 徐娅芬

(上海建桥学院珠宝学院, 上海 201306)

**摘 要:** 技术本科教育兼具传统高等教育和职业教育的双重特征, 在现今不同教育层次中逐渐凸显出其更加适应市场需求, 顺应时代的比较优势。本文以上海建桥学院珠宝学院为例, 基于技术本科教育的基本特征, 通过其与传统职业教育及传统本科教育的深入对比, 探讨新形势下珠宝专业人才培养模式的突破, 暨成果导向的教学模式、校企合作双向引智、发挥区域优势实现办学特色。

**关键词:** 技术本科; 珠宝专业; 培养模式改革

## On Reforming the Talent Training Mode of Jewelry Major: from the Perspective of Cultivating Applied Technology-Oriented Undergraduate

LIU Xianyu, ZHAO Jingna, WU Fan, YANG Tianchang, XU Yafen

(School of Jewelry, Shanghai Jianqiao University, Shanghai 201306, China)

**Abstract:** Technical-oriented undergraduate education has the dual characteristics of traditional higher and vocational education, which gradually highlights its comparative advantage in adapting to the market demand and among different education levels in nowadays. Taking School of Jewelry of Shanghai Jianqiao University as an example, based on the basic characteristics of technology-oriented undergraduate education, this paper discusses the breakthrough of jewelry professional talent training mode under the new situation, and the achievement oriented teaching mode, two-way talent introduction through school enterprise cooperation, and regional advantages to realize school running characteristics via in-depth comparison with traditional vocational and undergraduate education.

**Key words:** technology-oriented undergraduate; jewelry major; reforming the talent training mode

表 1 技术本科教育和传统职业教育以及传统本科教育的对比

Table 1 The contrast between technical undergraduate education, traditional vocational education and traditional undergraduate education

教育模式 对比方面	传统职业教育	技术本科教育	传统本科教育
办学层次	初等、中等或者高等教育 (以专科为主)	本科	本科
价值取向	强调技能型,主要解决 “做什么”和“如何做”的 问题	强调应用型、技术型,主要解 决“做什么”和“怎么做”的问 题,培养学生对世界的改造 能力	强调学术性,主要是解决 “是什么”和“为什么”的 问题,培养学生对世界的 认识能力
培养目标	掌握经验技术为主,要求 经过长时期实习养成某 一种职业所需的熟练技 能经验和有关知识	培养生产、建设、管理、服务 第一线工作,把科学技术、工 程原理转化为现实生产力的 技术型人才	培养从事研究、发现规律 的学术型人才和从事于 为社会谋求直接利益相 关的规划、决策、设计等 相关的人才
培养方式	按照某一个岗位设置的 工作技能设置课程	按照技术项目、行业以及岗 位群的变化设置专业,有一 定的定向性和地域性	学术定向,为学生接受同 一或者更高级别的教育 做准备
教学模式	实践课比重较大	注重实践课程的比重,采用 多元整合型课程模式	理论课程比重较大,采用 学科课程模式
教师队伍	双师双能型教师队伍 专职和兼职相结合	双师双能型教师队伍 专职和兼职相结合	学术型教师队伍 专职为主



主办单位

ORGANIZER

中国地质大学（武汉）珠宝学院

湖北省珠宝工程技术研究中心

联系方式

CONTACT INFORMATION

027-87482950

67883748

内部资料，请勿外传

